Subsurface Heating and Irrigation of Soils: Its Effect on Temperature and Water Content and on Plant Growth

by

E.W. R. Barlow

A. R. Sepaskhah

L. Boersma

Water Resources Research Institute

Oregon State University

Corvallis, Oregon

WRRI-23

March 1974

SUBSURFACE HEATING AND IRRIGATION OF SOILS: ITS EFFECT ON TEMPERATURE AND WATER CONTENT AND ON PLANT GROWTH

Project Completion Report

Prepared by

E. W. R. Barlow, A. R. Sepaskhah and L. Boersma
Department of Soil Science
Oregon State University

The work upon which this report is based was supported in part by funds provided by the OFFICE OF WATER RESOURCES RESEARCH, U.S. Department of the Interior, through the WATER RESOURCES RESEARCH INSTITUTE of the State of Oregon as authorized under the Water Resources Research Act of 1964, a research and development grant from the PACIFIC POWER AND LIGHT COMPANY, Portland, Oregon, and matching grant funds from the Oregon State University AGRICULTURAL EXPERIMENT STATION.

Project No. B-028-ORE
Matching Grant Agreement
No. 14-31-0001-3634

TABLE OF CONTENTS

TABLE OF CONTENTS

LIST OF TABLES

LIST OF TABLES

LIST OF TABLES

LIST OF FIGURES

LIST OF FIGURES

LIST OF FIGURES

LIST OF FIGURES

LIST OF FIGURES

PART I: EXPERIMENTAL ANALYSIS OF SUBSURFACE HEATING AND IRRIGATION ON THE TEMPERATURE AND WATER WATER CONTENT OF SOILS

A. R. Sepaskhah

INTRODUCTION

Statement of the Problem

Important climatic factors affecting plant growth are soil temperature and air temperature. The optimum soil temperature varies with plant species and variety. The optimum root temperature for species indigenous to warm climates is above that for temperate species (Neilsen and Humphries, 1966). It is known that within certain temperature ranges, biological activity doubles with each temperature increase of 10 C. But temperatures too low or too high are lethal to plants (Salisbury and Ross, 1969). In general, air temperature controls reproductive growth while vegetative growth is controlled by root temperature. High rates of production depend on early germination, emergence, and vigorous vegetative growth. In geographical regions where soil temperatures are not favorable for seed germination and early vigorous growth, high yields are not possible without increasing the soil temperature to an optimum level. Unfavorable soil temperatures at planting time often produce a poor stand and consequently a reduced yield. Retarded growth of young seedlings not only reduces yield but also adversely affects the quality of the crop produced (Richards et al., 1952). Favorable soil temperatures may make it possible to produce two or more crops per year or achieve earlier crop maturity which may have marketing advantages (Boersma, 1970).

Control of temperature in agricultural activities is limited primarily to greenhouse horticulture. Several approaches to increasing the soil temperature in the open field have been taken. Clarkson (1960) mulched soil with black polyethylene plastic. He observed that temperatures were 20-25 F higher at the surface of the mulch and 2 inches above the mulch than at corresponding locations on non-mulched fields. Petroleum mulch was used by Kowsar et al. (1969) to increase soil temperature. The higher temperature in mulched soil was attributed to a blackbody effect of the petroleum mulch and the higher thermal conductivity of the soil resulting from the conservation of soil water below the petroleum skin. Ridging may increase soil temperature by 3 C (Shaw and Buchele, 1957). Orientation of rows can affect soil temperature. Larson and Willis (1957) showed that with north-south rows more radiation is absorbed by the soil than with east-west rows. All these methods depend on available energy and may not increase the soil temperature to an optimum level under unfavorable circumstances.

Other methods for increasing the soil temperature have been discussed by Bunting and Cartwright (1957). They suggested that heating the soil by means of electrically energized heating cables would always be too expensive, but that it might be possible to use waste heat from power stations for this purpose. Boersma (1970) pointed out that surface irrigation is not a feasible method for imparting the energy in condenser cooling water to the soil. The large quantities of water that would be needed would keep the soil flooded most of the time. Boersma (1970) and Boersma and Rykbost (1973) proposed an integrated system for multiple use of the waste heat from power plants. They suggested, that as a part of an integrated complex warm water be circulated through an underground system of pipes thus heating the soil.

Underground heat sources impose a temperature field on the natural soil temperature distribution. The resulting temperature distribution depends on the source temperature, air temperature, and depth and spacing of the heat sources. Power plants with cooling towers are normally designed so that the temperature of the effluent is between 26.5 and 47.5 C (Yarosh et al., 1972). The temperature of the cooling water, the natural soil temperature regime, and the type of crop to be grown, are important factors to be considered in the design of a subsurface soil warming system.

Energy dissipation in the soil depends on the temperature gradient, thermal conductivity, and depth and spacing, of the heat sources. Heat source temperature, soil surface temperature, and depth of heat source are parameters that influence the magnitude of the temperature gradient. Soil thermal conductivity is a critical parameter in controlling the rate of energy dissipation from soil warming systems. The apparent thermal conductivity of the soil is a function of the physical properties of the soil. Important among these are soil texture, soil temperature, and soil water content. The total land surface area required to dissipate a given amount of energy, therefore, depends on the air temperature, heat source temperature, soil type, soil water content, and depth and spacing of the heat sources.

Potential Problems and Opportunities

Moisture migration due to temperature gradients occurs in the soil. This mechanism can produce a dry region around heat sources. Arman et al. (1964), Milne and Mochlinski (1964), and Boersma and Rykbost (1973) reported that this drying can occur at low as well as high temperatures of the heat sources and with any type of soil. Soil surrounding a heating cable is dried to a stage at which the capillary film of water between soil particles is broken. Rewetting the soil is usually very slow (Milne and Mochlinski, 1964). Rykbost (1973) found that the soil water content decreased in the 60-90 cm layer with heat sources at the 90 cm depth. A small but very dry core developed around the heat sources during the summer.

A continuous supply of water near the heat source would prevent the observed drying of the soil. Enough water should be supplied to maintain a constant and high level of water content. This system would make use of the thermal gradients as a driving force to distribute the water through the soil profile.

Subsurface irrigation even without heating the soil has given good results in terms of increased yields and decreased water requirements in comparison with other methods of water application (Hanson and Williams; 1968, Hanson et al., 1970). In principle, if water is introduced slowly into or near the root zone of a plant, it will spread by capillary action in the soil and thus become available for utilization by the plant. If the location of the water application point and the rate of application is properly chosen, it should be possible to supply the demand of the plant without any significant seepage losses and with the region of moist soil maintained below the soil surface to minimize evaporation. The amount of water saved would be a function of the type of crop, soil type, ambient conditions, and efficiency of the comparative methods. Hanson and Williams (1968) and Hanson et al., (1970) estimated potential water savings to exceed 25 percent over furrow irrigation for cotton in New Mexico. Zetzsche (1964) and Newman (1965) reported comparable 1963 cotton yields on 42 percent less irrigation water in Texas using subsurface irrigation. Furthermore, more nearly optimum soil water levels could be achieved with subsurface irrigation than with conventional methods of irrigation.

Scope of the Study

Experiments were set up in the laboratory to study the effect of heat source temperature on the temperature distribution around a line heat source in different soils. Different sinusoidal soil surface heat loads were applied to study the effect of different climatic conditions on the temperature distributions. Effects of heat source temperature, soil surface temperature, and soil texture on rate of heat dissipation were studied. Water was applied near the heat source to determine the rate of water application required to maintain a constant soil water content at different heat source temperatures. Water content distributions and rates of water application were measured.

Field conditions were simulated by packing soils in containers with inside dimensions of 48 x 40 x 4 cm. Thermal insulation was provided on all sides, except the soil surface. A heat source was placed at a depth of 32 cm and 1.5 cm from one side of the box. The soil slab and heat source thus represented a system of parallel line heat sources with a spacing of 77 cm placed at a depth of 32 cm with a lower boundary at 48 cm. Dimensions of the system were dictated by available laboratory equipment. The heat source consisted of a copper tube (O.D. = 0.7 cm) with a resistance heater imbedded in it. Its temperature was controlled thermostatically during each experiment. A porous tube (O.D. = 0.9 cm) with pore sizes ranging from 60 to 70 microns was placed immediately

above the heat source. Water was released from the tube to the surrounding soil. Water was supplied with a Mariotte bottle connected to the porous tube. The device was adjusted to maintain a soil water suction of 2 cm H_2O at the lower side of the porous tube.

Experimental Procedures

Values of the apparent thermal conductivity of the soil are needed to predict temperature distributions and energy dissipation rates for the proposed soil warming systems. The apparent thermal conductivity varies with soil water content, texture, and temperature. Experiments were conducted in the laboratory to measure the apparent thermal conductivity as a function of soil water content at 25 C and 45 C for Quincy, Cloquato, and Chehalis soils.

The particle size distributions and other specifications of the soils used in the experiments are shown in Table 1. Measurements were made at water contents ranging from oven dry to saturation and at 25 C and 45 C.

Table 1. Physical properties of the soils used.

Soil	Particle Size			Porosity	Water Content		Bulk Density
	Sand	Silt	Clay		-1500 Joules/kg	-30 Joules/kg	
	%	%	%	---------- cm^3/cm^3 ----------			g/cm^3
Quincy loamy sand	90	6	4	0.475	0.070	0.185	1.69
Cloquato loam	43	37	20	0.600	0.140	0.350	1.18
Chehalis silt loam	9	64	27	0.600	0.180	0.395	1.16

The samples were prepared by adding the amount of water required to bring a prepacked, air dry, sample to the desired water content. The air dry soil was packed in a glass jar that was tapped once on the top of the laboratory bench with each scoop of sample poured into it. The number of scoops per jar was the same for each sample. Predetermined quantities of water were applied to the samples such that no water was ponded on the soil surface. This method of water application prevented trapping of air in the samples. Samples with low water content were prepared by pouring air dry soil on a plastic sheet and spreading it evenly in a thin layer. Required amounts of water were then sprinkled onto the soil. It was shaken in a plastic bag to distribute the water uniformly and packed into the jars. These were capped with a lid with a hole in the center to

later receive the conductivity probe. The lid and the lid hole were masked by tape to prevent water loss by evaporation. The containers were kept in a constant temperature cabinet for 5-7 days to insure uniform distribution of water and temperature throughout the samples before the measurements were made. Cabinet temperatures of 25 C and 45 C were used.

Apparent thermal conductivities were obtained with a cylindrical probe (Schleirmacher, 1888; Hooper and Lepper, 1950), according to

$$T_2 - T_1 = \frac{q}{4\pi\lambda} \ln \frac{t_2}{t_1}, \qquad (1)$$

where $T_2 - T_1$ is the increase in temperature (C) near the heat source during the time period from t_1 to t_2 in seconds, q is the total amount of heat input (cal/cm sec), and λ is the apparent soil thermal conductivity.

Results

Results of the measurements are shown in Tables 2, 3, and 4. Theoretical values of apparent thermal conductivity were calculated according to the procedures described by de Vries (1963). Ratios of experimental and computed values are also shown in the tables. Results are shown graphically in Figures 1, 2, and 3.

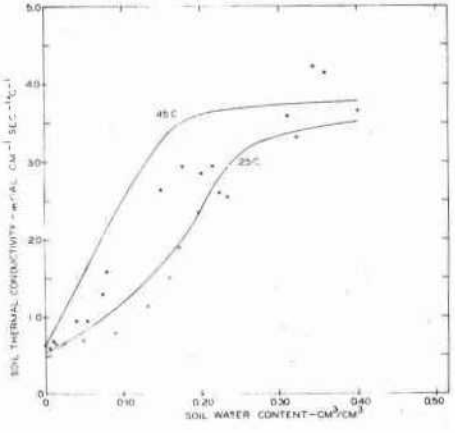

Figure 1. Apparent thermal conductivity of the Quincy soil as a function of water content measured at 25 C (open circles) and 45 C (closed circles). The solid line is based on calculations according to the de Vries (1963) model.

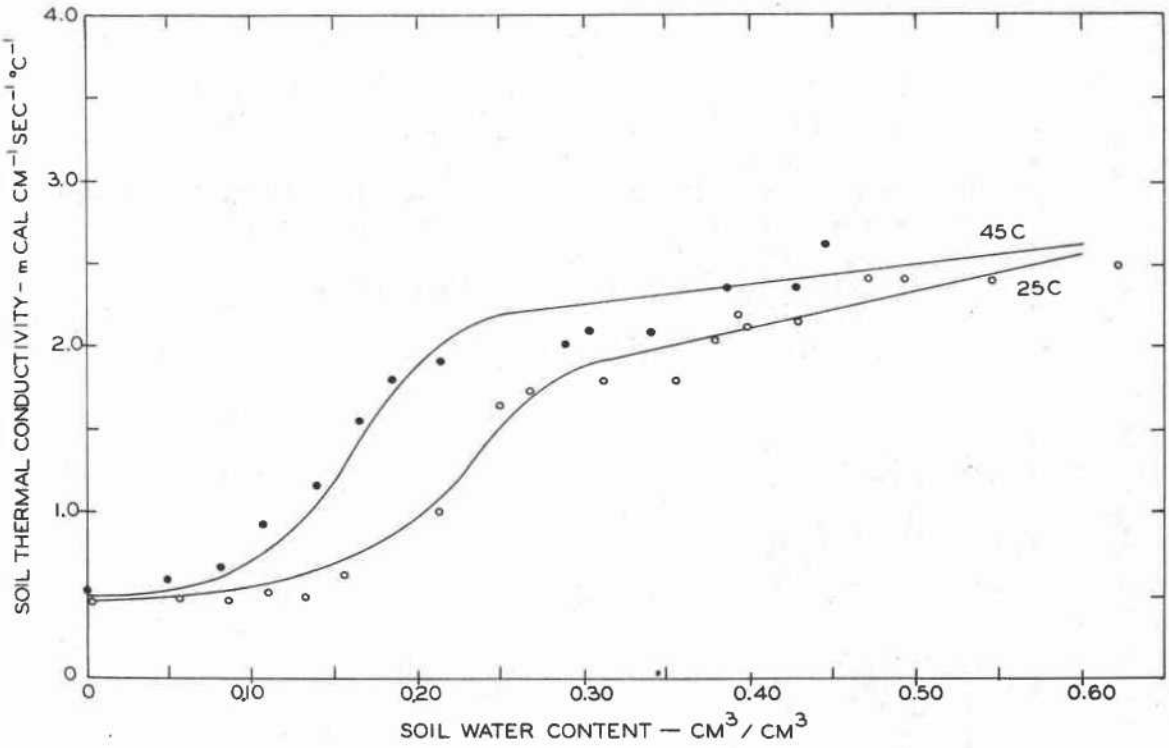

Figure 2. Apparent thermal conductivity of the Cloquato soil as a function of water content measured at 25 C (open circles) and 45 C (closed circles). The solid line is based on calculations according to the de Vries (1963) model.

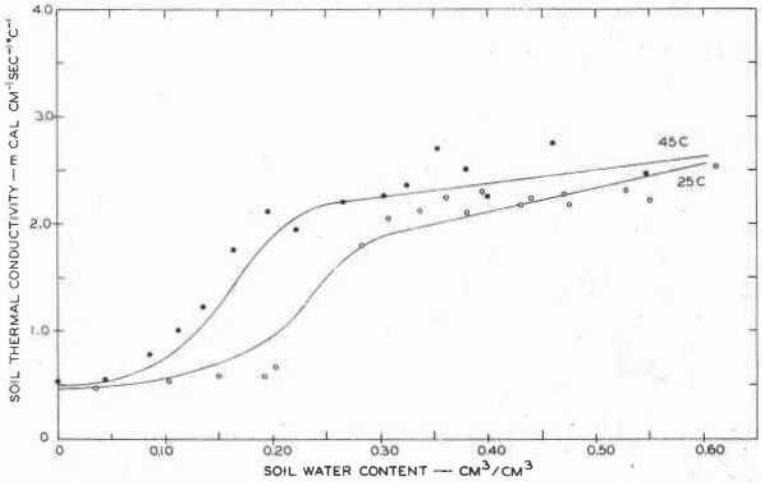

Figure 3. Apparent thermal conductivity of the Chehalis soil as a function of water content measured at 25 C (open circles) and 45 C (closed circles). The solid line is based on calculations according to the de Vries (1963) model.

Table 2. Experimental (λ_e) and computed (λ_c) values of apparent thermal conductivity for Quincy loamy sand at 25 and 45 C.

25 C				45C			
	Apparent Thermal Conductivity, λ		$\frac{\lambda_e}{\lambda_c}$		Apparent Thermal Conductivity, λ		$\frac{\lambda_e}{\lambda_c}$
X_w	(λ_e)	(λ_c)		X_w	(λ_e)	(λ_c)	
cm^3/cm^3	mcal/cm sec C			cm^3/cm^3	mcal/cm sec C		
0.004	0.60	0.55	1.09	0.000	0.63	0.65	0.97
0.014	0.64	0.60	1.07	0.010	0.66	0.82	0.81
0.024	0.66	0.66	1.00	0.039	0.93	1.33	0.70
0.049	0.68	0.82	0.83	0.953	0.94	1.58	0.60
0.090	0.79	1.10	0.72	0.073	1.28	1.92	0.67
0.132	1.14	1.45	0.79	9.978	1.59	2.17	0.73
0.159	1.51	1.78	9.85	0.148	2.63	3.23	0.81
0.172	1.90	1.97	0.97	0.176	2.94	3.66	0.80
0.196	2.35	2.36	1.00	0.200	2.85	3.67	0.78
0.223	2.60	2.95	0.88	0.213	2.94	3.68	0.80
0.233	2.54	2.98	0.85	0.311	3.58	3.73	0.96
0.322	3.30	3.27	1.01	0.342	4.22	3.75	1.13
0.400	4.14	3.52	1.18	0.354	4.14	3.75	1.10

Table 3. Experimental (λ_e) and computed (λ_c) values of apparent thermal conductivity for Cloquato loam sand at 25 and 45 C.

25 C				45 C			
	Apparent Thermal Conductivity, λ		$\frac{\lambda_e}{\lambda_c}$		Apparent Thermal Conductivity, λ		$\frac{\lambda_e}{\lambda_c}$
X_w	(λ_e)	(λ_c)		X_w	(λ_e)	(λ_c)	
cm^3/cm^3	mcal/cm sec C			cm^3/cm^3	mcal/cm sec C		
0.006	0.47	0.47	1.00	0.000	0.55	0.50	1.10
0.054	0.47	0.49	0.96	0.050	0.61	0.52	1.17
0.086	0.48	0.53	0.91	0.082	0.67	0.62	1.08
0.110	0.52	0.57	0.91	0.112	0.95	0.76	1.25
0.132	0.49	0.63	0.78	0.140	1.17	1.06	1.10
0.157	0.63	0.73	0.86	0.166	1.58	1.41	1.12
0.214	1.03	1.10	0.94	0.186	1.81	1.73	1.05
0.249	1.65	1.70	0.97	0.213	1.89	2.00	0.95
0.267	1.77	1.83	0.97	0.290	2.02	2.25	0.90
0.312	1.80	1.92	0.94	0.306	2.09	2.28	0.92
0.357	1.81	2.02	0.90	0.341	2.09	2.32	0.90
0.378	2.05	2.08	0.99	0.385	2.37	2.37	1.00
0.392	2.20	2.10	1.05	0.428	2.37	2.43	0.98
0.397	2.17	2.11	1.03	0.444	2.62	2.44	1.07
0.428	2.16	2.18	0.99				
0.471	2.41	2.27	1.06				
0.493	2.42	2.33	1.04				
0.544	2.39	2.44	0.98				

Table 4. Experimental (λ_e) and computed (λ_c) values of apparent thermal conductivity for Chehalis silt loam at 25 and 45 C.

25 C				45 C			
	Apparent Thermal Conductivity, λ				Apparent Thermal Conductivity, λ		
X_w	(λ_e)	(λ_c)	$\frac{\lambda_e}{\lambda_c}$	X_w	(λ_e)	(λ_c)	$\frac{\lambda_e}{\lambda_c}$
cm^3/cm^3	mcal/cm sec C			cm^3/cm^3	mcal/cm sec C		
0.035	0.48	0.47	1.02	0.000	0.53	0.50	1.06
0.104	0.54	0.57	0.95	0.045	0.52	0.53	0.98
0.150	0.58	0.70	0.83	0.087	0.80	0.68	1.18
0.193	0.60	0.91	0.66	0.111	1.01	0.84	1.20
0.203	0.67	0.98	0.68	0.136	1.22	1.05	1.16
0.282	1.78	1.85	0.96	0.164	1.77	1.45	1.22
0.308	2.07	1.91	1.08	0.194	2.10	1.85	1.14
0.340	2.14	1.99	1.08	0.219	1.96	2.05	0.96
0.360	2.26	2.03	1.11	0.265	2.19	2.22	0.99
0.379	2.13	2.08	1.02	0.302	2.26	2.26	1.00
0.394	2.32	2.10	1.11	0.325	2.37	2.29	1.04
0.428	2.20	2.18	1.01	0.353	2.70	2.32	1.16
0.440	2.26	2.21	1.02	0.380	2.52	2.35	1.07
0.469	2.31	2.27	1.02	0.401	2.24	2.38	0.94
0.474	2.20	2.28	0.97	0.459	2.75	2.45	1.12
0.529	2.33	2.40	0.97	0.555	2.44	2.58	0.95
0.550	2.24	2.45	0.91				

The computed results are in good agreement with experimental values for Cloquato and Chehalis soils. The computed values are systematically slightly higher at 25 C and slightly lower at 45 C at low water content for both these soils. This may be due to incorrectly having assumed a linear relationship between the effective thermal conductivity of the air and the soil water content at water contents below θ_e.

Experimental values for the Quincy soil (Table 2) at low water contents are systematically lower than the computed results. The quantity of water required to wet the soil samples to the desired level at low water content was very small. It was difficult to mix the required amount of water with the dry soil to obtain a uniform water content in the samples. Non-uniform water distribution at low water content could result in experimental values of apparent thermal conductivities lower than the values corresponding to the average water content.

Theoretical estimates of the apparent thermal conductivity of a soil can be obtained if the mineral composition, porosity, and water content and the thermal conductivities of each of these components are known. The accuracy of the thermal conductivities obtained by this procedure (de Vries, 1963) is sufficient for many practical applications. At water contents higher than 0.2 to 0.3 cm^3/cm^3, the predicted apparent thermal conductivity differed from the measured values by about 10 percent for Cloquato and Chehalis soils (Tables 3 and 4). The deviations were greater than 10 percent for Quincy at almost all water contents (Table 2), and at low water contents for Cloquato and Chehalis soils. Variation of the apparent thermal conductivity in a given soil at a given depth due to the nonhomogeneity of the soil and due to irregular changes in the water content may be expected to be of the order of 5 to 10 percent (de Vries, 1963).

Discussion

Thermal Conductivity as a Function of Particle Size

The coarse textured Quincy soil has a higher thermal conductivity than the fine textured Cloquato or Chehalis soils in the air dry state. This difference may be attributed to the lower thermal conductivity of the granular material in fine-textured soils. De Vries (1963) reported thermal conductivities of 21, 11, and 7 mcal/cm sec C for quartz, granite, and clay minerals, respectively. Nakshabandi and Kohnke (1965) also showed the apparent thermal conductivity of air dry soil to increase with particle size. Nagpal and Boersma (1974) comparing the thermal conductivities of glass bead media of different sizes could not show

the effect of grain size on the apparent thermal conductivity of the medium. Glass beads possess the same thermal conductivity regardless of bead size. These results suggest that the small differences in the thermal conductivities of the air-dry materials used in the experiments are due to differences in the thermal conductivities of the particle materials and not to the size of the particles.

Thermal Conductivity as a Function of Soil Water Content

Apparent thermal conductivities of the three materials remained unchanged as the water content increased from zero to certain specific values (Figures 1, 2, and 3). The amount of water in the soils at which the apparent thermal conductivities started to increase is shown in Figure 4 as a function of clay content at 25 and 45 C. The indicated behavior can be explained by soil-water interactions. At low water content molecules of water form only thin films on the soil particles. As more water is added the thickness of the water films increases and wedges are formed at the contact points between particles. At very low water content the water films on the surfaces are only a few molecules thick and water does not fill interstices between them (Wadsworth, 1944). The films are uniform and do not improve the thermal contact between soil particles, so that heat flow is not appreciably enhanced. The amount of water required to produce films of a given thickness depends on the specific surface area of the particles which is a function of particle size, shape, and clay content. Clay particles are small but have a high specific external and internal surface area. Clay soils need to absorb more water than sandy soils to produce the wedges which contribute to increased heat flow.

The water absorbed by the clay particles is tightly bound but can be driven off at higher temperatures. Examination of Figures 1, 2, and 3 shows that the water content at which the bound water can be driven off and contribute to heat flow decreases as a function of temperature (Figure 4).

The apparent thermal conductivities of the three soils increases with water content except at very low water content. The increase in the apparent thermal conductivity per unit of water added is greater in the coarse-textured soil than in the fine-textured soils at both temperatures. Similar observations were made by Smith (1939) and Nakshabandi and Kohnke (1965). The rate of increase of the apparent thermal conductivity with soil water content is highest at low water contents. Here the increase is due to the addition of water in the wedges at the particle contact points. The surface through which heat is conducted increases rapidly with the first increments of water added. With further additions of water, soil pores gradually are filled and the rate of increase of the apparent thermal conductivity becomes smaller.

Apparent thermal conductivity differences between the three soils are more pronounced at the higher water contents. This again shows the influence of the thermal conductivities of the particles themselves. The sandy soil had a higher apparent thermal conductivity at water contents near saturation. Similar results were obtained by Chudnovskii (1962). He measured the apparent thermal conductivities of quartz sand and of limestone with the same grain size distributions as a function of water content. The difference between the apparent thermal conductivities of the two materials was small at the dry condition, but at a water content of 20 percent, the ratio of apparent thermal conductivities of quartz sand and limestone was 1.5.

Thermal Conductivity as a Function of Soil Water Potential

When the apparent thermal conductivity is plotted as a function of soil water potential, a dissimilarity due to textural differences appears (Figure 5). These differences are greatest between coarse-textured (Quincy) and fine-textured (Cloquato and Chehalis) soils at high water potentials. No textural differences at soil water potentials lower than about -400 Joules/kg were found at 25 C. Results shown in Figure 5 are best understood by considering the soil water characteristic curves for the three soils (Figure 6). These graphs show that most of the soil water in Quincy loamy sand is withdrawn over a very narrow potential range, corresponding to the range over which its apparent thermal conductivity decreases (Figure 5). The soil water characteristic curves for Cloquato and Chehalis show that the gradual decrease of the thermal conductivities for these two soils corresponds with the gradual decrease of soil water content as the water potential decreases. Nagpal and Boersma (1974) reported pronounced textural differences in the relationship thermal conductivity - water potential for glass beads at water potentials higher than about -70 Joules/kg. The results shown in Figure 6 are in agreement with these findings.

Thermal Conductivity as a Function of Porosity

The apparent thermal conductivity of a porous medium is determined by the thermal conductivities of its constituent fractions (solid, water, and air). Porous materials with similar particles and similar total porosities should have unique thermal conductivities at various volumetric water contents. Skaggs and Smith (1967) calculated the thermal conductivity of a soil as a function of pore space and water content. Their results showed an increasing resistance to heat flow at identical water contents with increasing pore space. The effect of total pore space on the apparent thermal conductivity was most pronounced at the highest soil water contents.

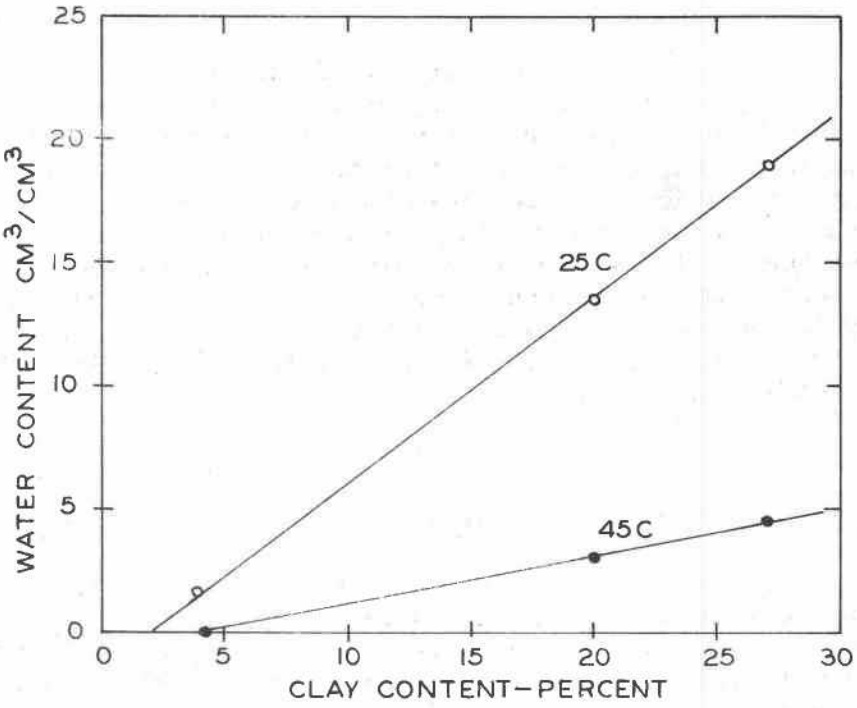

Figure 4. Maximum water content range below which the apparent thermal conductivity of the soils is constant, plotted as a function of the clay content, measured at 25 C (open circles) and 45 C (closed circles).

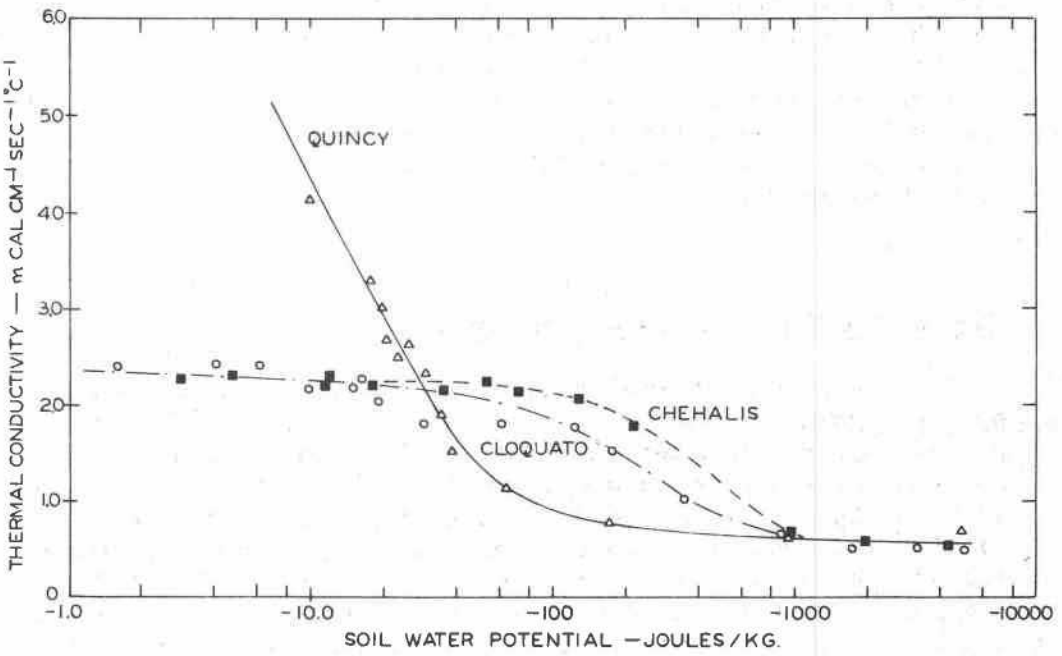

Figure 5. The apparent thermal conductivities of the Quincy, Cloquato, and Chehalis soils as a function of soil water potential at 25 C.

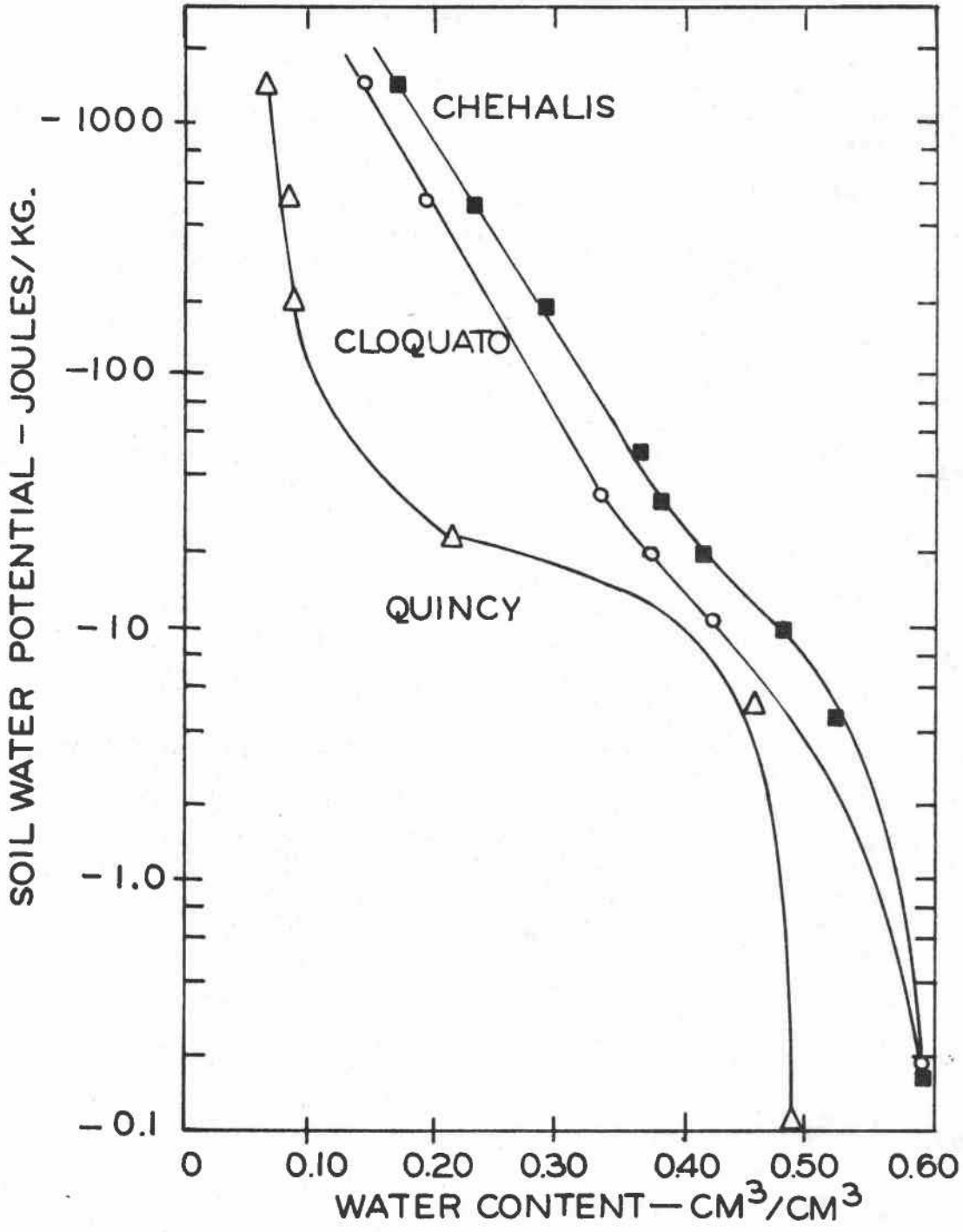

Figure 6. Soil water characteristic curves for the three soils used in the experiments. The data points shown were obtained with the pressure plate and the pressure membrane techniques. Packed cores were used for the measurements at potentials higher than -600 Joules/kg and bulk samples were used at lower potentials.

Cloquato loam and Chehalis silt loam have a porosity of 60 percent and the thermal conductivities of the particles are identical. Total porosity of the Quincy loamy sand is 46.5 percent and the thermal conductivity of its particles is higher. Similarities between the apparent thermal conductivities of the Cloquato and Chehalis soils as a function of soil water content and their difference from Quincy soil was therefore expected and in agreement with literature reports. Nakshabandi and Kohnke (1965) observed textural differences in the apparent thermal conductivity versus soil water content relationship for fine sand, silt loam, and clay with porosities of 40, 48, and 58 percent, respectively. These differences were attributed to differences in air-filled pore space at identical water contents. At higher water contents where good contact between particles increases the apparent thermal conductivity, the thermal conductivity of the particles themselves becomes important. The higher apparent thermal conductivity of the sand at identical water contents is in part due to the higher thermal conductivity of the sand particles.

Thermal Conductivity as a Function of Temperature

Apparent thermal conductivities did not change much by the increase in temperature from 25 C to 45 C at the very low water contents. The slight increase of the apparent thermal conductivities of dry soils with temperature can be attributed to increased thermal conductivity of the air at higher temperatures.

The apparent thermal conductivities of the soils increased appreciably as a function of temperature as soil water content increased. The configuration of the water films on the soil particles remains the same at a given water content at 25 and 45 C and it should not change the conduction between particles. But a substantial increase in the apparent thermal conductivity occurred as a result of the temperature increase. The higher apparent thermal conductivity at the higher temperature is due to enhanced vapor transfer through the air-filled pores. The increases in the apparent thermal conductivities as a result of the temperature increase from 25 to 45 C are smaller at the high water contents. This is so because air filled pore space available for vapor diffusion is less.

Effective thermal conductivity of an air-filled pore is due to heat conductance, λ_a and convective vapor movement, λ_v so that

$$\lambda_{eff.} = \lambda_a + \lambda_v, \qquad (2)$$

where λ_a changes slightly with temperature, increasing from 0.0615 to 0.0650 mcal/cm sec C as the temperature increases from 25 to 45 C. However, λ_v varies greatly with temperature.

For water contents less than θ_e, the effective conductivity of air varies as a result of decreasing relative humidity. It is usually assumed that λ_v decreases linearly with soil water content, from $\lambda_v = \lambda_v^s$ at $x_w = \theta_e$ to zero at $x_w = 0$, so that the effective conductivity of air in air-filled pores becomes:

$$\lambda_a + \lambda_v = \lambda_a + \frac{x_w}{\theta_e}(\lambda_v^s - \lambda_v), \tag{3}$$

where λ_v^s is the thermal conductivity due to vapor movement in water vapor saturated air and x_w is the volumetric water content. An expression was given by Krischer and Rohnalter (1940) to calculate λ_v^s as follows

$$\lambda_v^s = \frac{LD_o P}{RT\ (P-p_o)} \frac{dp_o}{dT}, \tag{4}$$

where λ_v is the latent heat of vaporization (cal/g), R is the gas constant (0.11 cal/g Kfor water vapor, D_o is the diffusion coefficient of water vapor in air (cm^2/sec), P is atmospheric pressure (mm Hg), p_o is the saturation vapor pressure (mm Hg), and dp_o/dT is the slope of the saturation vapor pressure versus temperature curve (mm Hg/C).

Ratios of the apparent thermal conductivities of the three soils at 45 C and 25 C are shown in Figure 7 as a function of the pore volume fraction available for vapor diffusion. The maximum values of the ratios are 2.15, 2.73, and 2.96, respectively. Comparison of these values with the ratio of dp_o/dT at 45 and 25 C, which is equal to 2.61, suggests that increased vapor diffusion was the prime mechanism causing the increase of apparent thermal conductivity with temperature at low soil water content. The ratio of $\lambda_{45}/\lambda_{25}$ approaches one at air-filled porosities higher than 0.95 and lower than 0.45. It never becomes equal to one because of the higher thermal conductivities of air and water at higher temperatures. The contribution of vapor diffusion to apparent thermal conductivity increases as soil water content decreases or the air-filled pore volume increases.

The ratios of $\lambda_{45}/\lambda_{25}$ are lowest for the Quincy sand. This is so because the apparent thermal conductivity of the sand particles is higher than that of the clay particles. The relative contribution of vapor transfer is therefore smaller.

The contribution of water vapor diffusion to the apparent thermal conductivity depends on the vapor pressure gradient and the diffusion coefficient. These parameters both increase with temperature. The vapor diffusion coefficient also increases with increasing air-filled porosity. Therefore, the temperature effect on the apparent thermal

conductivity is greatest in soil with the highest air-filled porosity. At extremely low water content the ratio $\lambda_{45}/\lambda_{25}$ decreases (Figure 7). This decrease occurs because the air-filled pores are not saturated with water vapor at these low water contents. Philip and de Vries (1957) have shown that when the soil air is not saturated with water vapor the value of λ_v is proportional to the relative humidity, p/p_o, thus:

$$\lambda_v = \frac{p}{p_o} \lambda_v^s \qquad (5)$$

and

$$\frac{p}{p_o} = \exp\left(\frac{4M\sigma}{\rho dRT}\right) \qquad (6)$$

where p is the water vapor pressure (mm Hg), M is the molecular weight of water (gram/mole), σ is the surface tension of water (dyne/cm), ρ is the density of water (gram/cm^3), d is the pore diameter (cm), R is the gas constant (8.314 x 10^7 erg/mole K), and T is the Kelvin temperature. At extremely low water content only small pores are filled with water. According to Equations 5 and 6, λ_v decreases and so does its contribution to the apparent thermal conductivity.

The maximum ratio of apparent thermal conductivities at 45 and 25 C occurred at the air-filled porosities of 0.78, 0.73, and 0.70 in Quincy, Cloquato and Chehalis soils respectively (Figure 7). These values correspond to water contents of 0.11, 0.15, and 0.18 cm^3/cm^3.

At high water contents the pore volume available for vapor diffusion is very small and discontinuous. The ratios approach one near saturation. Temperature was found to have only a small effect on the apparent thermal conductivities at water contents higher than .20, 0.25, and 0.30 cm^3/cm^3 in Quincy, Cloquato and Chehalis soils, respectively.

Conclusions

The apparent thermal conductivities of soils change with water content. The changes are greatest at water content levels between field capacity and wilting point. The apparent thermal conductivity does not vary with water content at extremely low levels. Water increases the thermal contact between soil particles and enhances heat flow in the soil by increasing soil apparent thermal conductivity. At low water contents, water molecules form layers on the surfaces of clay particles and do not contribute to heat flow. The water content at which the water begins to have an effect on the apparent thermal conductivity was proportional to the clay content.

In unsaturated soil, air-filled pores are available for vapor diffusion resulting from vapor density gradients. Vapor flow contributes to the apparent thermal conductivity. Its effect is greatest at low water contents where enough water is available to produce saturated conditions and enough pore space is present for vapor flow to occur.

The apparent thermal conductivity increased with temperature. This increase, due to an increase in the thermal conductivity of water, is negligible. Temperature has a significant effect on the apparent thermal conductivity by increasing the vapor pressure gradients in air-filled pores. In the range of water contents where vapor flow contributes significantly to the apparent thermal conductivity, the maximum $\lambda_{45}/\lambda_{25}$ values were 2.15, 2.73, and 2.96 for Quincy, Cloquato, and Chehalis soils, respectively. The value of the vapor pressure ratio at 45 and 25 C is 2.6 which is close to the maximum ratios obtained for the three soils. Vapor diffusion did not contribute significantly to the apparent thermal conductivity at water contents above field capacity where the air-filled pore volume available for vapor flow is small and probably discontinuous.

A plot of the apparent thermal conductivity versus soil water potential showed differences between soils with different textures except at water potentials lower than -300 to -400 Joules/kg.

The de Vries (1963) model can be used satisfactorily to calculate apparent thermal conductivities of soils using the thermal conductivities of the solid particles, porosity, and water content.

A temperature increase from 25 to 45 C increased the apparent thermal conductivity almost three times at low water content. This suggests that appreciable error may result from the use of a constant value for the thermal conductivity in heat flow problems in soils.

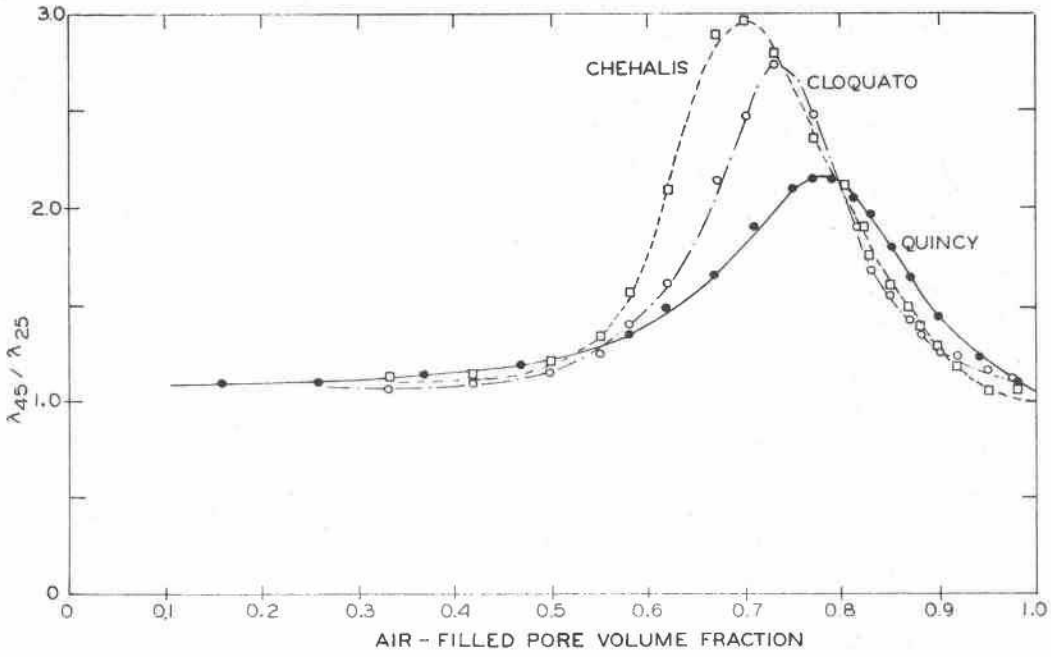

Figure 7. Ratios of the apparent thermal conductivities at 45 and 25 C ($\lambda_{45}/\lambda_{25}$) for the three soils as a function of the air-filled pore volume reported as a percentage of the total pore volume.

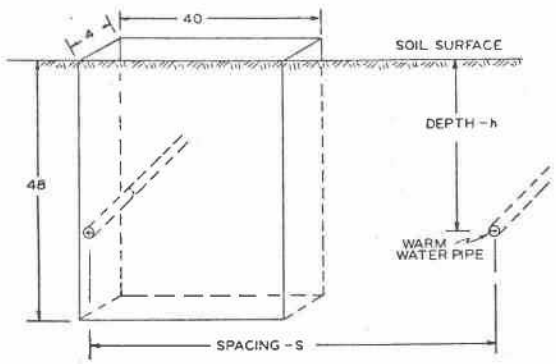

Figure 8. Geometry of the experimental soil slab used for the laboratory experiments. The heat source representing the warm water pipe was at a depth of 33 cm. The water source (not shown) was immediately above the heat source.

EXPERIMENTAL ANALYSIS OF SUBSURFACE SOIL WARMING AND IRRIGATION

Experimental Procedure

Soil columns were used in laboratory studies to simulate the proposed open field soil warming system. Soils were contained in a box 48 cm deep, 40 cm long, and 4 cm wide on the inside (Figure 8). The box was made of 0.5 cm thick acrylic plastic. Dimensions of the container were dictated by available materials and laboratory equipment. A heat source 0.7 cm in diameter consisting of a copper covered electrical resistance heating wire was placed 32 cm deep and 1.5 cm from the inside of the right hand wall of the box. This configuration simulated an open field soil warming system with heat sources buried 32 cm deep, 77 cm apart. Small holes were drilled through the wall of the box for the insertion of thermistors for temperature measurements.

An irrigation water source was placed above the heat source, 30 cm deep and 1.5 cm from the right hand wall of the box. It consisted of a porous tube, 3.5 cm long with and I. D. = 0.9 cm, made of synthetic material with pore sizes ranging from 60 to 70 microns. A graduated Mariotte bottle was connected to the porous tube such that a pressure of -2 cm H_2O was maintained in the soil next to it. The water source configuration simulated a subsurface irrigation system, 30 cm deep with a 77 cm spacing. Different evaporative conditions were simulated by sinusoidal surface heat loads, applied with a resistance heater 10 cm above the soil surface. Experiments were conducted at three different subsurface heat source temperatures.

Physical properties of the soils used are shown in Table 1. Air dried soil materials were packed in the acrylic containers and saturated with water from below until free water appeared at the soil surface. At this time the soil column was disconnected from the water source and excess water was allowed to drain. Surface evaporation was prevented during the drainage period. The column was then covered with styrofoam on all sides except at the surface and thermistors were inserted at the predetermined points. All preparations and experiments were conducted in a constant temperature room maintained at 22 $\pm$ 1 C.

Experiments were initiated by preparing soil columns as described above. The water content at a point close to the heat source was monitored with a gamma-ray attenuation system. Water was applied by the irrigation tube at a rate such that the water content at this particular point was not lowered from its initial value. This criterion produces a constant water content throughout the soil at each combination of experimental conditions. When the appropriate rate of water application was established, several readings of water content were taken with the gamma-ray attenuation system at predetermined points.

Each experiment was continued until an equilibrium water content distribution and temperature distribution was attained. Measurements were then continued for three days during which periodic measurements were made. A summary of the experiments is shown in Table 5.

Table 5. List of experiments conducted in the laboratory study of the soil warming system.

Experiment No.	Soil	Heat Source Temperature	Subsurface Irrigation	Peak Rate of Irradiation
		°C		Watt
1	Quincy	29	yes	0
2	Quincy	29	yes	13
3	Quincy	29	yes	52
4	Quincy	29	yes	117
5	Cloquato	36	yes	0
6	Cloquato	36	yes	13
7	Cloquato	36	yes	52
8	Cloquato	36	yes	117
9	Chehalis	44	yes	0
10	Chehalis	44	yes	13
11	Chehalis	44	yes	52
12	Chehalis	44	yes	117
13	Quincy	29	no	117

Temperature Distributions

Experimental Results

Temperature readings obtained at preselected points in time during three days while equilibrium conditions existed were averaged. Figure 9 shows the temperature as a function of depth at 0:00, 4:00, 8:00, 12:00, 16:00, and 20:00 o'clock in the heated Quincy loamy sand at heat source temperatures of 29, 36, and 44 C and a sinusoidal surface heat load with a maximum of 117 watts. The measurements were made in a vertical profile centered over the heat source. Subsurface heating raised the soil temperature throughout the profile. The temperature rise was highest near the heat source. The effect of heating on the temperature of the soil was small near the soil surface. The soil surface temperatures were below the air temperature at all heat source temperatures during the cooling period.

The soil surface temperatures at 8:00 o'clock were 19.6 and 22.4 C for heat source temperatures of 29 and 44 C, respectively. They were less than the room temperature of 23 C near the soil surface during the cooling

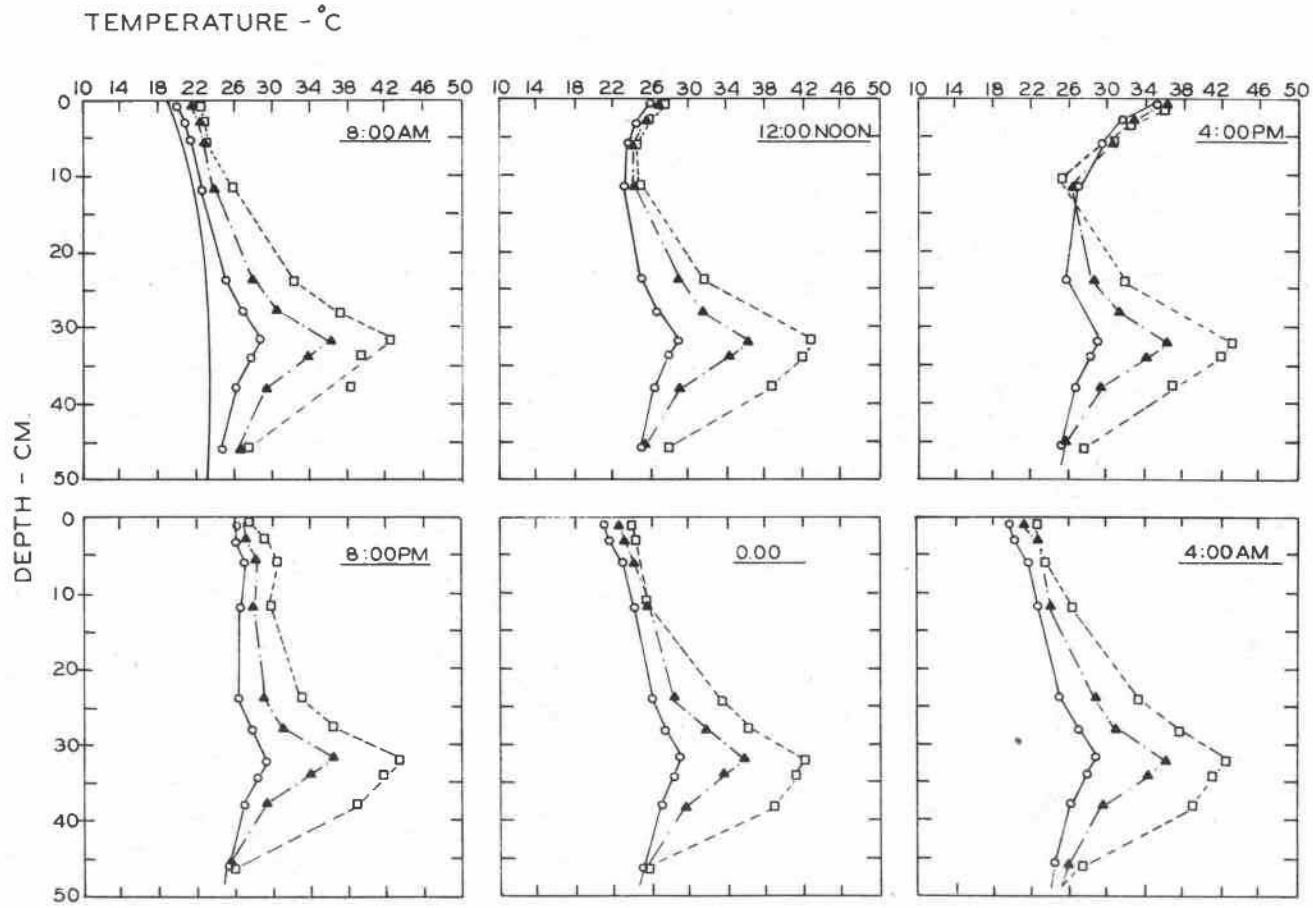

Figure 9. Soil temperature as a function of depth measured at four-hour intervals at heat source temperatures of 29 C (o), 36 C (x), and 44 C (□) in Quincy soil. Measuremtns were made in a vertical profile centered over the heat source.

period starting at 20:00 o'clock and terminating at 8:00 o'clock. The room temperature of 23 C was the upper limit of the daily room temperature variation. The thickness of the shallow surface layer with temperatures below 23 C at 8:00 o'clock was 19, 12, and 7 cm at heat source temperatures of 29, 36, and 44 C, respectively. The temperature of the surface layer increased during the heating period (12:00 to 16:00 o'clock) due to the surface heating.

Equilibrium temperature isotherms are shown in Figures 10, 11, and 12. No heat was applied at the soil surface in the experiments shown in these diagrams. The heat source temperature influenced the temperature of the area near the heat source greatly. Its effect decreased rapidly at points away from the heat source. The horizontal distance from the heat source at which a 5 C increase in soil temperature occurred is shown in Table 6 as a function of the temperature difference between heat source and the unheated soil surface. The relationship was dependent on the soil texture.

Table 6. Relationship between the horizontal distance (d) from the heat source, at which a 5 C temperature rise occurred and the difference in temperature between heat source and unheated soil surface (ΔT).

Soil	Source Temperature	ΔT	d
	°C	°C	cm
Quincy loamy sand	29	6	4.0
Quincy loamy sand	36	13	10.0
Quincy loamy sand	44	21	15.0
Cloquato loam	29	8	3.5
Cloquato loam	36	13	9.5
Cloquato loam	44	23	12.5
Chehalis silt loam	29	6	2.5
Chehalis silt loam	36	13	9.0
Chehalis silt loam	44	23	12.5

The isotherms shown indicate that a wide range of temperatures occurs in a profile heated with line heat sources. This can be important if the crop grown in the field has a narrow temperature range for optimum growth. Soil temperatures higher than the optimum root temperature may have an adverse effect on crop production. The optimum root temperature for many crops grown in temperate climates is about 25 C. Temperatures higher than 25 C were observed near the heat source. The distance over which temperatures higher than 25 C occurred was a function of the heat source temperature. The soil volume with temperatures higher than 25 C

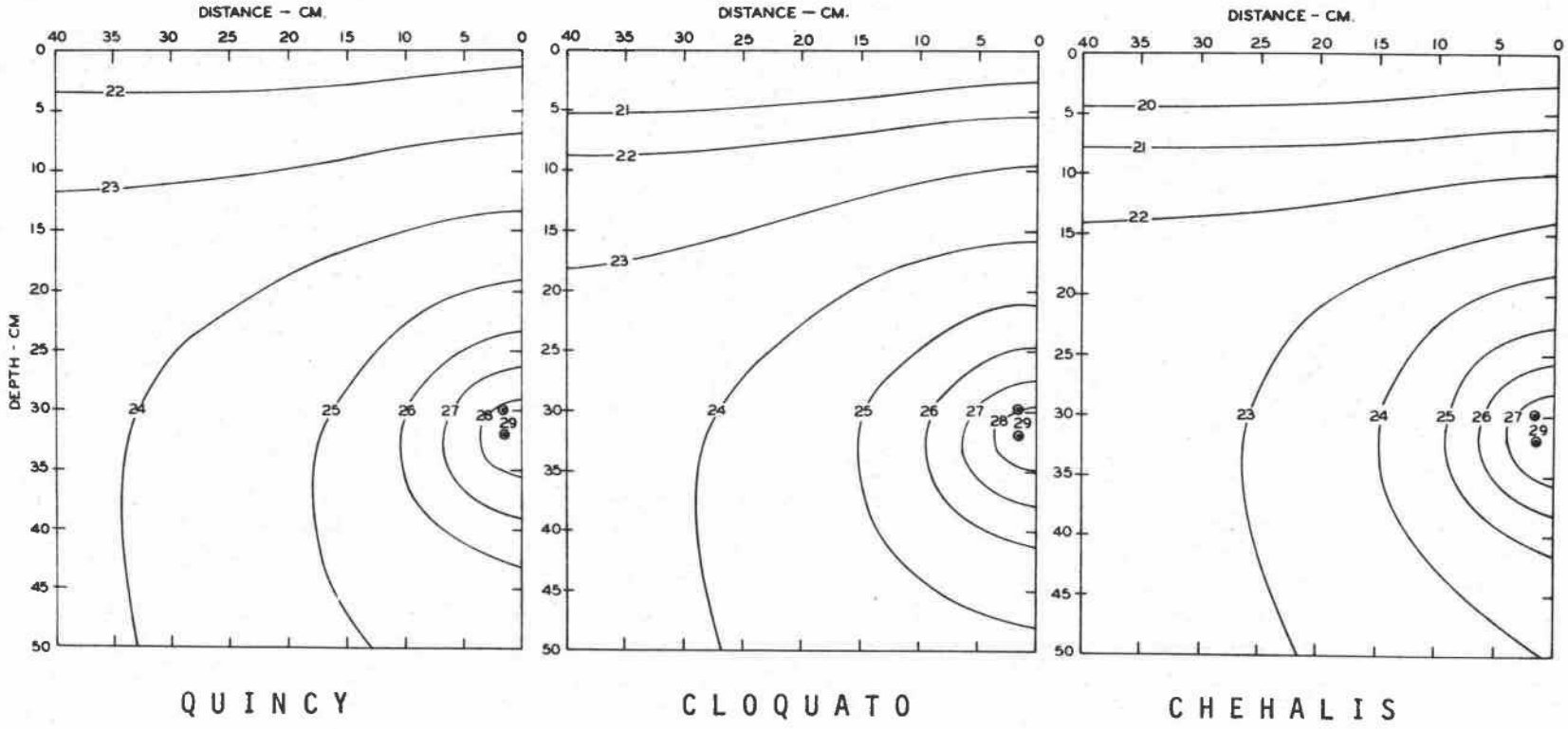

Figure 10. Measure equilibrium temperature isotherms for the Quincy, Cloquato, and Chehalis soils at a heat source temperature of 29 C. No heat was applied at the soil surface.

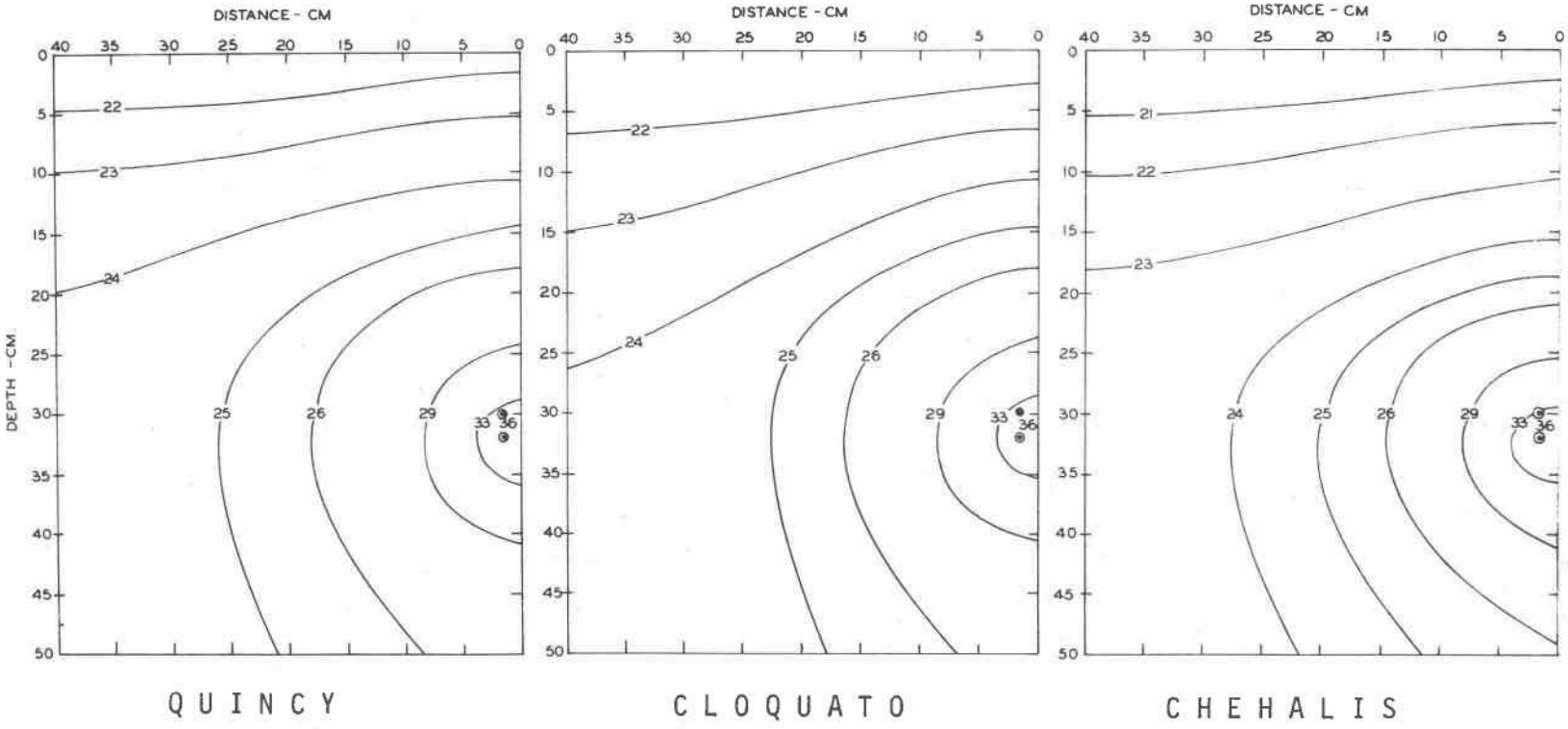

Figure 11. Measured equilibrium temperature isotherms for the Quincy, Cloquato, and Chehalis soils at a heat source temperature of 36 C. No heat was applied at the soil surface.

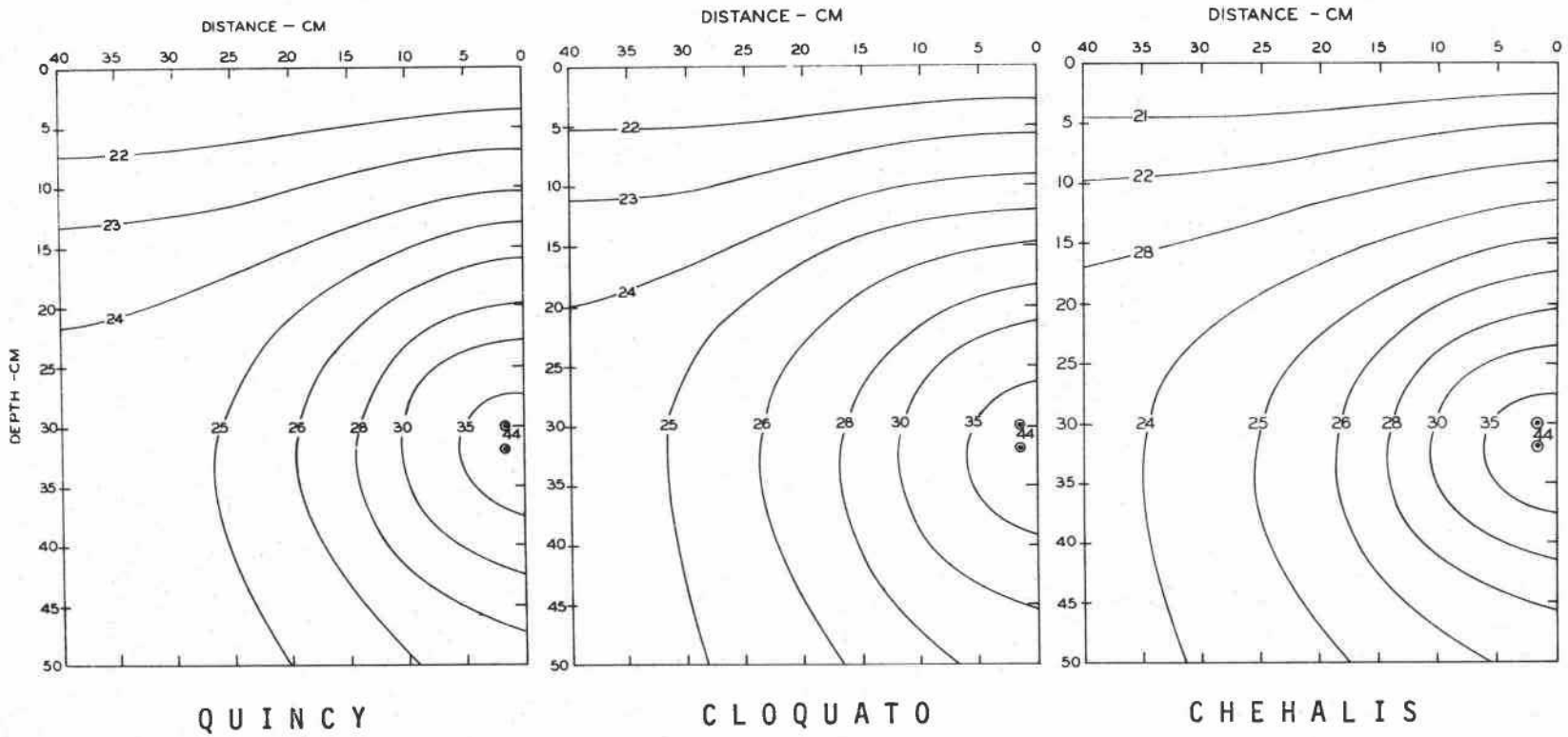

Figure 12. Measured (solid lines) and calculated (broken lines) equiligrium temperature isotherms for the Quincy, Cloquato, and Chehalis soils at a heat source temperature of 44 C. No heat was applied at the soil surface.

was very small at a heat source temperature of 29 C but was considerable at the heat source temperature of 44 C. The adverse effect of soil temperatures above 25 C could be prevented by planting some distance away from the heat source. Soil warming had little effect on the temperature of the upper 10 cm of the soil. This is the layer in which seed germination usually occurs. Optimum temperatures for germination of most seeds range from 15 to 40 C (Mayer and Poljakoff-Mayber, 1963). When the unheated soil temperature is lower than the optimum temperature for seed germination, soil warming will not help to improve the seed germination.

Theoretical Considerations

Equation 7, derived by Kendrick and Havens (1973) was used to calculate theoretical isotherms. This equation was developed for a semi-infinite medium with a constant surface temperature and constant apparent thermal conductivity throughout.

$$T_{(x,y)} - T_{su} = \frac{q}{2\pi\lambda}\left[\ln\sqrt{\frac{x^2+(h-y^2)}{x^2+(h+y)^2}} + \sum_{n=1}^{N}\ln\sqrt{\frac{(ns-x)^2+(h-y)^2}{(ns-x)^2+(h+y)^2}} + \sum_{n=1}^{N}\ln\sqrt{\frac{(ns+x)^2+(h-y)^2}{(ns+x)^2+(h+y)^2}}\right] \quad (7)$$

where x is the horizontal distance from the heat source (cm), h is the distance from soil surface to the heat source (cm), y is the vertical distance from the soil surface (cm), q is the heat flow rate per unit length of heat source (cal/cm sec), λ is the thermal conductivity of the soil (cal/cm sec C), $T_{(x,y)}$ is the temperature of the medium at any point in the system (C), and T_{su} is the soil surface temperature (C). Several simplifying assumptions should be considered in the application of Equation 7. These are: (i) constant, uniform soil apparent thermal conductivity, (ii) no radial temperature variation in the cross-section of the heat source, (iii) constant, uniform soil surface temperature, (iv) steady-state operation, (v) heat is transferred in the soil in the radial direction only, and (vi) all sources have the same temperature and dissipate heat at the same rate. Experimental conditions did not correspond to these assumptions. It was deemed desirable to test the validity of this equation for the experimental conditions.

The soil surface temperature varied during the day according to the applied surface heat load in several of the experiments. A daily average of the soil surface temperature was used in the calculations. The measured rates of energy dissipation per unit length of the heat source, q,

are shown in Table 7. An average apparent thermal conductivity for the soil column was used, although the conductivity was not uniform throughout the soil column because of variation in the soil water content and temperature. The soil column had a reflecting boundary at the lower end. Thus it did not present a semi-infinite medium as was assumed in the derivation of equation 7.

Table 7. Energy dissipation rates in Quincy, Cloquato, and Chehalis soils with different heat source temperatures and surface heat loads.

Heat Source Temperature	Max. Surface Heat Load	Energy Dissipation Rate Per Unit Length of Heat Source		
		Quincy	Cloquato	Chehalis
C	Watts	cal/cm sec		
29	0	0.0257	0.0275	0.0246
	13	0.0269	0.0213	0.0199
	52	0.0221	0.0203	0.0162
	117	0.0223	0.0210	--
36	0	0.0514	0.0454	0.0536
	13	0.0526	0.0444	0.0437
	52	0.0545	0.0466	0.0425
	117	0.0537	0.0456	0.0511
44	0	0.0784	0.0713	0.0588
	13	0.0787	0.0651	0.0558
	52	0.0734	0.0664	0.0481
	117	0.0682	0.0571	--

Results of the calculations are shown in Figures 10, 11, and 12. Agreement between measured and computed isotherms was good. A summary of the discrepancies between measured and calculated isotherms is shown in Table 8. Equation 7 underestimates temperatures near the heat source and overestimates temperatures near the soil surface. The heat source was placed 1.5 cm from the right hand side of the box. It heated a portion of the wall of the box near the heat sourc. Back radiation may have increased the temperatures of the soil around the heat source so that higher measured temperatures were obtained. Temperatures were overestimated near the lower end of the soil column. The measured temperatures converged to the air temperature at this boundary.

Figures 10, 11, and 12 show that the measured temperatures near the soil surface were always a few degrees lower than the calculated ones where a constant air temperature of 22$\pm$ 1C was imposed on the soil surface.

Table 8. Difference between measured temperatures and temperatures calculated according to the Kendrick and Havens (1973) model calculated-measured at the indicated grid points in C (top) and in percent of the measured value (bottom).

Depth	29C				36C				44C			
	5	15	25	35	5	15	25	35	5	15	25	35
cm	C											
Quincy												
5	-0.1	-0.1	-0.2	-0.3	-0.8	-0.5	0.6	-0.6	0.9	0.9	0.9	0.7
15	-0.2	-0.2	-0.3	-0.5	-0.3	-0.4	-0.8	-1.0	1.2	1.4	1.1	0.7
25	0.0	0.0	-0.2	-0.4	-0.3	-0.3	-0.	-0.8	0.5	2.0	1.6	1.1
35	0.1	0.0	-0.1	-0.3	-0.9	0.2	0.1	-0.5	0.0	2.1	2.5	1.5
45	-0.8	-0.3	-0.3	-0.5	-0.3	0.7	0.2	-0.4	2.5	2.3	2.5	2.0
Cloquato												
5	-0.9	-0.5	-0.6	-0.8	0.7	1.0	1.1	1.2	0.4	0.4	0.2	0.1
15	-0.4	-1.0	-1.2	-1.6	1.8	1.6	1.4	0.9	1.2	1.0	0.6	0.4
25	0.4	-0.3	-0.9	-1.4	2.2	2.7	0.9	1.1	1.7	1.6	1.6	0.8
35	0.6	0.0	-0.6	-1.0	2.5	3.3	2.4	1.3	2.0	2.7	1.9	1.2
45	0.4	-0.3	-0.6	-0.9	2.3	2.9	2.2	1.4	3.6	2.8	2.0	1.2
Chehalis												
5	1.2	1.2	1.0	0.8	1.5	1.8	1.8	1.7	0.8	1.0	0.8	0.6
15	0.7	0.7	0.5	0.2	2.3	2.7	1.9	1.1	1.8	1.0	1.1	0.5
25	1.4	1.0	0.9	0.5	2.7	2.6	2.6	1.5	2.0	2.4	1.8	1.1
35	0.2	1.4	1.1	0.7	1.7	3.1	2.7	1.9	0.9	2.5	2.6	1.7
45	1.8	1.2	1.1	0.9	3.6	3.1	3.0	1.9	3.5	3.2	2.9	1.9
	%											
Quincy												
5	0.4	0.4	0.9	0.9	3.5	2.2	2.7	2.7	3.9	4.0	4.1	3.2
15	0.8	0.8	1.3	2.1	1.2	1.6	3.3	4.2	4.6	5.6	4.6	3.0
25	0.0	0.0	0.8	1.7	1.0	1.1	0.4	3.3	1.6	7.3	6.3	4.5
35	0.4	0.0	0.4	1.3	2.9	0.7	0.4	2.0	0.0	7.4	9.7	6.1
45	3.0	1.2	1.2	2.0	1.1	2.7	0.8	1.6	8.5	8.5	9.8	8.1
Cloquato												
5	4.1	2.3	2.8	3.8	3.1	4.5	5.0	5.6	2.0	2.1	0.7	0.4
15	1.7	4.3	5.2	7.0	7.0	6.6	6.0	3.9	4.9	4.3	2.7	1.7
25	1.6	1.2	3.8	6.0	7.6	10.5	3.7	4.6	5.6	5.9	6.4	3.1
35	2.2	0.0	2.5	4.2	8.1	12.6	9.7	5.3	5.7	10.0	7.5	5.1
45	1.6	1.2	2.5	3.8	8.4	11.3	8.9	5.7	13.2	10.8	8.0	4.9
Chehalis												
5	5.8	5.9	5.0	4.0	6.9	8.5	8.6	8.2	3.6	4.7	3.8	2.8
15	3.0	3.1	2.3	0.9	9.7	11.6	8.3	4.8	7.2	4.2	4.7	2.2
25	5.6	4.2	3.9	2.2	9.6	10.3	10.9	6.4	6.6	9.2	7.3	4.6
35	0.8	5.8	4.8	3.1	5.4	12.0	11.1	8.1	2.6	9.1	10.4	7.1
45	7.4	5.1	4.8	4.0	13.7	12.4	12.5	8.1	12.7	12.4	11.7	7.9

The magnitude these differences decreased with depth, with only small differences existing between calculated and measured values at the 12 cm depth. The lower temperatures at the soil surface were the result of evaporative cooling.

It appears that equation 7 can be used to predict soil temperature isotherms for field conditions. The daily cycle of the soil surface temperature may be approximated with a constant average temperature.

Temperature Variations at the Soil Surface

Temperatures measured as a function of time and depth are shown in Tables 9, 10, and 11. Maximum and minimum temperatures estimated from the measured data as a function of depth are summarized in Table 12 for the three levels of radiation.

The largest amplitudes were obtained for the Cloquato and Chehalis soils. The amplitudes increased with higher heat flux density for all soils.

The temperature variation as a function of time and depth is given by van Wijk and de Vries (1963) as follows:

$$T_{(y,t)} = T_{ay} + A_0 \exp(-y/D) \sin (\omega t + \phi_0 - y/D), \qquad (8)$$

where $T_{(y,t)}$ is the temperature (C) at any depth y (cm) at time t (sec), T_{ay} is average temperature at any depth in the soil column during a period (C), A_0 is the surface amplitude (C), D is the damping depth (cm), ω is the angular frequence ($2\pi\nu$ where ν is the frequency of temperature variation) equal to 7.27×10^{-5} sec^{-1} for a diurnal variation, and ϕ_0 is the phase constant.

The phase constant can be calculated from

$$\omega t_1 + \phi_0 - \frac{y}{D} = \frac{\pi}{2}, \qquad (9)$$

where t_1 is the time at which the maximum temperature at a depth y occurs. Equation 8 describes the temperature variation about an average temperature at any depth. The average temperature at any depth can be written as follows:

$$T_{ay} = T_y + A_0 \exp(-y/D). \qquad (10)$$

Substitution of Equation 10 in the Equation 8 yields,

$$T_{(y,t)} = T_y + A_0[\exp(-y/D)]\{1 + \sin (\omega t + \phi_0 - y/D)\}, \qquad (11)$$

Table 9. Measured and calculated soil temperatures at the indicated depths for Quincy soil with a source temperature of 29 C at three radiation loads.

Time	1.0 cm		3.0 cm		6.0 cm		12.0 cm	
	meas.	calc.	meas.	calc.	meas.	calc.	meas.	calc.
13 Watts	C	C	C	C	C	C	C	C
4:00	21.5	21.5	21.0	21.7	22.6	22.0	23.3	22.7
8:00	21.6	21.7	21.5	21.9	22.7	22.1	23.3	22.7
12:00	21.9	22.3	22.0	22.4	22.8	22.5	23.4	22.9
16:00	22.6	22.5	22.5	22.6	23.1	22.7	23.6	23.1
20:00	21.8	22.3	21.7	22.4	22.9	22.5	23.6	23.4
24:00	----	21.7	----	21.9	----	22.3	----	22.9
52 Watts								
4:00	20.9	21.5	21.1	21.7	22.0	22.2	23.4	23.0
8:00	20.8	22.9	20.5	22.5	21.9	22.4	22.8	22.7
12:00	23.6	25.6	22.8	24.8	22.9	24.0	23.0	23.3
16:00	25.2	26.8	25.4	26.2	24.9	25.3	24.3	24.3
20:00	23.3	25.3	23.6	25.4	24.5	25.1	24.8	24.7
24:00	21.6	22.7	21.7	23.2	22.8	23.5	23.7	24.1
117 Watts								
4:00	20.4	20.5	20.4	20.8	21.9	21.7	22.8	22.2
8:00	20.9	23.5	20.8	22.4	21.7	22.5	22.8	21.8
12:00	26.7	29.8	25.9	27.9	23.8	26.3	23.1	23.4
16:00	32.6	33.0	32.4	30.9	29.1	29.2	26.4	25.5
20:00	24.8	29.9	26.0	29.4	26.4	28.3	26.8	25.4
24:00	21.3	23.7	21.6	24.9	23.0	24.6	24.3	24.2

Table 10. Measured and calculated soil temperatures at the indicated depths for Cloquato soil with a source temperature of 29 C at three radiation loads.

Time	1.0 cm		3.0 cm		6.0 cm		12.0 cm	
	meas.	calc.	meas.	calc.	meas.	calc.	meas.	calc.
13 Watts	C	C	C	C	C	C	C	C
4:00	19.0	18.6	19.1	19.1	21.1	19.8	22.2	21.0
8:00	19.6	19.0	19.4	19.3	21.0	19.5	21.9	20.5
12:00	19.7	20.1	19.8	20.3	21.2	20.2	22.1	20.7
16:00	21.0	21.0	21.0	21.2	22.0	21.1	22.6	21.4
20:00	20.4	20.7	20.7	21.0	22.1	21.4	22.9	21.9
24:00	20.0	19.5	20.3	19.9	21.8	20.7	22.7	21.7
52 Watts								
4:00	19.6	19.8	20.0	20.2	22.1	20.9	23.0	22.0
8:00	19.9	20.2	20.2	20.4	21.8	20.6	22.7	21.5
12:00	20.1	22.7	20.4	22.5	22.0	21.8	22.8	21.9
16:00	24.3	24.8	23.9	24.2	23.4	23.4	23.4	22.8
20:00	22.6	24.4	23.0	24.0	24.1	23.7	24.3	23.3
24:00	21.1	21.7	21.3	22.0	23.0	22.4	23.9	22.9
117 Watts								
4:00	22.0	21.2	22.0	21.5	23.9	22.5	24.4	23.3
8:00	22.1	22.4	21.7	22.1	23.3	21.7	23.6	22.5
12:00	23.0	30.0	22.7	27.4	23.9	24.4	24.0	23.1
16:00	35.5	36.4	32.5	32.3	27.8	27.9	25.1	24.5
20:00	29.7	35.2	30.0	31.7	30.0	28.6	26.4	25.3
24:00	24.2	27.6	24.1	26.4	26.0	26.0	26.1	24.8

Table 11. Measured and calculated soil temperatures at the indicated depths for Chehalis soil with a source temperature of 29 C at three radiation loads.

Time	1.0 cm		3.0 cm		6.0 cm		12.0 cm	
	meas.	calc.	meas.	calc.	meas.	calc.	meas.	calc.
13 Watts	C	C	C	C	C	C	C	C
4:00	18.7	19.7	19.2	20.0	21.4	20.3	22.2	21.3
8:00	20.4	20.7	20.8	21.0	21.6	20.6	22.4	21.3
12:00	21.2	22.4	21.4	22.7	21.8	21.5	22.7	21.7
16:00	21.7	23.1	22.6	23.4	22.6	22.2	22.9	22.1
20:00	20.9	22.1	21.4	22.4	22.4	21.9	22.9	22.2
24:00	20.6	27.4	20.7	20.7	22.3	21.0	22.5	21.7
52 Watts								
4:00	22.3	21.1	22.7	21.4	23.8	21.2	24.2	23.1
8:00	22.5	22.8	22.7	22.5	23.6	21.9	24.1	22.7
12:00	24.5	26.3	24.0	25.2	24.0	23.6	24.1	23.2
16:00	29.0	28.0	28.4	26.8	26.4	25.2	25.4	24.1
20:00	25.1	26.3	26.1	25.9	26.4	25.2	25.9	24.5
24:00	22.8	22.8	23.0	23.0	24.6	23.6	24.8	24.1
117 Watts								
4:00	23.9	22.6	24.5	23.0	25.5	23.6	26.1	25.0
8:00	23.3	24.7	23.6	24.4	24.7	23.6	25.2	24.1
12:00	27.2	31.5	25.6	29.5	24.9	26.8	24.8	25.0
16:00	36.7	35.1	----	33.3	30.1	30.0	----	26.8
20:00	39.7	34.1	31.1	31.9	30.7	30.1	28.4	27.7
24:00	24.9	27.3	25.4	26.8	26.7	26.8	27.0	26.8

Table 12. Maximum and minimum temperatures, amplitudes, and time lags as a function of depth for Quincy, Cloquato, and Chehalis soils with a heat source temperature of 29 C at three surface heat loads.

Soil	Maximum Surface Heat Load	Depth	Temperature		
			Maximum	Minimum	Amplitude
	Watts	cm	°C	°C	°C
Quincy	13	1	22.6	21.5	0.55
		3	22.5	21.0	0.75
		6	23.1	22.6	0.25
		12	23.6	23.2	0.20
	52	1	25.2	20.4	2.40
		3	25.4	20.5	2.45
		6	25.4	21.7	2.85
		12	24.8	22.8	1.00
	117	1	32.6	20.4	6.10
		3	31.4	20.4	5.50
		6	29.2	21.7	3.75
		12	27.2	22.7	2.25
Cloquato	13	1	21.0	18.6	1.20
		3	21.1	18.5	1.30
		6	22.1	20.6	0.75
		12	22.9	21.4	0.75
	52	1	24.8	19.6	2.60
		3	24.6	19.6	2.50
		6	24.4	21.6	1.40
		12	24.3	22.5	0.90
	117	1	37.3	21.7	7.80
		3	34.4	21.4	6.50
		6	30.3	23.3	3.50
		12	27.1	23.6	1.75
Chehalis	13	1	22.2	18.7	1.75
		3	22.6	19.2	1.70
		6	22.6	21.1	0.75
		12	22.9	22.0	0.45
	52	1	29.0	22.1	3.45
		3	28.4	22.4	3.00
		6	26.8	23.5	1.65
		12	25.9	24.0	0.95
	117	1	36.7	23.3	6.70
		3	35.1	23.6	5.75
		6	31.6	24.6	3.50
		12	28.4	24.8	1.80

where T_y is calculated with equation 7.

Equations 9 and 10 were used to calculate the soil temperature variation as a function of time and depth. A period of 24 hours was used in these calculations. The damping depth, D, is related to the thermal properties of the medium and the angular frequency by the equation

$$D = \left(\frac{2\lambda}{C\omega}\right)^{\frac{1}{2}}. \qquad (12)$$

The surface amplitudes A_0 used in Equation 11 were calculated from the equation

$$A_z = A_0 e^{-z/D}, \qquad (13)$$

were A_z is the amplitude (C) at any depth. A_z values for each soil and radiation intensity are shown in Table 13. The plot of ln A_z versus depth in cm, gives a straight line with a negative slope, which is the reciprocal of the damping depth. The intercept of this straight line with the ln A_z axis is ln A_0. The results of these operations are shown in Table 13. Results of the calculations of the soil temperatures as a function of time and depth in the three soils at a heat source temperature of 29 C and at different radiation intensities are shown in Tables 9, 10, and 11. Observed temperatures were lower than calculated near the soil surface for all samples. Differences at the 1 cm depth were time dependent in all samples. The differences were higher at the time of rising and falling temperature. This is due to the fact that the rate of energy supply at the surface did not follow a perfect sinusoidal fluctuation while a sinusoidal model was used.

Conclusions

The effect of heat source temperature on soil surface temperature is small in moist soils. Heat source temperatures of 29 and 44 C increased the surface temperatures only 2 and 4 C respectively. The surface temperature is mainly influenced by air temperature and not by heat source temperature. The proposed system of soil warming can not be expected to improve soil surface temperatures much to improve conditions for seed germination in the spring. Other means for increasing the temperature of the soil surface, like petroleum mulching (Kowsar et al., 1969) must be used.

A portion of the soil column with heat source temperatures of 36 and 44 C had higher temperatures than the optimum range for plant growth. High soil temperatures in the root zone can be prevented by placing the heat sources deeper and farther apart.

Table 13. Surface amplitudes and damping depths as a function of surface heat load for Quincy, Cloquato, and Chehalis soils with a heat source temperature of 29 C.

Soil	Surface Heat Load	Surface Amplitude	Damping Depth
	Watts	°C	cm
Quincy	13	0.6	14.1
	52	2.9	11.8
	117	6.9	10.6
Cloquato	13	1.3	9.2
	52	3.0	9.9
	117	9.5	6.4
Chehalis	13	1.9	8.3
	52	3.9	8.2
	117	7.7	8.2

Energy Dissipation Rates

The duration of the time periods during which the heat source was energized were recorded with a Rustrak event recorder. Rates of energy input were calculated from these measurements. Results of energy input measurements and experimental conditions are summarized in Table 14. These rates increased with heat source temperature for all three soils. The energy dissipation rates were highest in the Quincy soil and lowest in the Chehalis soil for each temperature treatment.

The energy dissipation rates were plotted as a function of the difference between the average temperature of the heat source and the average temperature at the 1 cm depth (Figure 13). For the purpose of this analysis the daily average temperature at the 1 cm depth was used for the experiments with fluctuating surface temperatures. The correlation between the energy dissipation rates and the temperature differences was determined by using a least square method to fit the equation:

$$F = A + B(T_s - T_{su}), \qquad (14)$$

where F is the rate of energy loss ($cal/cm^2 min$), T_s is the heat source temperature (C), T_{su} is the average soil temperature at 1 cm (C), and A and B are constants. The solid lines shown in Figure 13 were calculated using Equation (14) and values of A and B shown in Table 15.

Table 14. Heat source temperatures, soil surface temperatures, and energy dissipation rates for Quincy, Cloquato, and Chehalis soils for the indicated surface radiation loads.

Surface Heat Load	Heat Source Temperature			Average Temperature at depth of 1 cm			Energy Dissipation Rate		
	Quincy	Cloquato	Chehalis	Quincy	Cloquato	Chehalis	Quincy	Cloquato	Chehalis
Watts	C	C	C	C	C	C	---------cal/cm^{2}min----------		
0	29.3	28.2	29.0	21.5	18.8	19.8	0.0385	0.0412	0.0368
13	29.3	28.0	28.4	21.9	19.8	20.8	0.0404	0.0320	0.0299
52	29.0	28.2	28.9	22.5	21.3	24.4	0.0332	0.0305	0.0243
117	29.1	28.3	29.1	24.4	26.2	27.8	0.0335	0.0318	--
0	37.2	35.2	36.4	20.5	20.7	20.2	0.0770	0.0681	0.0804
13	36.7	35.1	35.8	20.0	20.9	21.0	0.0789	0.0666	0.0655
52	36.8	34.8	35.5	22.7	22.0	21.8	0.0818	0.702	0.0637
117	36.4	34.7	35.2	27.0	23.8	24.2	0.0810	0.0684	0.0768
0	43.3	46.9	46.9	21.2	21.1	20.1	0.1176	0.1070	0.0881
13	42.5	46.1	46.3	21.5	21.4	20.7	0.1180	0.0976	0.0887
52	42.8	45.6	42.7	23.4	21.8	22.3	0.1101	0.0996	0.0722
117	42.9	45.9	--	27.1	24.3	--	0.1023	0.0856	--

Table 15. Parameters of regression models obtained from data in Table 14, correlation coefficients, and calculated thermal conductivities for Quincy, Cloquato, and Chehalis soils.

Soil	Intercept A	Slope B	Correlation Coefficient R	Slope of Line Through Origin, B^1	Calculated Thermal Conductivities
	$cal/cm^2 min$	$cal/cm^2 min\ C$		$cal/cm^2 min\ C$	cal/cm min C
Quincy	0.00204[a]	0.00531	0.97**	0.00543	0.17
Cloquato	0.00499[b]	0.00390	0.99**	0.00417	0.13
Chehalis	0.01395[b]	0.00287	0.97**	0.00360	0.11

**Statistically significant at the 1 percent level.

[a]Statistically negligible at the 1 and 5 percent level.

[b]Statistically negligible at the 1 percent level only.

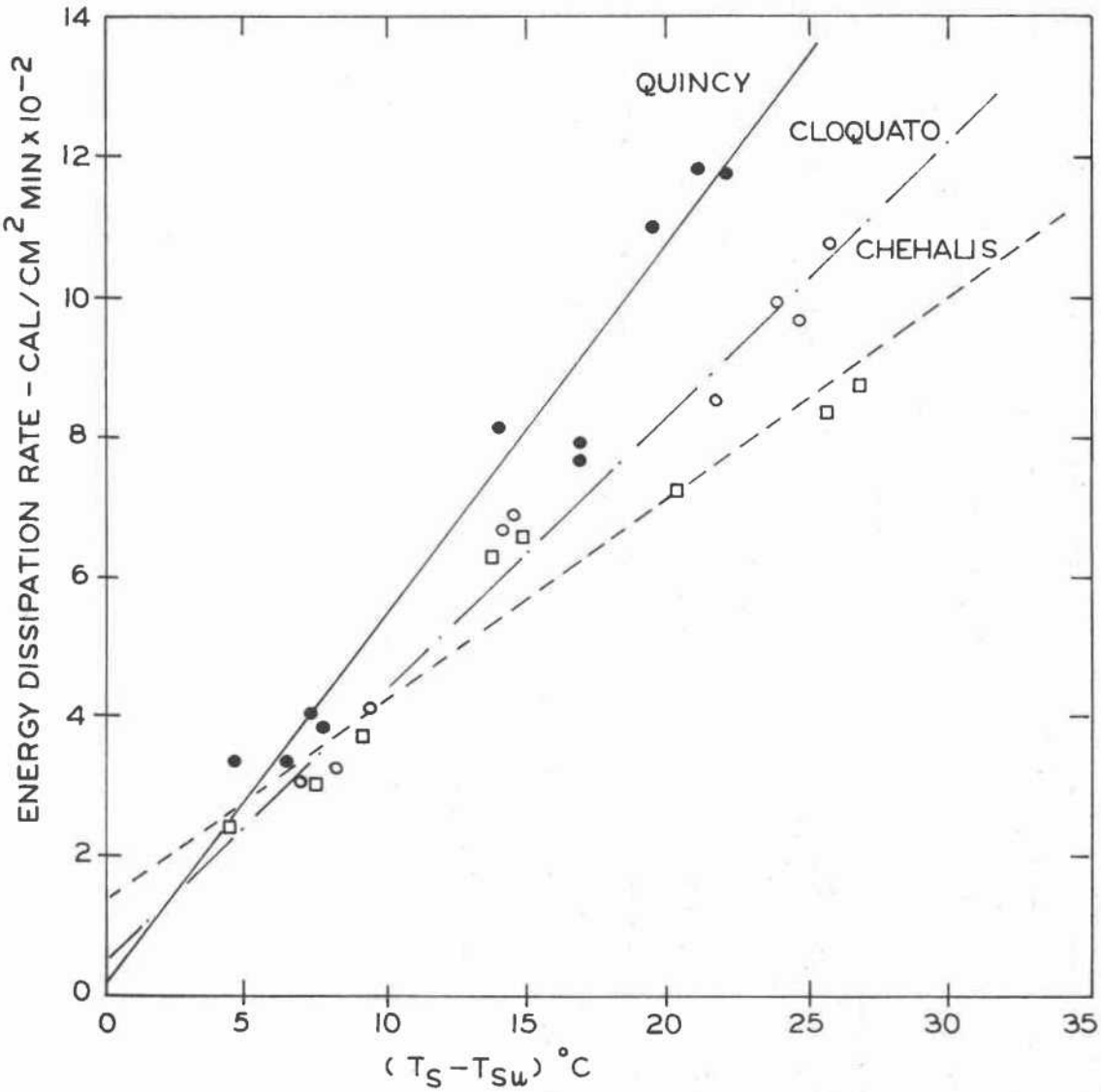

Figure 13. Mean daily energy dissipation rates as a function of the difference between mean daily heat source temperature and mean daily soil temperature at a depth of 1 cm.

The value of B (slope of lines) is determined in part by the thermal conductivity of the soil. It was highest for Quincy soil and lowest for Chehalis soil. The regression lines should pass through the origin. This result was not obtained. The regression lines intercept the ordinate at 0.00204, 0.00499, and 0.01395 for Quincy, Cloquato, and Chehalis soils, respectively. This deviation may have been caused by several factors which include: (i) experimental error, (ii) non-steady-state conditions, (iii) leakage of energy from the heat source or from the lower end of the soil column, (iv) thermal inertia due to poor contact between electrical elements and the cover of the heat source, so that additional energy was required to raise the temperature of the electrical element to overcome this contact resistance, (v) underestimation of the differences between heat source and soil surface temperatures resulting from the use of the temperature at a depth of 1 cm. Furthermore, data points in Figure 13 were obtained from different experimental soil columns with small differences in the water content and hence thermal conductivity.

The possibility of energy leakage from the lower end of the soil column was investigated. Temperature gradients were calculated from temperature measurements obtained with thermistors placed at the lower acrylic wall of the soil container. Temperature gradients which caused heat leakage occurred over areas near the side of the box below the heat source. Total rate of energy leakage was calculated by multiplying the temperature gradients, energy leakage area, and thermal conductivity of the acrylic material. The rate of energy loss was found to be less than 5 percent of the total heat input at the heat source at a 44 C heat source temperature. This percentage would be less for lower heat source temperatures. The rate of energy loss at the lower end of the column was low because of the low thermal conductivity of the acrylic material. This material has a thermal conductivity of about 0.45 mcal/cm sec C which is less than that of air dry soil. The thermal conductivity of moist soil is more than 5 times that of the acrylic plastic.

A statistical analysis showed that the value of the intercept of Equation 14 with the ordinate, did not differ significantly from zero. Hence, using regression analysis, straight lines were fit to the data in Figure 13 which went through the origin according to the equation

$$F = B^1 \Delta T, \tag{15}$$

stating that the rate of energy loss, F, is proportional to the difference in temperature at the heat source and soil surface, ΔT. The values of B^1 are shown in Table 15.

Equation 15 can be used to describe the rate of energy loss in soil warming systems. According to Kendrick and Havens (1973).

$$B^1 = \frac{2\pi\lambda}{\ln\left(\frac{2h-r}{r}\right) + \sum_{n=1}^{N} \ln\left[\frac{(ns)^2+(2h-r)^2}{(ns)^2+r^2}\right]} \tag{16}$$

Using the design parameters, s = 77 cm, h = 32 cm, r = 0.5 cm and N = 0 (for the laboratory column), the value $B^1 = 0.033\lambda$ was obtained.

$$B^1 = 0.033\lambda$$

Thermal conductivities were calculated by substituting values of B^1 from Table 15. Calculated values of λ are shown in Table 15. Results are in agreement with the measured values at the same water content.

Equation 15 can be written as

$$F = G\lambda\Delta T, \tag{17}$$

where

$$G = \frac{2\pi}{\ln\left(\frac{2h-r}{r}\right) + \sum_{n=1}^{N} \ln\left(\frac{(ns)^2+(2h-r)^2}{(ns)^2+r^2}\right)} \tag{18}$$

The parameter G can be called the "shape factor" since it depends only on the depth, spacing, and the radius of the heat source. The solution of Equation (18) is independent of N for values greater than 6. Depth and spacing influence the "shape factor", G, more than the radius of the heat source. The G value increases 43 percent by a ten-fold increase in the heat source radius at a depth and spacing of 30 and 30 cm, respectively. A five-fold increase in spacing (from 30 to 150 cm) with a heat source radius of 0.5 cm increased G values only 31 percent. The G value increases 29.5 percent by increasing the depth six-fold (from 30 cm to 180 cm) at a spacing of 30 cm and heat source radius of 0.5 cm. At a given heat source radius, spacing has the greatest influence on the "shape factor" at the shallow depths. At a heat source radius of 1.0 cm an increase in spacing from 60 cm to 120 cm decreases G values 67 and 37 percent at 30 and 150 cm depths.

Land Area Requiremtns

Thermal conductivity values shown in Table 15 and a ΔT value of 20 C were used to calculate the total land area required to dissipate the waste energy generated by a 1000 MWe power plant with an efficiency of 34 percent. It was found that 2841, 3714, and 4390 hectares would be required for Quincy, Cloquato and Chehalis soils, respectively, with the heat sources buried 32 cm deep and 77 cm apart. A temperature change along the pipes was not taken into account in these calculations.

The shape factor is constant for a given installation, but values, of ΔT and λ depend on the physical properties of the soil, source temperature, and climatological factors. Energy dissipation rates may therefore be expected to vary seasonally. Irrigation and precipitation also

cause seasonal changes. The rate of energy loss is more sensitive to the thermal conductivity and ΔT than to the depth, spacing, and radius of the heat source. In the Willamette Valley, Oregon high rates of energy loss occur during the cold season when the air temperature is low and the soil water content is high due to high precipitation and low evaporation rates. High soil water content corresponds to high soil thermal conductivity. Temperature differences between the soil surface and the heat source are low during the warm season and the soil water content at that time is also low due to lack of rainfall. These conditions result in low rates of energy loss during the summer. Raising the heat source temperature increases ΔT and hence the rate of heat dissipation for a given climatological condition. The value of ΔT increases 78, and 167 percent by increasing the heat source temperature from 29 to 36 and 44 C respectively with a soil surface temperature of 20 C. Such an increase in ΔT increases the heat dissipation rate or decreases the total land area required to dissipate a given amount of waste heat. Results obtained by Rykbost (1973) indicate that a three-fold seasonal variation in energy dissipation rate occurred in the Willamette Valley, Oregon with a minimum in the late summer and a maximum in the late winter.

Daily Heat Flux Cycle at the Soil Surface

Heat flux at the soil surface of the columns with sinusoidal radiation loads can be analyzed using a model formulated by Gardner and Hanks (1966). The heat absorbed by a layer of thickness, Δy, is used to evaporate water and raise the temperature of the material in this layer. The total heat flux ($cal/cm^2 min$), ΔH, into a layer of thickness, Δy, can be written as

$$\Delta H = \frac{EL + C\Delta T\Delta y}{\Delta t} \qquad (19)$$

or

$$\Delta H = L \frac{\Delta\theta}{\Delta t} \Delta y + C \frac{\Delta T}{\Delta t} \Delta y, \qquad (20)$$

where E is the evaporation ($cm = \Delta\theta \cdot \Delta y$), L is the heat of vaporization of water ($580 cal/cm^3$), C is the heat capacity of layer Δy, including water ($cal/cm^3 C$), ΔT is the change in temperature in time interval t(C), Δy is the thickness of the layer (cm), Δt is the time interval (min), and $\Delta\theta$ is the change in water content (cm^3/cm^3).

The first member of the right side of Equation 20 represents the heat used for evaporation and the second member the heat used for increasing the temperature of the material. When the soil water content does not change (dry condition or fixed soil water content), $\Delta\theta = 0$ and Equation 20 becomes:

$$\Delta H = C\frac{\Delta T}{\Delta t} \Delta y, \qquad (21)$$

which is the sensible heat flux at the soil surface.

The soil water content remained unchanged during each experiment. Therefore, Equation 21 can be used to calculate the sensible heat flux at the soil surface for the experiments with sinosoidal heat loads. These calculations were made by dividing the column into layers varying in thickness, Δy. The temperatures of the layer $T_{\Delta y}$, is given by:

$$T_{\Delta y} = T_{(y_1+y_2)/2} \qquad (22)$$

For selected times t, the sensible heat flux was calculated using Equations 21 and 22. The heat capacity values needed in Equation 21 are given by

$$C = x_s C_s + x_w C_w + x_a C_a \quad (Cal/cm^3 C), \qquad (23)$$

where x is the volume fraction, C is the heat capacity, and the subscripts s, w, and a denote the solid, liquid, and gas phases. Since C_a is very small, the term $x_a C_a$ is usually neglected. The heat capacities of the soils were calculated using heat capacity values of 0.68, 0.56, 0.56, and 1.0 $cal/cm^3 C$ for the soil particles of the Quincy, Cloquato, and Chehalis soils, and water, respectively.

Results of the calculations are shown in Figures 14, 15, and 16. These figures show the sensible heat flux for Quincy, Cloquato and Chehalis soils as a function of time for the 13, 52, and 117 watts surface heat loads. The daily total of energy exchanged at the soil surface can be obtained by integrating the area under curves. The results are shown in Table 16. The quantities of sensible heat into and out of the soil columns were not exactly the same. The small discrepancies were caused by errors in estimating the temperatures and heat capacities.

Table 16. Energy exchanged at the surface of soil columns of Quincy, Cloquato, and Chehalis soils with different surface heat loads and a heat source temperature of 29 C.

Soil	Surface Heat Load	Sensible Heat Flux	
		In	Out
	Watts	cal/cm^2	cal/cm^2
Quincy	13	9.7	9.6
	52	27.9	29.4
	117	63.4	64.7
Cloquato	13	9.3	8.7
	52	27.7	28.5
	117	53.4	61.0
Chehalis	13	9.0	9.2
	52	28.5	29.3
	117	52.3	53.6

Conclusions

The energy dissipation rate was highest in Quincy soil and lowest in Chehalis soil at a given temperature difference between heat source and soil surface. When the surface temperature remains constant, the energy dissipation rate increases with heat source temperature. The results obtained showed good agreement with predictions from the theoretical model presented by Kendrick and Havens (1973).

This model was developed for steady state conditions with a constant soil surface temperature. Analysis of this study showed that it can be used to predict the energy dissipation rate for non-steady state conditions with a varying soil surface temperature, by using an average surface temperature. The model appears to be adequate for predicting land area requirements for the dissipation of given amounts of waste energy.

The total land area required to dissipate the waste energy from a 1000 MWe power plant is higher in Chehalis soil than in Quincy soil. The land area required depends more on the thermal conductivity and the difference between heat source and soil surface temperature than on the depth and spacing.

Water Movement

Soil Water Distribution Without Subsurface Irrigation

Quincy soil was subjected to a daily surface irradiation cycle with a maximum rate of heat application of 117 watts for seven consecutive days with the heat source temperature at 29 C. The initial soil water content was 0.30 cm^3/cm^3. Changes in the initial soil water content were measured with a gamma ray attenuation system at four hour intervals at 78 positions in the soil column. The water content distribution existing on the seventh day is shown in Figure 17. The soil water content was lowest in the region near the heat source and increased gradually at points away from it. The water content was 0.04 cm^3/cm^3 near the heat source and 0.14 cm^3/cm^3 at the 5 cm depth. Plants cannot survive in Quincy soil when the water content decreases below 0.10 cm^3/cm^3. The soil water content was less than this critical value over most of the soil column. Soil water depletion also decreased the apparent thermal conductivity of the soil, making the system less efficient as a heat dissipation mechanism.

In a drying soil column with no subsurface heating, the water content is usually highest in the lower region of the column and decreases gradually toward the evaporating site at the soil surface. The soil water content distribution in the column with soil warming was quite different. It was lowest near the heat source and increased toward the soil surface.

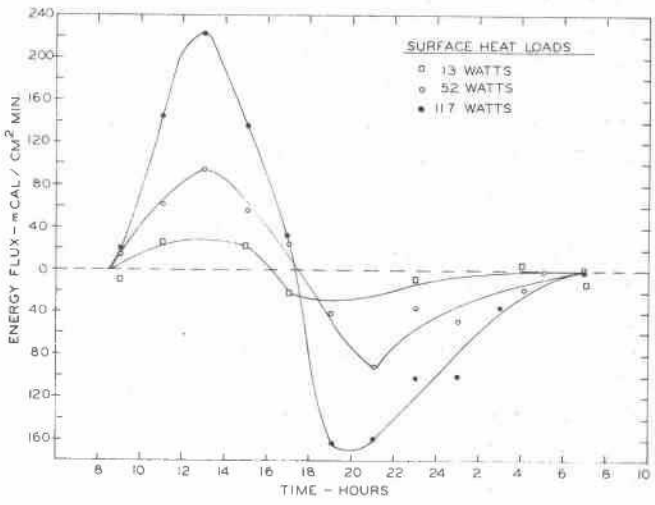

Figure 14. Daily energy flux cycles at the surface of the Quincy soil column at three surface heat loads and a heat source temperature of 29 C.

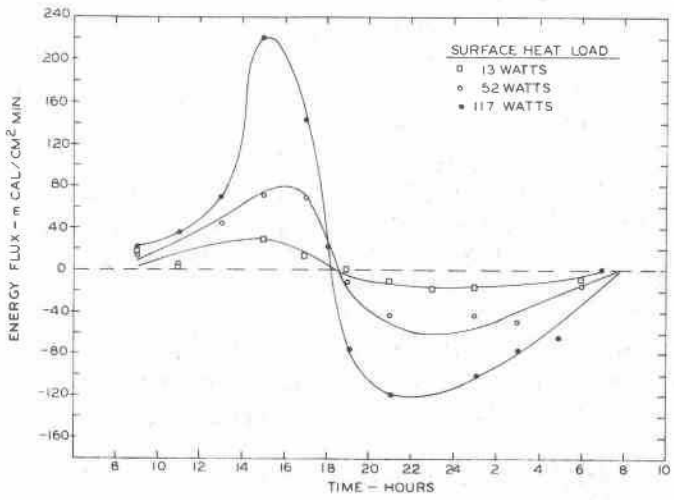

Figure 15. Daily energy flux cycles at the surface of the Cloquato soil column at three surface heat loads and a heat source temperature fo 29 C.

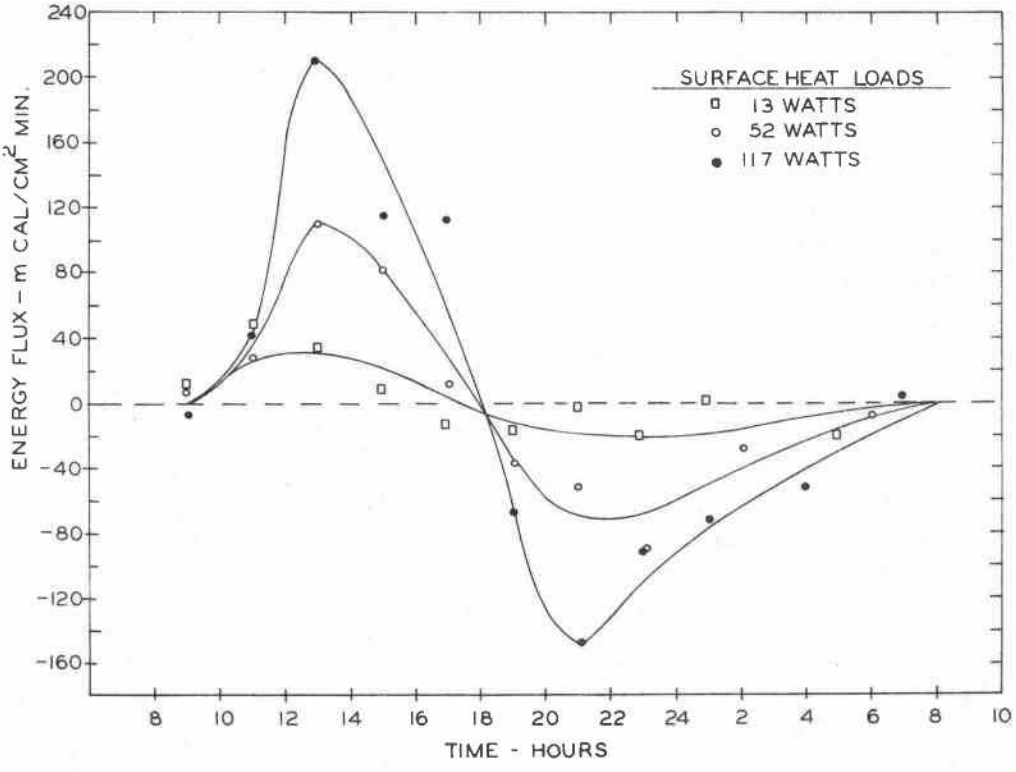

Figure 16. Daily energy flux cycles at the surface of the Chehalis soil column at three surface heat loads and a heat source temperature of 29 C.

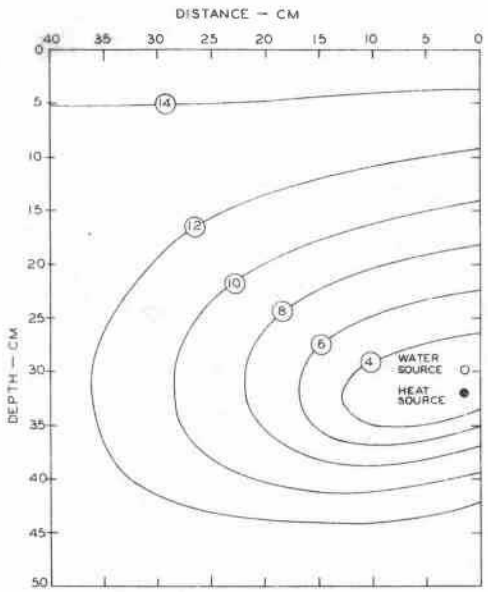

Figure 17.
Distribution of water in a Quincy soil exposed to a heat source temperature of 29 C for seven days at a room temperature of 22 C. Heat was applied at the soil surface as described in the text. The solid lines connect points of the same water content. They are labelled in percent of total volume. The initial water content was .30 cm^3/cm^3. No water was added to the soil surface or near the heat source.

Water depletion near the heat source occurs as a result of mass flow and vapor flow. Surface tension of water decreases with increasing temperature, thus weakening the forces retaining water in the warm regions and causing mass flow toward the cool regions to occur. This mechanism continues until all the capillary water has been removed and the capillary channels are broken. At this water content the hydraulic conductivity of the soil is very low. As the soil water content decreases, large interconnecting air filled pores become available for vapor diffusion. The water vapor pressure in the pore spaces in the high temperature regions exceeds that in the lower temperature regions. Hence water vapor movement is initiated. The vapor pressure gradients are maintained by evaporation in the high temperature regions and condensation in the low temperature regions. The vapor movement and subsequent condensation creates a hydraulic gradient opposite to the temperature gradient. The evaporation may be compensated for by a return flow of water resulting from these hydraulic gradients. If the ratio of hydraulic conductivity to vapor diffusivity is very low, the vapor diffusion process ceases only when all capillary water has been removed from the high temperature region. The water content of the soil next to the heat source at which an equilibrium between evaporation and return mass flow is established depends on the heat source temperature, soil type, and rate of liquid and vapor transfer.

Once most of the capillary water has been removed, the hydraulic conductivity is very low. Consequently, even by ceasing energy input at the heat source, a zone once dried out may take a long time to regain its normal water content (Milne and Mochlinski, 1964; Boersma and Rykbost, 1973). Milne and Mochlinski observed the recovery of water in soil around power transmission lines when water was available to wet the soil profile. They reported that the water content in the wet zone of a sandy soil recovered from about 2.7 percent to about 5.0 percent, but in the dry zone only from about 0.4 percent to 0.6 percent. They also found that the recovery of water in clay soil was negligible.

Soil Water Distribution with Subsurface Irrigation

Soil columns packed with Quincy, Cloquato, and Chehalis soils were subjected to heat source temperatures of 29, 36, and 44 C and daily cycles of surface irradiation with maximum rates of heat application of 0, 13, 52, and 117 watts. The soil water content at a point close to the heat source was monitored continuously with the gamma-ray attenuation system. Water lost by evaporation at the soil surface was replaced from a porous cup located 2 cm above the heat source. Water was applied at 4 hour intervals until midnight. The next supply of water was made at 8:00 a.m. in the morning. Water was applied from the subsurface irrigation system at a rate such that the water content at the point close to the heat source did not decrease below its initial value. Water requirements to prevent drying around the heat source were determined by trial and error. Arbitrary rates of water were initially applied and the water content at a point near the heat source was monitored by the gamma-ray attenuation system at short

time intervals between consecutive water application periods. The accepted water application rate was the one which resulted in a water content variation of less than 0.005 cm^3/cm^3 at this point during the water application intervals.

When a constant rate of water application was obtained for a particular treatment, application was continued at this rate for three days. During this period, several readings of soil water content were taken with the gamma-ray attenuation system at predetermined points in the soil columns. Averages of these readings were calculated and used to plot the soil water distribution in the soil columns. An example is shown in Figure 18. The soil water content decreased toward the soil surface with the steepest gradients immediately above the heat source. Average values of soil water content as a function of depth were calculated for two regions each 5 cm wide. These are shown in Figure 19. The region labeled "over" was above the heat source, while the region labeled "away" was centered 20 cm from the heat source. The water contents of the regions are shown in Tables 17, 18, and 19 as a function of depth, heat source temperature, and rate of surface irradiation. Data for Chehalis soil with heat source temperatures of 44 C were not obtained due to a mechanical failure of the equipment. The soil water content was highest in the regions near the heat and water source and gradually decreased towards the soil surface. The water content near the heat and water sources was nearly the same at all heat source temperatures and surface heat loads. The soil water content of the surface layer was lowest at the highest rate of surface heat application.

Comparison of Figure 17 with Figure 18 shows that it was possible to supply water to the entire column and maintain a high water content with the subsurface irrigation system. The soil water content was near field capacity, which is generally the optimum water content for crop production, throughout the column. The subsurface water application rates that were attained appear adequate to meet the evaporation needs in subsurface heating and irrigation systems for different climatic conditions.

Water Application Rates

Water application rates from the subsurface irrigation system, required to prevent drying around the heat sources for different soils at different heat source temperatures and surface heat loads, are shown in Table 20. Water requirements increased with surface heat load (potential evaporation) and heat source temperature. The water requirements were higher for the Quincy soil than for the Cloquato or Chehalis soils. This is so because the Quincy soil with its coarse texture has a higher hydraulic conductivity than the Cloquato and Chehalis soils.

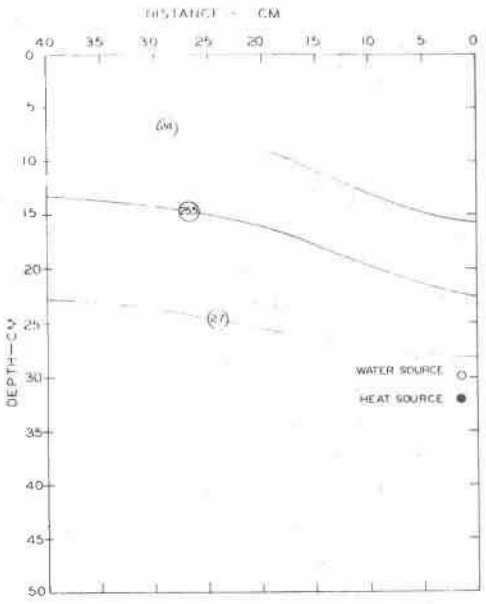

Figurs 18.
Distribution of water in the Quincy soil exposed to a heat source temperature of 36 C with water being added near the heat source at the rate required to maintain a constant water content. The solid lines connect points of the same water content and are labeled in percent of total volume

Figure 19. Positions of the soil column regions identified as "over" and "away" from the heat source.

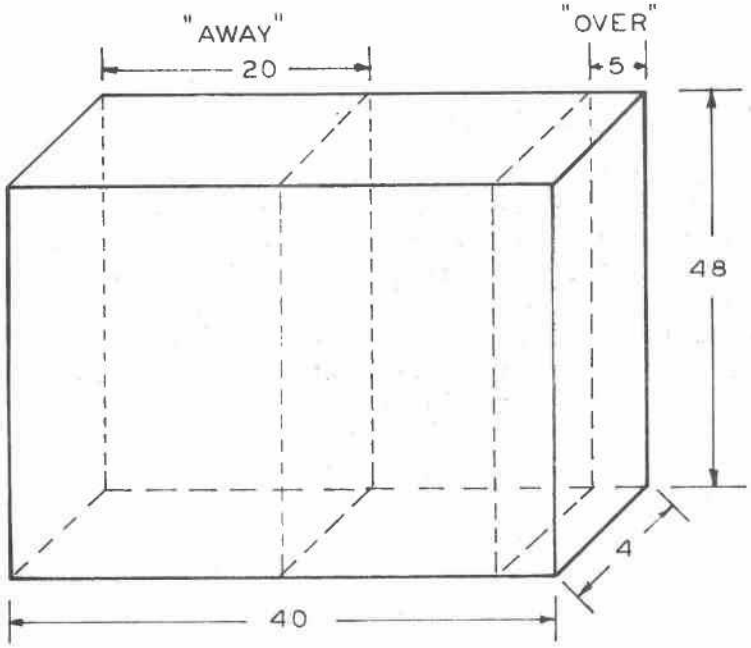

Table 17. Average soil water content "over" and "away from" the heat source as a function of depth in the Quincy soil column at the indicated surface heat loads and heat source temperatures.

Heat Source Temperature	Depth	0 Watts		13 Watts		52 Watts		117 Watts	
		"over"	"away"	"over"	"away"	"over"	"away"	"over"	"away"
C	cm	cm^3/cm^3							
29	1	0.123	0.202	0.128	0.195	0.120	0.194	0.109	0.184
	4	0.190	0.205	0.192	0.195	0.179	0.189	0.161	0.177
	8	0.170	0.174	0.175	0.214	0.177	0.202	0.155	0.180
	15	0.248	0.214	0.245	0.209	0.233	0.227	0.217	0.219
	25	0.280	0.299	0.278	0.300	0.266	0.288	0.248	0.281
	29	0.271	0.300	0.272	0.296	0.257	0.296	0.226	0.288
	33	0.296	0.319	0.295	0.334	0.297	0.324	0.287	0.316
	46	-----	-----	-----	-----	-----	-----	0.289	0.323
36	1	0.170	0.178	0.148	0.166	0.149	0.156	0.122	0.114
	4	0.178	0.180	0.169	0.175	0.160	0.167	0.153	0.152
	8	0.169	0.214	0.158	0.204	0.155	0.193	0.153	0.188
	15	0.206	0.187	0.180	0.232	0.168	0.222	0.165	0.222
	25	0.235	0.236	0.230	0.230	0.233	0.239	0.228	0.237
	29	0.217	0.238	0.225	0.227	0.230	0.240	0.247	0.248
	33	0.241	0.227	0.253	0.234	0.252	0.235	0.253	0.249
	46	0.243	0.252	0.246	0.250	0.243	0.252	0.242	0.252
44	1	0.156	0.156	0.133	0.143	0.107	0.120	0.096	0.113
	4	0.193	0.197	0.186	0.178	0.174	0.182	0.174	0.184
	8	0.229	0.222	0.222	0.212	0.206	0.198	0.206	0.192
	15	0.241	0.282	0.237	0.275	0.217	0.251	0.211	0.241
	25	0.269	0.275	0.285	0.282	0.291	0.278	0.286	0.290
	29	0.253	0.282	0.260	0.295	0.268	0.284	0.271	0.279
	33	0.295	0.286	0.303	0.286	0.300	0.276	0.202	0.282
	46	0.297	0.323	0.297	0.323	0.289	0.305	0.295	0.318

Table 18. Average soil water content "over" and "away from" the heat source as a function of depth in the Cloquato soil column at the indicated surface heat loads and heat source temperatures.

Heat Source Temperature	Depth	0 Watts		13 Watts		52 Watts		117 Watts	
		"over"	"away"	"over"	"away"	"over"	"away"	"over"	"away"
C	cm	cm^3/cm^3							
29	1	0.279	0.248	0.195	0.231	0.153	0.180	0.103	0.133
	4	0.319	0.331	0.275	0.307	0.226	0.254	0.234	0.230
	8	0.463	0.429	0.426	0.398	0.417	0.394	0.397	0.396
	15	0.446	0.433	0.411	0.390	0.390	0.371	0.413	0.411
	25	0.502	0.535	0.485	0.531	0.475	0.527	0.477	0.497
	29	0.501	0.476	0.498	0.459	0.497	0.449	0.485	0.510
	33	0.505	0.535	0.496	0.527	0.501	0.528	0.517	0.541
	46	0.552	0.574	0.565	0.566	0.559	0.557	0.569	0.576
36	1	0.474	0.525	0.470	0.518	0.469	0.501	0.458	0.458
	4	0.462	0.531	0.468	0.527	0.460	0.494	0.457	0.460
	8	0.495	0.474	0.498	0.476	0.485	0.481	0.476	0.473
	15	0.512	0.466	0.508	0.471	0.495	0.466	0.495	0.466
	25	0.448	0.499	0.447	0.502	0.426	0.493	0.446	0.488
	29	0.478	-----	0.479	-----	0.469	-----	0.466	-----
	33	0.468	0.485	0.473	0.487	0.470	0.476	0.468	0.474
	46	0.501	0.471	0.500	0.464	0.481	0.451	0.492	0.485
44	1	0.441	0.451	0.442	0.452	0.441	0.453	0.454	0.454
	4	0.455	0.461	0.467	0.455	0.452	0.450	0.441	0.441
	8	0.453	0.472	0.450	0.477	0.444	0.468	0.438	0.452
	15	0.480	0.491	0.469	0.481	0.474	0.475	0.471	0.471
	25	0.485	0.507	0.490	0.507	0.485	0.503	0.483	0.504
	29	0.485	0.517	0.486	0.515	0.489	0.513	0.495	0.511
	33	0.504	0.516	0.508	0.514	0.511	0.514	0.513	0.515
	46	0.592	0.583	0.534	0.575	0.532	0.570	0.530	0.570

Table 19. Average soil water content "over" and "away from" the heat source as a function of depth in the Chehalis soil column at the indicated surface heat loads and heat source temperatures.

Heat Source Temperature	Depth	0 Watts		13 Watts		52 Watts		117 Watts	
		"over"	"away"	"over"	"away"	"over"	"away"	"over"	"away"
C	cm	cm^3/cm^3							
29	1	0.279	0.283	0.241	0.249	0.243	0.254	0.219	0.222
	4	0.321	0.342	0.307	0.316	0.314	0.327	0.301	0.303
	8	0.366	0.357	0.348	0.339	0.350	0.351	0.339	0.335
	15	0.397	0.352	0.371	0.381	0.384	0.427	0.367	0.411
	25	0.475	0.446	0.449	0.421	0.466	0.435	0.457	0.429
	29	0.467	0.462	0.424	0.432	0.447	0.446	0.430	0.438
	33	0.466	0.455	0.451	0.432	0.462	0.449	0.450	0.435
	46	0.506	0.555	0.504	0.523	0.514	0.543	0.497	0.527
36	1	0.466	0.411	0.432	0.401	0.421	0.401	0.404	0.371
	4	0.431	0.400	0.412	0.396	0.411	0.392	0.395	0.364
	8	0.455	0.416	0.440	0.408	0.433	0.401	0.431	0.390
	15	0.484	0.482	0.469	0.476	0.456	0.472	0.447	0.465
	25	0.496	0.484	0.486	0.475	0.475	0.469	0.461	0.458
	29	0.488	0.474	0.476	0.465	0.474	0.465	0.476	0.469
	33	0.474	0.502	0.468	0.487	0.472	0.480	0.472	0.479
	46	0.529	0.525	0.508	0.513	0.497	0.515	0.480	0.518

Table 20. Water application rate as a function of heat source temperature. surface heat load, and soil type.

Heat Source Temperature	Surface Heat Load	Water Application Rate		
		Quincy	Cloquato	Chehalis
C	Watts	mm/day		
29	0	3.00	2.25	1.50
	13	3.75	3.00	2.63
	52	4.50	3.38	3.00
	117	4.88	3.38	3.19
36	0	3.75	3.00	1.88
	13	4.50	3.75	2.25
	52	4.88	4.13	3.00
	117	5.25	4.50	3.75
44	0	4.50	3.38	2.25
	13	4.88	4.13	3.00
	52	5.63	4.88	3.38
	117	6.00	5.63	3.75

Water Application Rates as a Function of Heat Source Temperature

The water application rates were plotted as a function of the temperature difference between the heat source and the soil surface at different surface heat loads (Figures 20, 21, 22, and 23). These rates were evaluated in terms of potential evaporation rates for the laboratory conditions as measured by a weighing procedure. The soil container was filled with water and subjected to the different radiation cycles used in the experiments. The decrease in weight of the column over a period of time was used to estimate the potential evaporation for the laboratory conditions. These rates were 2.5, 3.3, 5.2 and 10.3 mm/day at sinusoidal surface heat loads with peak rates of 0, 13, 52 and 117 watts, respectively.

The water application rates increased with increasing temperature differences between the heat source and soil surface for all three soils. Straight lines were drawn through the experimental points and the slopes of these lines (mm/day C) were obtained. No statistical procedure was used since adequate data points were not available for each line. The results are given in Table 21. The rates were highest for the Quincy soil and lowest for the Chehalis soil. The rates increased with increasing surface heat load because more energy for evaporating water was available at the soil surface.

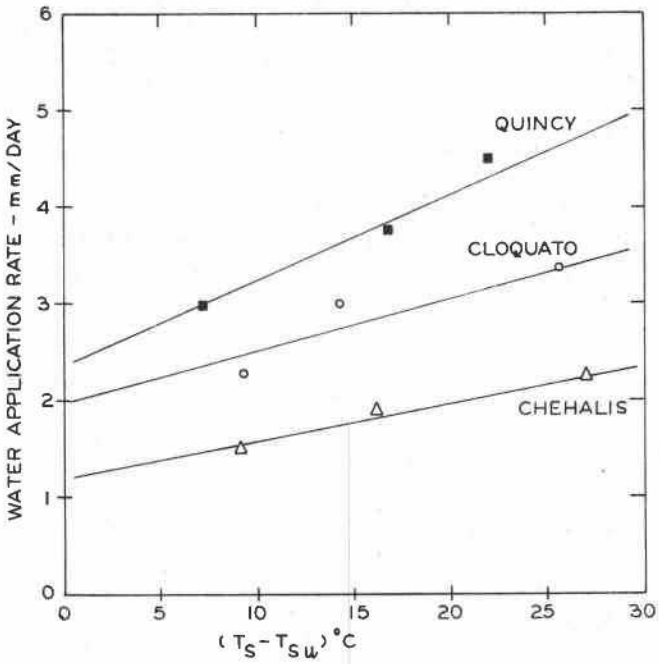

Figure 20. Water use rates as a function of the temperature difference between heat source and soil surface for Quincy, Cloquato, and Chehalis soils with no surface heating.

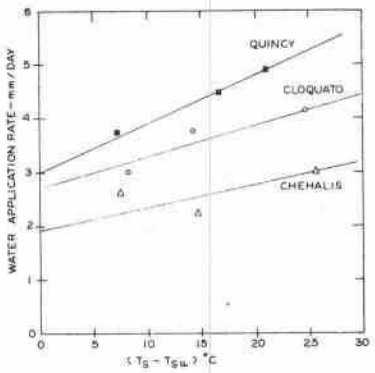

Figure 21. Water use rates as a function of the temperature difference between heat source and soil surface for Quincy, Cloquato, and Chehalis soils at a surface heat load cycle with 13 watts maximum rate.

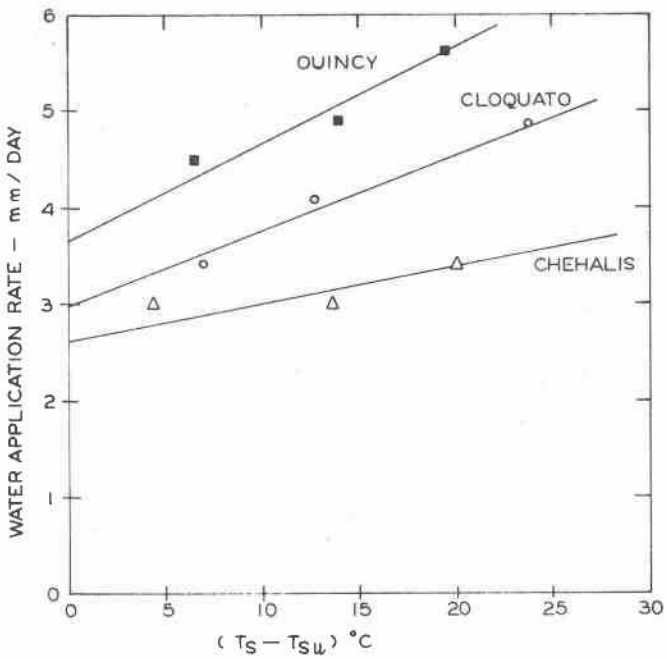

Figure 22. Water use rates as a function of the temperature difference between heat source and soil surface for Quincy, Cloquato, and Chehalis soils at a surface heat load cycle with a 52 watts maximum rate.

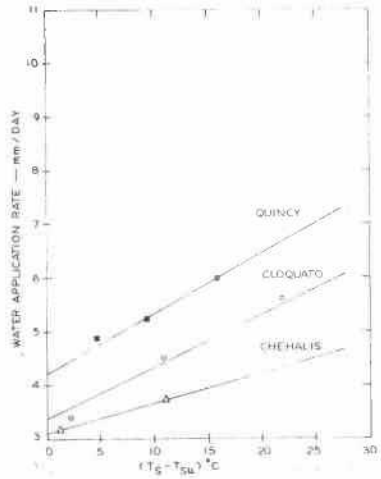

Figure 23. Water use rates as a function of the temperature difference between heat source and soil surface for Quincy, Cloquato, and Chehalis soils at a surface heat load cycle with a 117 watts maximum rate.

Table 21. Rate of increase of water application rate per unit temperature difference between heat source and soil surface at different surface heat loads for Quincy, Cloquato and Chehalis soils.

Surface Heat Load	Water Use Rate/($T_s - T_{su}$)		
	Quincy	Cloquato	Chehalis
Watts	mm/day C		
0	0.075	0.056	0.039
13	0.091	0.059	0.042
52	0.100	0.078	0.040
117	0.113	0.100	0.057

Rates of Water Loss with Subsurface Irrigation but No Subsurface Heating

The rates of water flow that would occur in the soil columns without subsurface heating but with subsurface water application, at the imposed surface heat loads were obtained. The assumption that these rates are proportional to the temperature differences as shown in Figures 20 through 23 was used for this analysis. Temperature differences for the experiments were assumed to be the differences between the daily average temperatures at the soil surface and the average temperature of the column equilibrated at room temperature without subsurface heating. Using these temperature differences, water loss rates were obtained from Figures 20 through 23. Results are shown in Table 22.

Table 22. Rates of water loss from Quincy, Cloquato, and Chehalis soils without subsurface heating, but with subsurface water application.

Surface Heat Load	Measured Evap. Rate	Rate of Water Loss (mm/day)		
		Quincy	Cloquato	Chehalis
Watts	mm/day	mm/day		
0	2.5	2.45	2.05	1.30
13	3.3	3.10	2.80	1.95
52	5.2	3.65	3.00	2.65
117	10.3	3.80	3.20	2.90

The rate of water application without subsurfave heating is highest for the Quincy soil and lowest for the Chehalis soil. The Quincy soil with its higher hydraulic conductivity passes water more easily. The Quincy soil can meet the evaporative demand at surface heat loads of 0 and 13 watts, but not at the higher surface heat loads. The Cloquato and Chehalis soils can not meet these evaporative demands. The hydraulic conductivities of these soils are inadequate to sustain the required flow rates. The soil surface layers of Cloquato and Chehalis soils therefore dried at the higher surface heat loads (Tables 17, 18, and 19).

As the surface heat load increases a layer of soil near the surface dries out. This dry soil layer then becomes a barrier to water movement. Hence, the rate of water loss increased little by increasing the heat load from 52 to 117 watts.

Water Application Rates in Relation to Crop Requirements

Potential evaporation rates and consumptive use values for the Willamette Valley growing season are shown in Table 23. Evaporation in the laboratory, measured by the weighing procedure varied from 7.50 cm/month to 30.90 cm/month. Table 24 shows the consumptive use rates for alfalfa and water application rates achieved with the subsurface irrigation system without subsurface heating and with a heat source temperature of 44 C. The laboratory conditions cover the range of potential evaporation occurring in the Willamette Valley (Table 23). The water supplied by the subsurface irrigation system is not sufficient to meet the highest crop requirements as indicated by the consumptive use for alfalfa when no energy is supplied at the heat source. However, with a heat source temperature of 44 C sufficient water can be supplied to meet the crop requirements in Quincy and Cloquato soils, but not in Chehalis soils.

Table 23. Potential evaporation and consumptive use in the Willamette Valley.

Month	Field* Potential Evaporation	Consumptive* Use For Alfalfa
	cm/month	cm/month
April	6.90	4.03
May	14.27	10.43
June	16.30	13.35
July	24.18	16.23
August	20.19	14.03
September	12.29	9.70
October	6.06	3.68

*Data obtained from Watts et al. (1968).

Table 24. Rates of water loss from heated soil columns compared with consumptive use rates for alfalfa.

Consumptive use for Alfalfa	Heat Source Temp.	Surface Heat Load	Water Application Rate With No Subsurface Heating		
			Quincy	Cloquato	Chehalis
cm/month	C	Watts	cm/month		
10.43		0	7.35	6.21	3.81
13.35		13	9.24	8.34	5.85
16.23		52	10.24	9.00	7.74
14.03		117	11.25	9.21	8.61
			Water Application Rate With Subsurface Heating		
10.43	44	0	13.50	10.14	6.75
13.		13	14.64	12.39	9.00
16.23		52	16.89	14.64	11.14
14.03		117	18.00	16.89	11.25

Subsurface Irrigation near Power Transmission Lines

Drying of the soil near power transmission lines has been observed. Extremely high cable temperatures due to drying of the soil resulted, which caused power transmission failure. Cooling the cables was proposed to eliminate this problem. Maintaining a high soil water content in the soil profile was also recommended by power transmission engineers. The practical value of water cooling for power transmission cables in the ground was examined by Milne and Mochlinski (1964) and Arman et al. (1964). Cooling was done by circulating water in pipes near the cables or by irrigating the soil with a perforated pipe from which water seeped into the soil near the cable right below. A huge volume of water was required for cooling with the piping system as compared with the irrigation method. The space between the circulating pipe and cables still dried out. This led to lower heat exchange rates between the circulating water and the cable. Subsurface irrigation was more efficient in cooling the cables. The function of the water was strictly to maintain a high apparent thermal conductivity in the soil. The amount of water required was small compared with that needed for the removal of heat by the circulation method. It was estimated that the irrigation method of cooling only used 10 percent of the water needed for the circulation method of cooling (Arman et al., 1964).

Conclusions

Surface evaporation and temperature gradient induced water flow depleted the soil water to below the wilting point in only a few days in soils heated with subsurface heat sources. Water depletion was most severe near the heat source.

Subsurface irrigation provides water to the soil to substitute for the water evaporated at the soil surface and migrated from the heat source region under temperature gradients. Subsurface irrigation makes it possible to maintain a soil water content near field capacity. As a result of the higher soil water content, the apparent thermal conductivity in soil with subsurface irrigation is 4 to 6 times greater than that in soil column with no subsurface irrigation for fine textured and coarse textured soils respectively. Hence the total land area required to dissipate a given amount of heat decreases 4 and 6 times in fine textured and coarse textured soils, respectively.

The subsurface irrigation system by itself is not sufficent to supply the consumptive use demand for crops in the Willamette valley. However, when used in conjunction with the subsurface heating system, subsurface irrigation would be a feasible irrigation method.

BIBLIOGRAPHY

Arman, A. N., D. M. Cherry, L. Gosland, and P. M. Hollingsworth. 1964. Influence of soil moisture migration on power rating of cables in H. V. transmission systems. Proc. IEE, 3:1000-1016.

Boersma, L. 1970. Warm water utilization. p. 74-112. In: S. P. Mathur and R. Stewart (ed.). Proceedings of the Conference on the Beneficial Uses of Thermal Discharges. New York State Department of Environmental Conservation. September 17-18. Albany, New York. 227 p.

Boersma, L. and K. A. Rykbost. 1973. Integrated systems for utilizing waste heat from steam electric plants. Journal of Environmental Quality. 2:179-187.

Bunting, A. H. and P. M. Cartwright. 1957. Agronomical aspects of environmental control. p. 96-110. In: J. P. Hudson (ed.). Control of the Plant Environment. Butterworths Scientific Publications, London.

Clarkson, V. A. 1960. Effect of black polyethylene mulch on soil and microclimate temperature and nitrate level. Agronomy Journal 52:307-309.

Chudnorskii, A. F. 1962. Heat transfer in the soil. Published for the National Science Foundation, Washington, D. C., by the Israeli Program for Scientific Translations, Jerusalem, 164 p.

de Vries, D. A. 1952. Thermal conductivity of soil. Mededelingen van de Landbouwhogeschool te Wageningen 52:1-73.

de Vries, D. A. 1963. Thermal properties of soils. p. 210-235. In: W. R. van Wijk (ed.). Physics of plant environment. North-Holland Publishing Company, Amsterdam.

Gardner, H. R. and R. J. Hanks. 1966. Evaluation of the evaporation zone in soil by measurement of heat flux. Soil Science Society of American, Proceedings 30:425-428.

Hanson, E. G. and B. C. Williams. 1968. Subsurface irrigation of cotton. p. 281-292. In: Proceedings of the National Irrigation Drainage Specialty Conference, Phoenix, Arizona. American Society of Civil Engineers.

Hanson, E. G., B. C. Williams, D. D. Fangmier, and D. C. Wilke. 1970 Influence of subsurface irrigation on crop yields and water use. p. D1-D13. In: Proceedings of National Irrigation Symposium, University of Nebraska, Lincoln.

Hooper, F. C. and F. R. Lepper. 1950. Transient heat flow apparatus for the determination of thermal conductivities. Transactions of the American Society of Heating Ventilating Engineers 56:309-324.

Kendrick, J. H. and J. A. Havens. 1973. Heat transfer models for a subsurface, water pipe, soil warming system. Journal of Environmental Quality 2:188-196.

Kowsar, A., L. Boersma, and G. D. Jarman. 1969. Effect of petroleum mulch on soil water content and soil temperature. Soil Science Society of America, Proceedings 33:783-786.

Krischer, O. and H. Rohnalter. 1940. Warmeleitung und Dampfdiffusion in feuchte Gutern. V. D. I. Forschungsheft. 402 p.

Larson, W. E. and W. O. Willis. 1957. Light, soil temperature, soil moisture and alfalfa red clover distribution between corn rows at various spacings and row directions. Agronomy Journal 49:422-426.

Mayer, A. M. and A. Poljakoff-Mayber. 1963. The germination of seeds. Pergamon Press, New York. 236 p.

Milne, A. G. and K. Mochlinski. 1964. Characteristics of soil affecting cable ratings. Proc. IEE, 3:1017-1039.

Nagpal, N. K., and L. Boersma. 1973. Air entrapment as a possible source of error in the use of a cylindrical heat probe. S SSA Proceedings 37:828-833.

Nakshabandi, G. A. and H. Kohnke. 1965. Thermal conductivity and diffusivity of soils as related to moisture tension and other physical properties. Agricultural Meteorology 2:271-279.

Nielsen, K. F. and E. C. Humphries. 1966. Effect of root temperature on growth. Soil and Fertilizers 29:1-7.

Newman, J. S. 1965. Evaluation of subirrigation for crop production. Proceedings of West Texas Water Conference 3:97-103.

Philip, J. R. and D. A de Vries. 1957. Moisture movement in porous materials under temperature gradients. American Geophysical Union, Transactions 38:222-232.

Richards, S. J., R. M. Hagan, and T. M. McCalla. 1952. Soil temperature and plant growth. p. 303-480. In: Byron T. Shaw (ed.). Soil Physical Conditions and Plant Growth. Academic Press, New York.

Rykbost, D. A. 1973. An evaluation of soil warming for increased crop production. Ph. D. thesis. Oregon State University, Corvallis. 275 numb. leaves.

Schleirmacher, von A. 1888. Ueber die Warmeleitung der Gase. Annalen der Physik und Chemie 8:623-646.

Shaw, R. H. and W. F. Buchele. 1957. The effect of the shape of the soil surface profile on soil temperature and moisture. Iowa State College Journal of Science 32:95-104.

Skaggs, R. W. and E. M. Smith. 1967. Apparent thermal conductivity of soil as related to soil porosity. Paper No. 67-114 presented at the Annual Meeting of the ASAE at Saskatoon, Saskatchewan, June 27-30.

Smith, W. O. 1939. Thermal conductivities in moist soils. Soil Science Society of America, Proceedings 4:32-40.

Smith, W. O. and H. G. Byers. 1938. The thermal conductivity of dry soils of certain of the great soil groups. Soil Science Society of America, Proceedings 3:13-19.

van Wijk, W. R. and D. A. de Vries. 1963. Periodic temperature variation in a homogeneous soil. p. 102-143. In: W. R. van Wijk (ed.). Physics of Plant Environment. North-Holland Publishing Company. Amsterdam.

Wadsworth, H. A. 1944. An interpretation of the moisture content-surface force curve for soils. Soil Science 58:225-242.

Watts, D. G., C. R. Dehlinger, J. W. Wolfe, and M. N. Shearer. 1968. Consumptive use and net irrigation requirements for Oregon. Agricultural Experiment Station, Oregon State University, Corvallis. Circular of Information No. 628.

Yarosh, M. M., B. L. Nichols, E. A. Hirst, J. W. Michel, and W. C. Yee. 1972. Agricultural and aquacultural uses of waste heat. ORNAL-4797; US-48-Biology and Medicine; UC-80-Reactor Technology, Oakridge National Laboratory, Oakridge, Tennessee, 54 numb. leaves.

Zetzsche, J. B., Jr. 1964. Evaluation of subirrigation with plastic pipe. American Society of Agricultural Engineers. Paper No. 64-731. St. Joseph, Michigan.

PART II: PHYSIOLOGICAL EFFECTS OF LOW ROOT TEMPERATURES ON THE GROWTH OF CORN SEEDLINGS

E. W. R. Barlow

INTRODUCTION

Low root temperatures limit the rate of water uptake by plants. Lowering the soil temperature decreases the rate of movement of water from the soil to the absorbing surfaces of the roots. The translocation of water through the roots is also decreased. A first consequence of lowering the root temperature is that a water stress is imposed on the shoots. In the following experiments the effect of lowering the root temperature on plant growth was evaluated by measuring the effects on plant water potential and its relation to leaf elongation, photosynthesis, and transpiration.

The mild to moderate phase of water stress which may result from low root temperatures is of interest because even well watered plants commonly experience mild to moderate water stress during the course of a clear sunny day (Turner and Begg, 1973; Carbon, 1973). In spite of the frequency of its occurrence, the effect of mild to moderate water stress on plant growth has not been investigated thoroughly. This may be so because it has not been considered important since mild water stress is not visually obvious and must be detected by plant water potential measurements. Relative water content (relative turgidity) is rather insensitive as a measure of mild water stress because a very small change in water content can correspond to a decrease of several bars in the leaf water potential and a large decrease in the turgor pressure (Hsiao, 1973).

Cell expansion generally is considered to be the parameter most sensitive to a small decrease in plant water potential (Iljin, 1957; Slatyer, 1969; Kramer, 1969; Hsiao, 1973). This hypothesis was first made in 1908 by Balls and later confirmed by Loomis in 1934. More recently the availability of linear variable differential transducers (LVDT's) that enable leaf elongation to be monitored on a minute by minute basis, have enabled Acevedo, Hsiao and Henderson (1971) and Barlow and Boersma (1972) to measure the extremely rapid response of leaf elongation to small changes in plant water potential. The rapid changes in the rate of cell expansion are due to the decrease in cell turgor pressure that occurs when the leaf water potential decreases quickly (Boyer, 1968; Green, 1968; Hsiao, 1973).

Photosynthesis is believed to be less sensitive to water stress than leaf elongation, but this has not been demonstrated conclusively by concurrent measurements on the same plant (Wardlaw, 1969; Boyer, 1970a; Acevedo et al., 1971). Wardlaw (1969) measured both net photosynthesis and leaf elongation, but not water potential, on the 7th and 8th leaves of water stressed Lolium temulentum plants for 3 days. He found that leaf elongation began to decline 10 hours after the onset of mild water stress, while photosynthesis was not affected until 22 hours had elapsed. Boyer (1970a) measured leaf enlargement, net photosynthesis and leaf water potential on different corn plants subjected to the same water stress for a number of days and reported that leaf enlargement decreased sharply at a leaf water potential of -2 to -4 bars and completely stopped at -8 bars whereas net photosynthesis was not affected greatly until the leaf water potential was at least -12 bars. These measurements were made over a 24 hour dark period. The relationship between net photosynthesis and leaf enlargement may not be the same when measured in the light. Finally Acevedo et al. (1971) monitored leaf elongation and net photosynthesis simultaneously on a water stressed corn plant and found elongation to be sharply reduced before photosynthesis was noticeably affected. However Acevedo et al. did not report the leaf water potentials at which the changes in leaf elongation and net photosynthesis took place.

This summary would indicate that a clearer understanding of the relationship between leaf elongation, photosynthesis, and leaf water potential may be gained by simultaneously monitoring these parameters on a plant subjected to a short term water stress such as that normally encountered in the diurnal stress cycle in the field.

If mild stress causes a sharp reduction in the rate of leaf elongation, it is of interest to consider the physiological effects of this reduction on other plant functions, in particular photosynthesis. The most immediate effect of a reduction in the rate of cell expansion is a concurrent decrease in the photosynthate requirement for the biosynthesis of cell walls and protoplasm in the elongating cell. This would result in an accumulation of photosynthate in the sink region and then a decrease in the size of the growth-sink for photosynthate in the elongating leaf.

In other physiological studies, where photosynthate sink size has been manipulated by chemical, environmental or excision treatments, substantial reductions in the photosynthetic rate of the source leaf have resulted (Humphries, 1963; Burt, 1966; Sweet and Wareing, 1966; King, Wardlaw and Evans, 1967). These studies have led to a revival of interest in the source-sink hypothesis (Boussingault, 1868) which postulates that the rate of photosynthate accumulation in the leaf is an internal factor controlling photosynthesis. The evidence for the source-sink hypothesis was reviewed by Neales and Incoll (1968), who concluded that while there is a sound physiological basis for the hypothesis, its biochemical basis suffers from a lack of evidence. Subsequent to this review the photosynthetic carboxylating enzymes of both C_3 and C_4 plants have been shown to have allosteric properties (Preiss and Kosuge, 1970; Coombs, Baldry and Bucke, 1973), thereby suggesting the possibility of photosynthate regulation of

these enzymes. Despite these promising discoveries the mechanism of photosynthate regulation of photosynthesis in the source leaf remains to be demonstrated.

In spite of its unproven biochemical mechanism, the source-sink hypothesis does provide a mechanism whereby mild water stress may decrease photosynthesis indirectly by causing photosynthate to accumulate in the sink leaf and ultimately in the source leaf. Although much of the direct effect of water stress on reducing photosynthesis has been ascribed to stomatal closure (Brix, 1962; Troughton, 1969; Boyer, 1970b; Kreideman and Smart, 1971), there is increasing evidence that changes in intracellular processes also may be important (Slavik, 1965; Boyer and Bowen, 1970; Redshaw and Meidner, 1972). None of the above workers measured photosynthate levels in their plants, but Redshaw and Meidner (1972) did postulate that the intracellular factor affecting photosynthesis in their experiments may have been a photosynthate accumulation. In contrast Boyer and Bowen (1970) concluded that at leaf water potentials below -11 bars the intracellular factor affecting photosynthesis was a reduction in photochemical activity. Other workers have reported no decrease in photochemical activity of plants until water stress became very severe (Nir and Poljakoff-Mayber, 1967; Santarius, 1967). Consequently the mechanism of intracellular inhibition remains an open question with the possibility of photosynthate regulation under conditions of mild stress certainly not excluded. Finally it should be noted that stomatal closure could result from prior changes in intracellular processes; e. g. Meidner (1962) has shown the size of the stomatal aperture in corn leaves to be very sensitive to the internal CO_2 concentration.

In addition to its possible regulation of photosynthesis, a reduction in cell expansion can also affect the relative plant growth rate, in the long term, by affecting the photosynthetic area available for light interception (Slatyer, 1973).

Because of the importance of cell enlargement to the growth of the plant and its susceptability to mild water stress a series of laboratory experiments were conducted to, firstly examine the effects of temperature induced mild water stress on leaf elongation and the effects of leaf elongation on other plant functions, and secondly to examine some of the key axioms of the source-sink hypothesis as applied to water stress. The experiments included the measurement of leaf elongation, net photosynthesis, transpiration rates, and soluble carbohydrate levels of young corn plants subjected to different levels of water stress of varying duration. These experiments were followed by studies of the effect of mild water stress, sufficient to reduce the rate of leaf elongation on the metabolism of both the elongating leaf and the mature leaf supplying the elongating leaf with photosynthate.

SEQUENTIAL EFFECTS OF LOWERING THE ROOT TEMPERATURE ON LEAF ELONGATION, PHOTOSYNTHESIS, AND TRANSPIRATION

Introduction

This experiment involved the simultaneous measurement of leaf elongation, net photosynthesis, and transpiration rates at successively lower values of ψ_c during short stress periods imposed sequentially by lowering the root temperature in small increments during a 12 hour period. These measurements made the evaluation of the relative sensitivity of leaf elongation, photosynthesis, and transpiration to water stress of increasing severity, possible.

The continuous measurement of photosynthesis and transpiration also made it possible to partition the diffusive resistances to carbon dioxide transfer into stomatal and mesophyll components. The theory and methodology of these calculations is described in Appendix I.

The source-sink hypothesis postulates regulation of photosynthesis by a feed-back type mechanism operating at the molecular or organelle level. Therefore, if such an intracellular mechanism is controlling the photosynthetic rate in a water-stressed plant, any decrease in the rate of photosynthesis should be accompanied by a concurrent increase in the mesophyll resistance to carbon dioxide transfer.

In this experiment, 2 to 3 week old corn plants were water stressed for periods up to 10 hours by rapidly lowering the root temperature (Brouwer, 1964). The simultaneous measurements of leaf elongation, photosynthesis, transpiration, and leaf water potential were conducted during this short stress period. Because low root temperatures have been shown to influence the activity of the shoot meristem in young corn plants (Watts, 1972b), the influence of shoot meristem temperature on the above physiological parameters also was evaluated.

Methods and Materials

Description of Apparatus

In order to measure simultaneously the rate of net photosynthesis, transpiration and leaf elongation, and the leaf water potential, it was necessary to construct a carbon assimilation system that incorporated an *in situ* leaf thermocouple psychrometer and a linear variable differential transducer (LVDT).

An open carbon assimilation system operating in the differential mode, similar to that described by Bierhuizen and Slatyer (1964) was constructed. The system is illustrated diagrammatically in Figure 24.

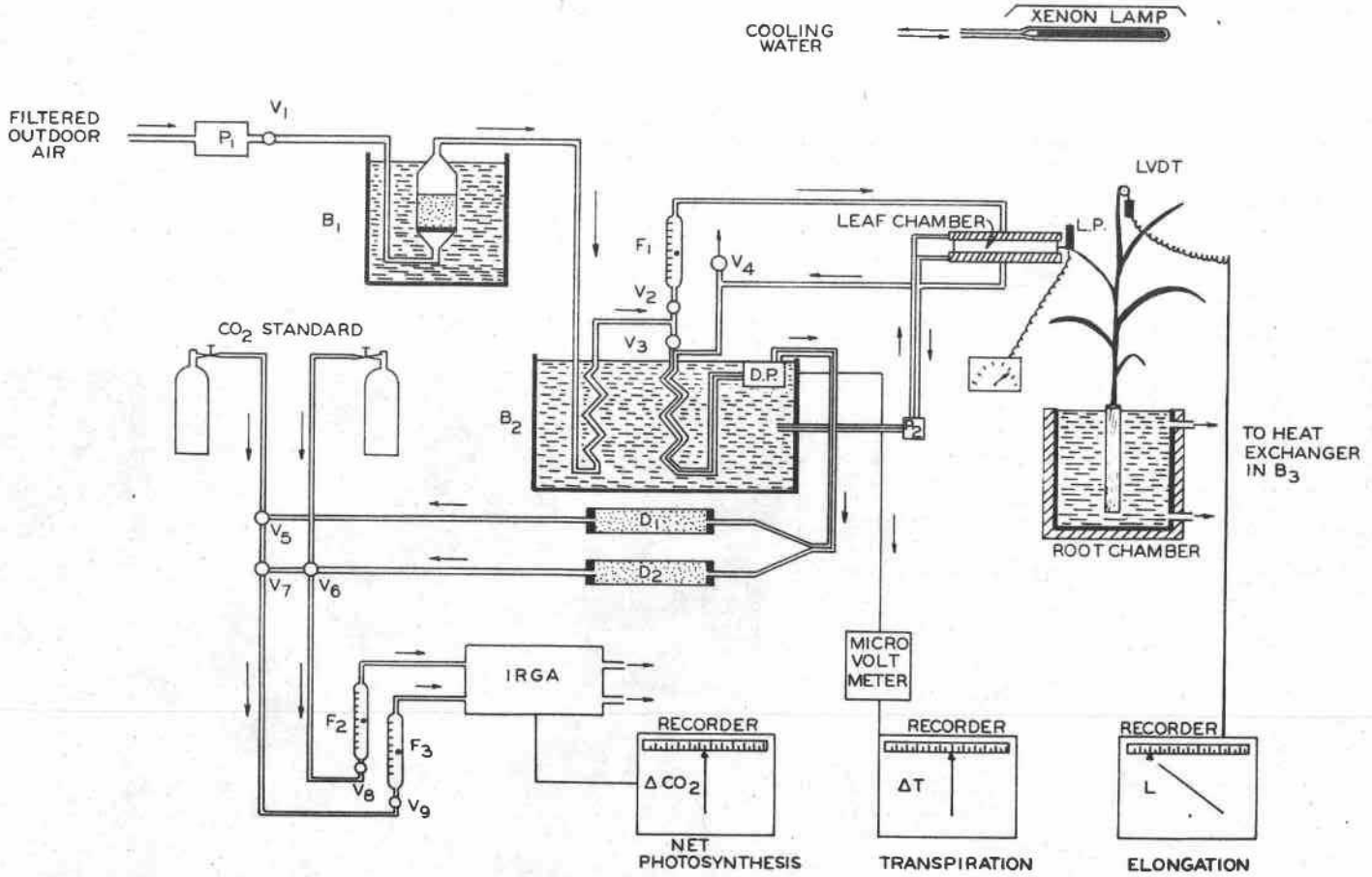

Figure 24. Schematic diagram of the carbon assimilation system used for the experiments. Symbols are explained in the text.

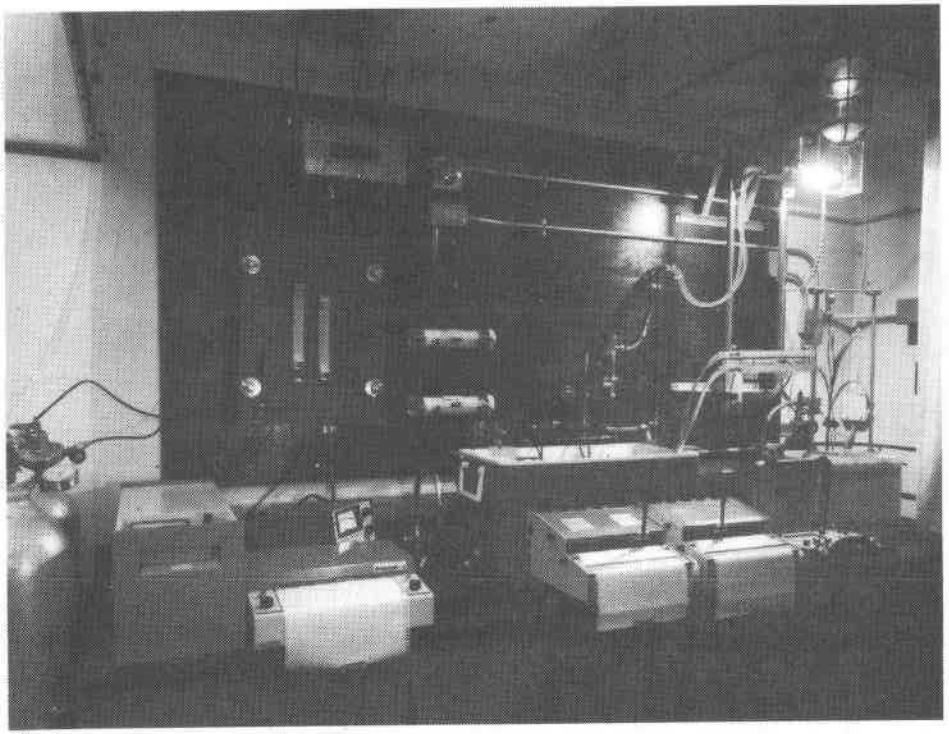

Figure 25. Photograph of the carbon assimilation system in operation.

A photograph of the equipment is shown in Figure 25. The essential features of this system are described below.

Air Control System. The first requirement of the system was to control the CO_2 concentration, water vapor pressure, temperature and flow rate of the air entering the leaf chamber. A near constant CO_2 concentration was attained by pumping atmospheric air through an air inlet filter on top of the building and well removed from any exhaust ducts. The CO_2 concentration of the atmospheric air was free from rapid variations, the maximum rate of change recorded being 2 vpm hour $^{-1}$. Because the infrared gas analyzer (IRGA) was operated in the differential mode using the inlet air as a reference gas, gradual variations less than 2 vpm hour $^{-1}$ did not affect the precision of the CO_2 measurement.

The flow rate of entering atmospheric air, drawn from the roof by pump P_1, was regulated by a valve V_1. The temperature and relative humidity were adjusted by successive passage through two temperature controlled water baths (B_1 and B_2). First the air was passed through a sintered glass diffuser, containing 500 cm^3 of distilled water, in water bath B_1, saturating it at the temperature of B_1, then it passed through a copper coil in bath B_2 set at the temperature desired in the leaf chamber. The relative humidity of the air directed to the leaf chamber was thus equal to the ratio of the saturation vapor pressure (S.V.P.) at the temperature of the bath B_1 over the S.V.P. at the temperature of the bath B_2. After passing bath B_2 the air flow was divided. The reference air steam went directly to the differential psychrometer via regulating valve V_3 through a copper coil in bath B_2. The air stream enroute to the leaf chamber passed through regulating valve V_2 and flowmeter F_1 (1-9 L min $^{-1}$ capacity) to regulate and measure the flow rate. The proportion of inlet air flowing through the reference and leaf chamber channels were regulated by V_3 and V_2 respectively. After passing across the leaf in the leaf chamber, the sample air flowed on through a copper coil parallel to the reference air line in bath B_2 to the differential psychrometer via exhaust valve V_4 and a copper coil in bath B_2. The sample air flow was reduced to a rate equalling that of the reference air flow entering the differential psychrometer by regulation of exhaust valve V_4.

The sample and reference air streams then followed parallel, but separate paths through the differential psychrometer, drying columns D_1, D_2, switching valves V_5, V_6, V_7, regulating valves V_8, V_9, flowmeters F_2, F_3 (0.1 to 1.5 L min $^{-1}$ capacity) to the IRGA.

The twin drying columns were modified lucite laboratory gas drying columns in which air passed first through indicating drierite then anhydrous magnesium perchlorate.

Switching valves V_5, V_6, V_7 permitted entry of CO_2 standards into the system for calibration of the IRGA at the beginning of each run. Regulating valves V_8 and V_9 are used to equalize the flow of the standard CO_2 gases. These valves (V_8 and V_9) did not regulate the flow of the leaf chamber and reference air, which was achieved by valves V_1, V_2, V_3, and V_4. Flowmeters

F_2 and F_3 monitored the flow rate of air in the reference and leaf chamber channels, respectively, coming from the differential psychrometer to the IRGA.

Throughout the gas system 0.635 mm O.D. (1/4") copper tubing was used wherever possible. Where flexible connections were required, 0.635 mm O.D. (1/4") high density nylon tubing was used. All conections were made with Swagelock gas-tight fittings.

Because the accuracy of the measurement of CO_2 exchange is most often limited by the accuracy with which the air flow through the leaf chamber is known (Janac, Catsky and Jarvis, 1971), flowmeter F_1 was calibrated in situ with a wet test gas meter.

The Leaf Chamber. The leaf chamber was constructed of lucite with inside dimensions of 25 x 12.5 x 2.5 cm, as illustrated in Figure 26. The upper and lower surfaces of the chamber consisted of walls 1.25 cm apart forming water jackets, through which water from bath B_2 was circulated by pump P_2 (Figure 24). The leaf was held in position in the center of the chamber by nylon threads stretched across it. The air inlet and outlet on opposite sides of the chamber consisted of 24 pairs of holes (0.4 mm diameter) spaced 1 cm apart along a 10 mm O.D. lucite distribution tube. An equal number of holes faced downwards, and upwards at an angle of 45^{o}, to ensure equal air flow rate across each side of the leaf. Uniform air mixing within the chamber was ensured by two electric fans in the bottom of the chamber whose speed was controlled by a variable DC power source. With the leaf in position, an air tight seal between the upper and lower half was obtained with thick (4 mm) closed-cell neoprene rubber. The chamber halves were held together with 10 lightly tightened wing nuts.

A 40 SWG Type T thermocouple was attached to the center nylon suspension thread so that it pressed against the underside of the leaf, for leaf temperature measurements.

Transpiration Measurements. The transpiration rate of the leaf in the leaf chamber was determined by measuring the difference between the water vapor pressures of the air passing over the leaf and the reference air stream with the differential psychrometer positioned in bath B_2 (Figure 27). The basic design of the differential psychrometer was similar to that described by Slatyer and Bierhuizen (1964).

The sample and reference air streams were first brought to the same temperature by passing through separate copper coils, soldered together and placed in bath B_2. The air flows were then introduced to identical wet bulb probes positioned in a 7.5 x 5 x 5 cm lucit block also situated in bath B_2 (Figure 24). A 40 SWG Type T thermocouple was placed at the tip of each lucite wet bulb probe which was covered with a small diameter cotton sleeve wick. The probes were sealed and held at the center of each inlet tube (6.75 mm diameter) by 2 O-rings on the probe bases (Figure 27). The effective cross-sectional area of the wet bulb probe was

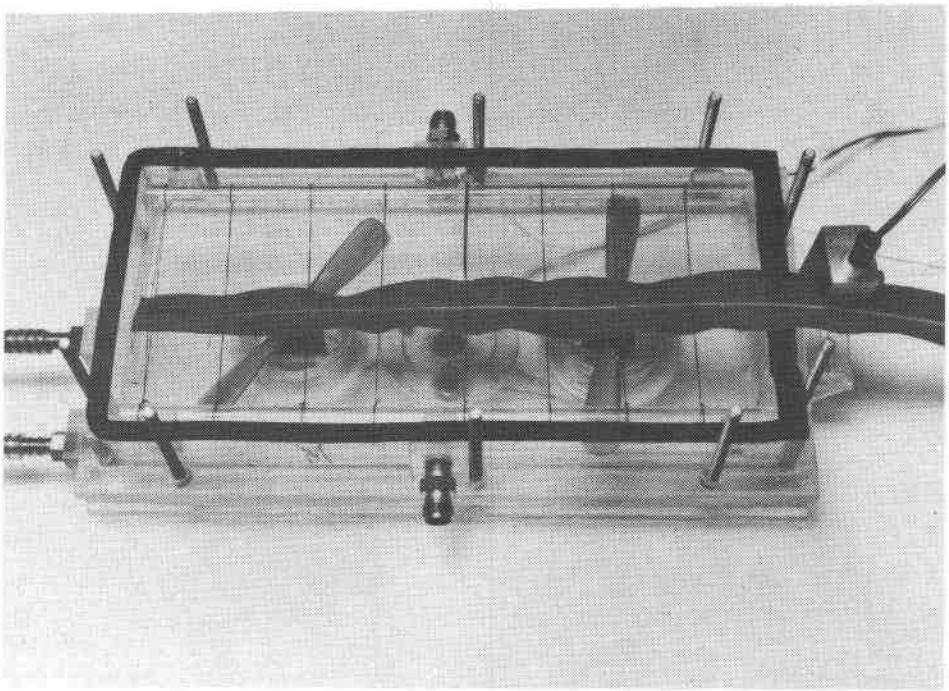

Figure 26. The leaf chamber, with the top removed, showing the experimental leaf held in place by the nylon threads, and the attachment of the in situ thermocouple psychrometer immediately outside the chamber.

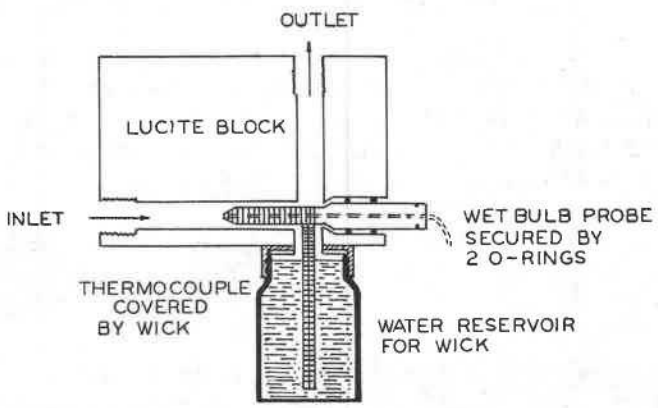

Figure 27. Cross-section of the wet bulb assembly of the differential psychrometer used for transpiration measurements.

15.5 mm^2 leaving a cross-sectional area of 20.0 mm^2 for air flow. With an air flow of 500 $cm^3 min^{-1}$, the ventilation rate was 12.5 m min^{-1}. The wick reservoirs were 25 ml scintillation vials with the caps glued to the lucite block. The seals between bottle and cap were obtained with silicone rubber gaskets.

A third thermocouple of the same type was placed in water bath B_2. The thermocouples were wired to measure the difference between the wet bulb temperatures of the air streams and the actual wet bulb temperature of the air leaving the leaf chamber. The thermocouple output was measured with a Keithley 150B Microvoltmeter and recorded on a potentiometric recorder.

For this differential psychrometer arrangement the psychrometric equations for the air streams may be written(Bierhuizen and Slatyer, 1964) as

$$(e_{wr}-e_r) = A(t-t_{wr}), \tag{24}$$

and

$$(e_{ws}-e_s) = A(t-t_{ws}), \tag{25}$$

where t is the temperature of the airstreams or the temperature of water bath B_2 since both air streams have passed through copper coils in this bath, t_{wr} and t_{ws} are the wet-bulb temperatures of the reference and sample air streams respectively, e_{wr} and e_{ws} are the respective saturated water vapor pressures of the air streams at this wet bulb temperature, and e_r and e_s are the actual vapor pressures. A is the psychrometric constant.

Subtracting (24) from (25) yields

$$\Delta e = e_r - e_s = A(t_{wr}-t_{ws}) + (e_{wr}-e_{ws}). \tag{26}$$

From this equation Δe, the difference in vapor pressure of the two air streams caused by leaf transpiration can be calculated. since $(t_{wr}-t_{ws})$ is measured with the differential psychrometer and $(e_{wr}-e_{ws})$ can be obtained from tables. Δe can be converted to water vapor concentration (c) in mg L^{-1} using the equation

$$c = \rho\left(\frac{\Delta e}{e_s}\right), \tag{27}$$

where e_s and ρ are the saturation vapor pressure and density of water vapor at the B_2 bath temperature, respectively. The transpiration rate (E) can be calculated using the equation

$$E = \frac{cF}{S}, \tag{28}$$

where S is the area of the leaf in the leaf chamber, and F is the flow

rate through the leaf chamber measured with flowmeter F_1. A sample calculation of transpiration rate using the above method is presented in Appendix II.

The differential psychrometer was calibrated with a Cambridge Dew-Point Hygrometer using saturated air at several temperatures. A wide range of relative humidities and air flow rates were used. A comparison between results obtained with the differential psychrometer and the Cambridge Dew-Point Hygrometer is presented in Appendix III. The effect of air flow rate on psychrometer response is illustrated in Figure 28. It shows that maximum wet bulb depression occurred at flow rates as low as 300 $cm^3 min^{-1}$. The IRGA ideally requires a gas flow rate of 500 to 1000 $cm^3 min^{-1}$, so that the differential psychrometer easily satisfied the design criteria of the system.

Photosynthesis Measurements. Net photosynthesis was measured by determining the difference in CO_2 concentration (ΔCO_2) between the leaf chamber and reference air streams, with an infrared gas analyzer (IRGA). Before passing through the IRGA the air streams were dried, because water vapor interferes with the measurement of CO_2 by the IRGA.

The photosynthetic rate was then calculated with the equation

$$P_n = \frac{\Delta CO_2 \times F}{S}, \qquad (29)$$

where ΔCO_2 is in mg L^{-1}, F is the flow rate measured with flowmeter F_1 in L min^{-1}, and S is the leaf area in cm^2.

The IRGA was calibrated with standard CO_2 mixtures. Air with a calibrated CO_2 concentration approximately equal to that of the air to be used in system was passed through both sample and reference tubes, while the analyzer was zeroed. With this mixture flowing through the reference tube, a calibrated mixture with a lower concentration (50-100 vpm lower) was passed through the sample tube allowing the analyzer output to be adjusted to the sensitivity required. Within these narrow concentration ranges the analyzer output was essentially linear and no further calibration gas was required (Janac, Catsky and Jarvis, 1971). In normal operation the analyzer output was recorded with a 10 mv potentiometric strip chart recorder.

Light Source. Light was provided by a 2500 watt xenon long arc lamp mounted in such a way that its height above the plant, and thus light intensity, could be easily varied. The lamp was equipped with a quartz outer and an infrared (IR) inner filter to reduce excessive ultra-violet and IR transmission (Jarman, Barlow, and Boersma, 1974). With this filter combination, the lamp produced a visual spectrum similar to natural sunlight (Figure 29). Although the lamp still exhibited a prominant infrared peak at 900 nm, the total energy emitted in the IR region was only 44% of the total radiation, which is very similar to natural daylight.

In addition to varying lamp height above the plants, the intensity of radiation could be varied by three choke taps. On the high power setting the lamp produced a radiant flux of 965 watts m^{-2} (1.38 langley min^{-1}) and

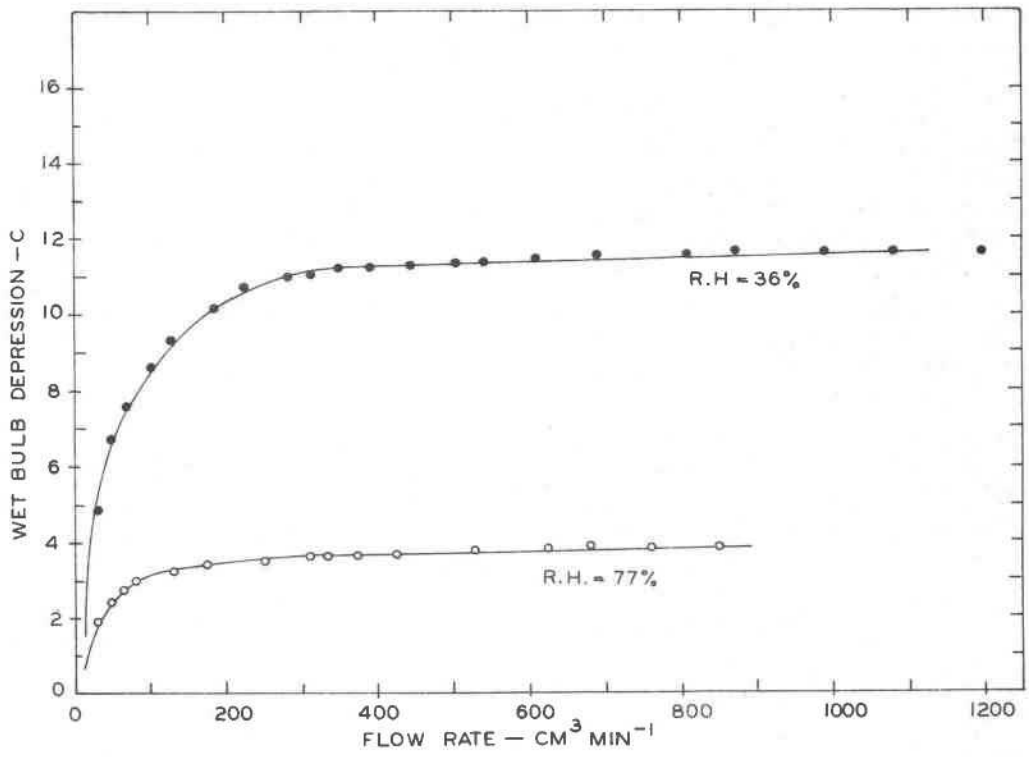

Figure 28. The effect of air flow rate on the performance of the differential psychrometer, illustrating the psychrometer to be fully ventilated at air flow rates as low as 300 cm^3 min^{-1}.

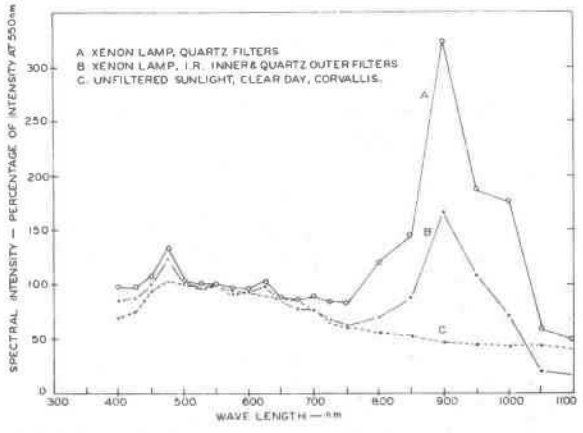

Figure 29. Spectral distribution of the radiant energy produced by the 2500 watt xenon long-arc lamp using an infrared filter, compared to the spectral distribution of unfiltered sunlight.

a visual luminous flux of 7550 ft. c. at a distance of 38 cm from the burner. The radiant flux of the lamp on the medium and low power settings were respectively 75 and 50 percent of the high power setting.

Leaf Elongation Measurements. The leaf length was monitored continuously with a linear variable differential transducer (LVDT), connected to a potentiometric chart recorder (Hsiao, Acevedo, and Henderson, 1970; Barlow and Boersma, 1972). The LVDT is an electromechanical transducer which produces an electrical output proportional to the displacement of a separate moveable iron core. A cotton thread taped to the tip of the youngest unrolled leaf connected it to the LVDT core via a low friction pulley. The iron core weighed less than 2 g and did not affect the rate of elongation, after an initial stretching period.

Leaf Water Potential ψ_c. An *in situ* leaf thermocouple psychrometer (Neumann and Thurtell, 1972) constructed after the design of Campbell and Campbell (1974) was used to monitor the water potential of the leaf being used for net photosynthesis and transpiration rate measurements. It was supported by the leaf chamber, but attached to the leaf outside the chamber. Before the psychrometer was attached to the leaf, the contact area was wiped with a Kimwipe moistened with xylene which removed part of the cuticle. The area was then cleaned with distilled water and thoroughly dried. The psychrometer was attached by placing the leaf in the slit of the block assembly and sealing the thermocouple assembly to the leaf with a 90% lanolin-10% bees-wax mixture (Campbell and Campbell, 1974). The psychrometer output was measured with a Wescor HR-33 Dewpoint Microvoltmeter. Prior to use, the psychrometer was calibrated using small pieces of filter paper (Whatman #1) moistened with KCl solutions of known water potential.

The initial equilibration time of the thermocouple psychrometer, after it was attached to the leaf was 1-3 hours. In practice, the *in situ* leaf psychrometer was always given an equilibration time of 12 hours or more by attaching it to the leaf the night before beginning experimental measurements. After this initial equilibration period, the time necessary to adjust to changes in ψ_c was approximately 15 minutes. On corn it was necessary to facilitate vapor transfer by removing part of the cuticle with xylene to achieve the indicated equilibration times. However, with other plant species such as soybean and cocklebur cuticle removal was not necessary to obtain reasonable equilibration times. Apparently the stomata, situated in the enclosed area of the corn leaf, closed quickly in response to the darkness imposed by the thermocouple assembly, making it necessary to obtain vapor equilibrium by the cuticular pathway.

Control of Root and Shoot Environment. A lucite root chamber measuring 21.5 x 19.5 x 31 cm and insulated with polystyrene, was used to control root temperature and soil water potential (Figure 24). The temperature of the osmotic solution in the chamber was controlled by continuously circulating the osmotic solution through a heat exchanger placed in water bath B_3 (Figure 24). The temperature of the soil contained in the cellulose

acetate membranes in this chamber was monitored by a type T thermocouple placed in the soil. This thermocouple was calibrated against a Hewlett-Packard quartz thermometer.

The entire carbon assimilation system was situated in a controlled environment growth room.

Experimental Procedure

Corn (Zea mays L. var. Pride 5) plants were grown in a reach-in growth chamber. When the plants reached the 7 leaf stage (2-3 weeks old), the roots were enclosed in a cellulose acetate membrane and placed in the temperature controlled osmotic root chamber located in the controlled growth room set at 27.5 $\pm$ 1 C and a R.H. of 55 $\pm$ 1%. Plants were placed in the chamber one day before the experiments were initiated to allow acclimatization.

The bottom section of the leaf chamber together with the in situ thermocouple psychrometer was placed on the 5th leaf of the corn plant, the night before the experiment was started. The narrow distal portion of this leaf was cut off to enable a uniform broad section to be placed in the chamber (Figure 26). The cut end was sealed with a nonphytotoxic 90% lanolin-10% bees-wax mixture.

Net photosynthesis, transpiration, and ψ_c were measured on the 5th leaf because Hofstra and Nelson (1969) have shown by C^{14} translocation studies on Pride 5 corn plants of the same age, that the 5th leaf is the major source of photosynthate for the rapidly expanding 7th leaf.

On the morning of the experiment the LVDT was connected to the 7th leaf by a piece of cotton thread stuck to the tip of the leaf with a small piece of "scotch" tape. At the beginning of each experimental run the IRGA was calibrated using standard CO_2 mixtures, and the zero base lines of both IRGA and differential psychrometer were established by passing reference air through both branches of the system, by-passing the leaf chamber. The leaf chamber was then sealed by placing the upper half in position, and connected to the gas system.

The height of the xenon lamp above the leaf chamber was adjusted in each experiment so that the light intensity at the surface of the leaf in the chamber was about 381 W m^{-2} (3900 ft. c.). The quantum flux was 753 μ Einstein m^{-2} s^{-1}.

The temperatures of the water baths B_1 and B_2 (Figure 24) were adjusted so that the air entering the chamber was at the same temperature and relative humidity as the growth room, namely 27.5 C and 55% respectively.

Experimental measurements were commenced 1 1/2 - 2 hours after the light was turned on by determining the initial nonstress rate of net photosynthesis, transpiration, and leaf elongation, at a root temperature of

27.5 C. After steady state values were achieved at this temperature, the root temperature was decreased 3.5 to 4.5 C by lowering the temperature, of water bath B_3. When the thermocouple, placed in the soil with the roots, indicated that a new equilibrium had been achieved, the plant was allowed to grow for another 45 minutes at this temperature, before ψ_c root and leaf temperatures were measured. Then the root temperature was lowered again and the procedure was repeated. In this manner the root temperature was incrementally lowered to approximately 10 C to obtain a series of successively lower values of ψ_c.

In a second series of experiments the root temperature was maintained at 27.5 C while the temperature of the shoot apical meristem was varied between 5 and 30 C. This was accomplished by placing a lucite water jacket around the meristem region of the corn stalk (Watts, 1972b). The lucite chamber, which was 5 cm high and 3.2 cm in diameter, was sealed to the corn stalk with a catalytic type silicone rubber, the day before beginning measurements. Water from bath B_3 was circulated through the chamber to control meristem temperature. A type T thermocouple was inserted in the outlet of the chamber to monitor its temperature. The experimental procedure discribed above was followed in these experiments. In all experiments, measurements were completed within 10 hours of exposing the plants to light.

Calculation of Transfer Resistances

The total resistance to water vapor transfer by the leaf, Σr_{H_2O} was calculated from the equation (Appendix I).

$$\Sigma r_{H_2O} = \frac{[H_2O]_c - [H_2O]_a}{E} . \qquad (30)$$

E was the measured rate of transpiration. The water vapor concentration within the leaf, $[H_2O]_c$ was calculated from leaf temperature data, assuming the air within the leaf to be saturated (Gaastra, 1959). The water vapor concentration $[H_2O]_a$ of the air entering the leaf chamber was measured by the reference wet bulb of the differential psychrometer. The boundary layer resistance to CO_2 transfer r_{a1} as measured with leaf models constructed of blotting paper, was 0.96 sec cm^{-1}.

The total resistance to CO_2 transfer was calculated from the equation

$$\Sigma r_{CO_2} = \frac{[CO_2]_a - [CO_2]_{chl}}{P_n} . \qquad (31)$$

P_n is the net photosynthetic rate, $[CO_2]_a$ is the CO_2 concentration of the air entering the leaf chamber, and $[CO_2]_{chl}$ is the CO_2 concentration at the chloroplast fixation sites, which is assumed to be zero (Gaastra, 1959). The validity of the latter assumption has recently been challenged by Whiteman and Koller (1968), who proposed that the CO_2 concentration at

the compensation point provides a better estimate of $[CO_2]_{chl}$. However, it is unlikely that the assumption of $[CO_2]_{chl} = 0$ resulted in a significant error in these experiments because Forrester, Krotkov, and Nelson (1966), and Moss (1971) have shown the CO_2 compensation point of Zea mays L. to be zero. Because of the above observation and the impracticality of determining the CO_2 compensation point at each level of water stress, the assumption of $[CO_2]_{chl} = 0$ was used in these calculations.

The stomatal resistance to CO_2 transfer was calculated from

$$r_s = \Sigma r_{H_2O} \left(\frac{D_{H_2O}}{D_{CO_2}}\right) - r_a. \qquad (32)$$

A value of 1.60 was used for the diffusitivity correction term (Fuller, Schettler, and Giddings, 1966). The mesophyll resistance to CO_2 transfer was calculated from the equation

$$r_m = \Sigma r_{CO_2} - (r_a + r_s). \qquad (33)$$

A sample calculation of these resistances is presented in Appendix II.

Results and Discussion

Under the constant environmental conditions of the growth room the photosynthetic rate of nonstress control plants was almost constant for a 12-hour light period (Table 25). Consequently, the effects of temperature and water stress on photosynthesis and transpiration have been reported as a percentage of the nonstress rate measured on the day of experimentation.

The net photosynthesis values shown in Table 25 are somewhat lower than those previously reported for Zea mays L. (Hesketh, 1967), because the light intensity was low (381 w m^{-2}). This low light intensity was used because higher light intensities were found to severely inhibit leaf elongation (Figure 30). The inhibition of leaf elongation, by the light intensity of 980 w m^{-2} was probably due to the direct inhibitory effect of light on leaf elongation (Sachs, 1965) and lowering of the leaf water potential caused by the intense radiation (Figure 30). The inhibitory effects of high light intensities and large radiant fluxes on leaf elongation have been noted previously by Loomis (1934), and Hsiao, Acevedo, and Henderson (1970). Therefore, because the aim of this experiment was to measure the response of leaf elongation to plant water stress, a lower light intensity (381 w m^{-2}) that did not severly inhibit leaf elongation (Table 25) was selected.

Table 25. The diurnal pattern, in the rates of leaf elongation (leaf 7), net photosynthesis, transpiration (leaf 5), and the leaf water potential (leaf 5) of a control plant growing at a root temperature of 27.5 C and a soil water potential of -0.35 bars. The light intensity was 381 w m^{-2}.

Time	Water Potential	Elongation	Net Photosynthesis	Transpiration
hrs	Bars	$\mu m\ min^{-1}$	$mg\ CO_2\ dm^{-2}\ hr^{-1}$	$gH_2O\ dm^{-2}\ hr^{-1}$
900	-6.3	45.4	30.9	2.233
1100	-6.5	73.5	30.9	2.233
1300	-6.7	71.6	31.0	2.224
1500	-6.7	72.8	32.8	2.224
1700	-6.6	73.1	32.4	2.250
1900	-6.7	74.0	31.5	2.250
2100	-6.7	71.5	30.8	2.227

Lowering the root temperature from 27.5 to 10.0 C in small increments had a different effect on leaf elongation then on net photosynthesis and transpiration (Figure 31). The rate of leaf elongation decreased steadily with each decrease in root temperature until it reached zero at a root temperature of 12 C. In contrast, net photosynthesis and transpiration were still proceeding at more than 80% of the nonstress rate when the root temperature reached 12 C. The effects of low root temperature on leaf elongation are at least two-fold. Firstly, lowering the root temperature can decrease the rate of water adsorption by the plant roots and thereby induce water stress within the plant (Kuiper, 1964; Kleinendorst and Brouwer, 1970). In this experiment the ψ_c decreased with each decrease in root temperature below 27.5 C (Figure 32), indicationg that low root temperatures reduced the rate of water uptake by the root system. However, the extent of this reduction was not constant with each decrease in root temperature, as there was a sharp discontinuity in the curve at a critical temperature in the vicinity of 13 C. This would indicate a change in the activation energy for water transport at this critical temperature. Discontinuous temperature response curves have been previously reported for water uptake, membrane ATPase activity, membrane permeability, and mitochondrial respiration (Kuiper, 1964; Kemp, Groot, and Reitsma, 1969; Hope and Aschberger, 1970; Lyons and Raison, 1970). The likely causes of these changes were recently reviewed by Kuiper (1972), who postulated that they may be correlated with changes in membrane structure. In particular, a hydrophobic melting of the membrane lipid molecules may begin at the critical temperature resulting in a transition in membrane structure from the lamellar to the globular phase, which is more permeable to water. Such a structural change may be accompanied by a collapse of the ice-like water structure to form polarized water around the lipid protein structure. It is also possible that this change from the lamellar to the globular phase could be caused by a change in the supply of metabolic energy resulting from conformational changes of key enzymes.

The second manner in which soil temperature may influence the rate of leaf elongation is by directly affecting the temperature of the shoot apical meristem (Watts, 1972a, 1972b). When corn is in the 7 leaf stage the apical meristem is close to the soil surface and tends to follow soil temperature rather than air temperature because of conduction up the stalk and the flow of cold liquid up the xylem (Beauchamp and Torrance, 1969; Watts, 1972b). Low soil temperatures do not affect directly the temperature of the plant leaves (Beauchamp and Torrance, 1969) or their physiological function. Consequently low root temperatures influence leaf elongation directly by the temperature effect on the apical meristem and indirectly by lowering ψ_c and cell turgor but only affect net photosynthesis and transpiration indirectly by decreasing ψ_c.

In order to evaluate the effect of successively lower ψ_c values on these functions, it was necessary to quantify the direct effect of low soil temperatures on shoot apical meristem activity and leaf elongation in the absence of water stress. This was accomplished by growing corn plants at a soil temperature of 27.5 C, and independently varying the temperature of

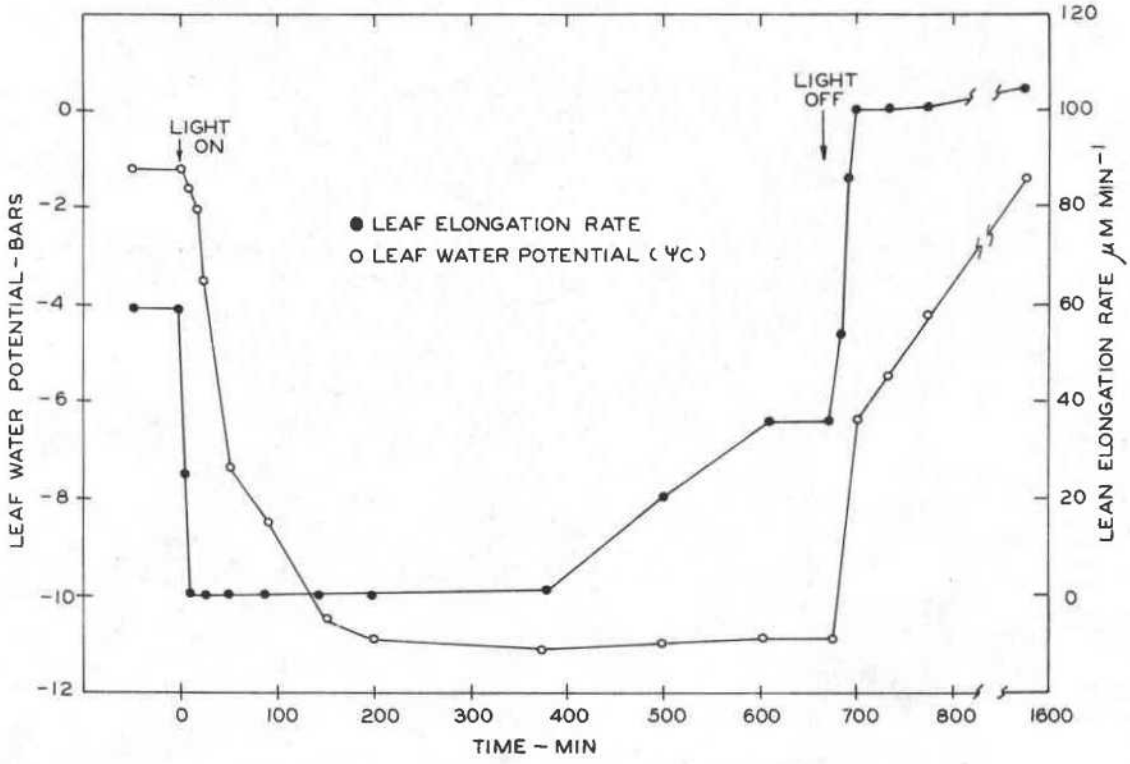

Figure 30. Changes in leaf elongation (leaf 7) and leaf water potential (leaf 5) during a 700 minute illumination period at a high light intensity (980 wm^{-2}).

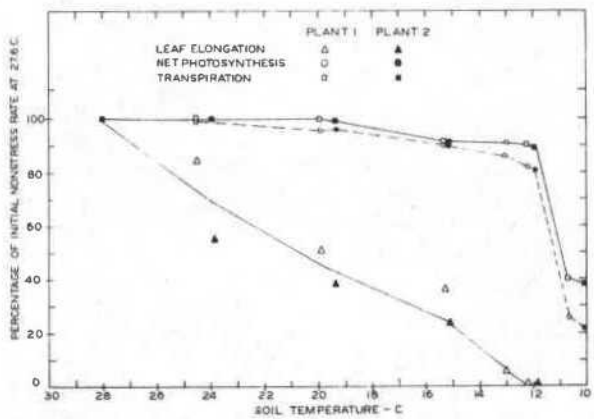

Figure 31. Steady state rates of leaf elongation (leaf 7), net photosynthesis and transpiration (leaf 5) of a corn plant with 7 unrolled leaves at soil temperatures ranging from 10 to 30 C.

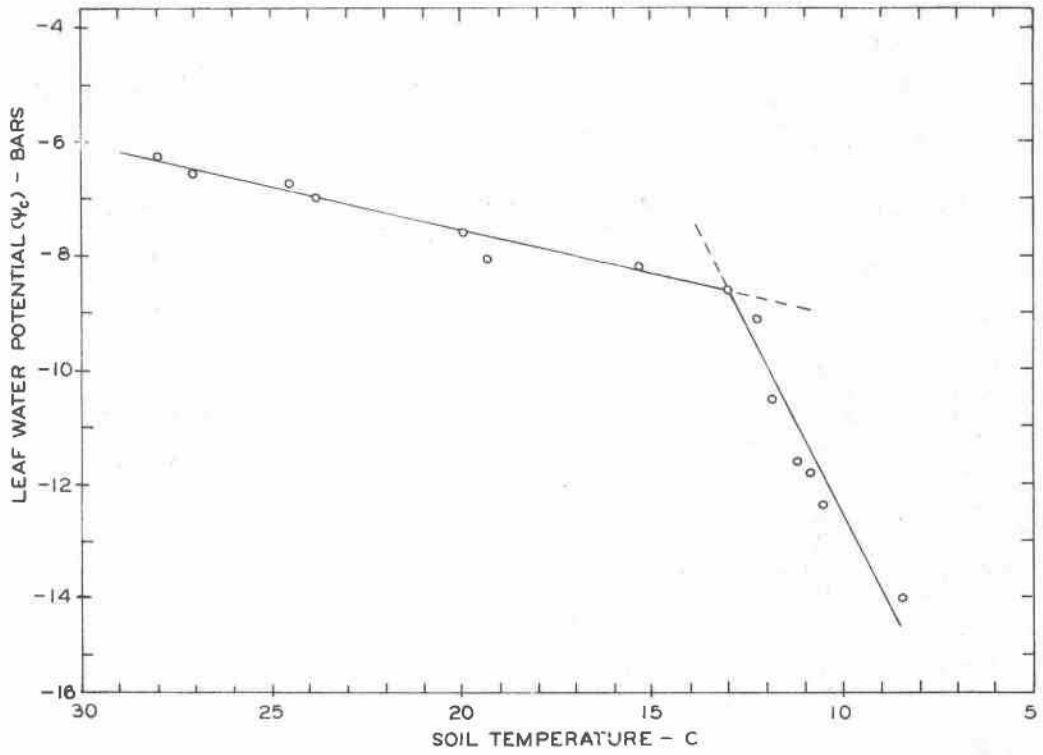

Figure 32. Steady state water potentials of the 5th leaf of a 7 leaf corn plant at soil temperatures ranging from 10 to 30 C. The shoot environment was controlled at 27.5 C and 55% relative humidity.

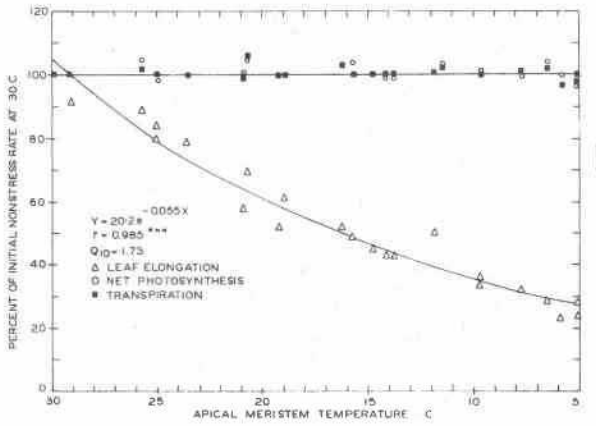

Figure 33. Steady state rates of leaf elongation (leaf 7), net photosynthesis, and transpiration (leaf 5) of a corn plant with 7 unrolled leaves growing at a soil temperature of 27.5 C and shoot appical meristem temperatures ranging from 5 to 30 C.

the shoot apical meristem by enclosing it in a small lucite water jacket connected to a controlled temperature recirculating water bath. In this manner, leaf elongation, net photosynthesis, and transpiration were measured at shoot apical meristem temperatures varying from 5 to 30 C (Figure 33).

Lowering the shoot apical meristem temperature in small increments of 5 C did not affect net photosynthesis or transpiration Furthermore, the ψ_c of the experimental plant did not decrease by more than 0.7 bars in any experiment. However, the shoot meristem activity, as measured by the rate of leaf elongation was affected markedly by lowering its temperature. Unlike the effect of root temperature on ψ_c, leaf elongation was a continuous exponential function of meristem temperature down to 5 C. The Q_{10} of leaf elongation throughout the entire temperature range was constant at 1.73 which was slightly lower than the Q_{10} value of 2 for leaf growth reported by Chao and Loomis (1948) and Watts (1972b). The water jacket did not enclose all of the elongating region as well as the meristem, so that some elongation may have continued irrespective of the meristem temperature. Furthermore, the high evaporative demand in the growth room caused a large flux of warm water to continuously move through the cooled meristem, and it is unlikely that the temperature of the meristem inside the enclosing leaf sheaths was as low as that of the circulating water. Both factors would tend to decrease the observed Q_{10} value.

The lack of an effect of the low meristem temperatures on net photosynthesis, transpiration, and ψ_c would indicate that these had little effect on translocation or other physiological functions, except for decreasing the apical meristem activity. This is consistent with the work of Thrower (1965) and Weatherly and Watson (1969) who found that translocation was restricted somewhat at chilling temperatures, but that it did not stop until the temperature was below 0 C.

The important observation from the meristem collar experiment (Figure 33) was that although decreases in the temperature of the apical meristem did decrease the leaf elongation rate, meristem temperatures as low as 5 C did not stop the leaf elongation. In contrast a soil temperature of 12 C stopped leaf elongation (Figure 31). Furthermore at temperatures ranging from 15 to 30 C approximately 65% of the reduction in the rate of leaf elongation can be attributed to the lowering of the apical meristem temperature (Figure 34). Below the critical temperature of approximately 13 C the ψ_c decreased rapidly (Figure 34) and sub-threshold cell turgor pressures were probably the major factor limiting leaf elongation in this region (Figure 34).

The effect of ψ_c on net photosynthesis, transpiration, and leaf elongation can now be evaluated by plotting the ψ_c values obtained in the root temperature experiment in Figures 35 and 36. Duplicate experiments are plotted separately because the ψ_c values for each plant at each soil temperature were different and a composite curve of both plants lacked clarity. It was not possible to make a quantitative correction for the effect of lowered meristem temperature on leaf elongation. Consequently the leaf

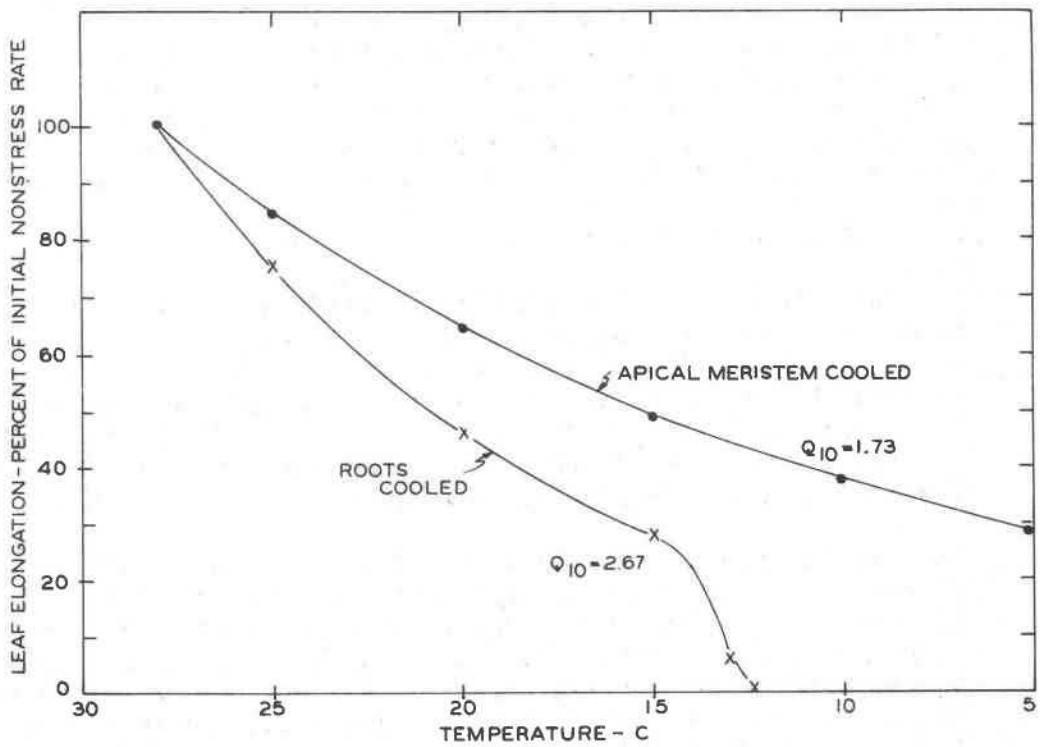

Figure 34. The elongation rate of the 7th leaf of young corn plants exposed to either soil or apical meristem temperatures ranging from 5 to 30 C.

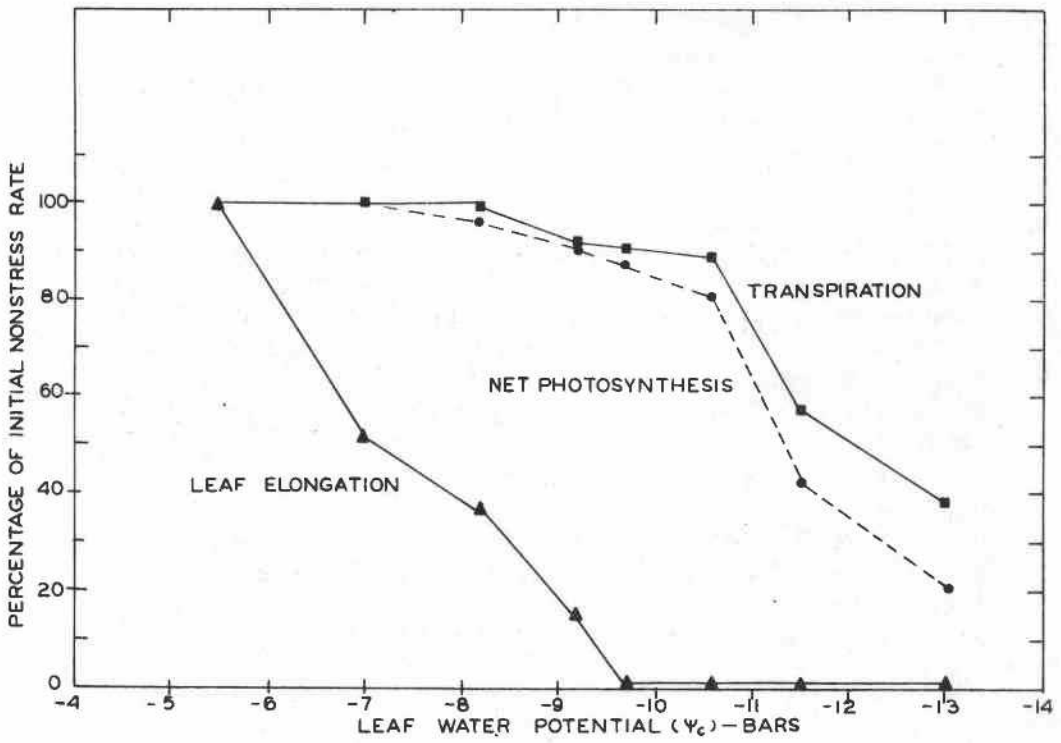

Figure 35. Steady state rates of leaf elongation (7th leaf), net photosynthesis, and transpiration (5th leaf) of a corn plant with 7 unrolled leaves as a functfòn of the water potential of the 5th leaf. Plant 1.

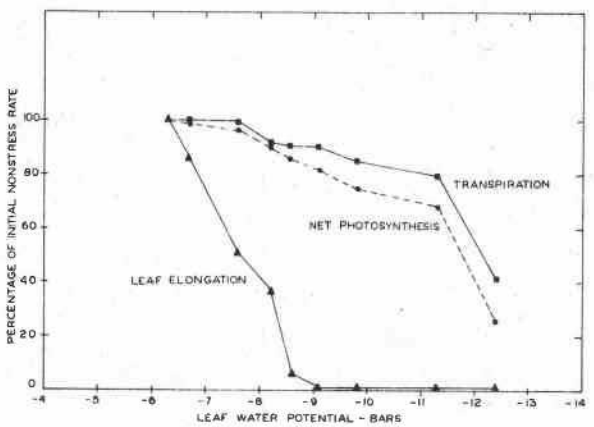

Figure 36. Steady state rates of leaf elongation (7th leaf), net photosynthesis, and transpiration (5th leaf) of a corn plant with 7 unrolled leaves as a function of the water potential of the 5th leaf. Plant 2.

elongation rate plots in Figures 35 and 36 show leaf elongation rate decreasing prematurely because most of the reduction in leaf elongation at high ψ_c values (higher soil temperatures) is due to the effect of soil temperature on apical meristem activity.

The sensitivity of leaf enlargement to small changes in ψ_c (Hsiao, 1973) was demonstrated clearly by the short term steady state measurements of this experiment. Each decrease in the ψ_c resulted in a decrease in the rate of leaf elongation (Figures 35 and 36). Leaf elongation eventually ceased at a ψ_c of -9.1 in one plant and -9.6 bars in another, which is in good agreement with the value of -9.2 bars obtained by long term steady-state measurements. Both Boyer (1970a) and Acevedo et al. (1971) reported that corn plants of similar age stopped leaf enlargement at a ψ_c of -7 to -8 bars. The discrepancy between these estimates is probably due to differences in light intensity as Boyer made his measurements in the dark, and Acevedo et al. used a light intensity of 1100 ft. c., which is less than 1/3 of that used in this experiment. It is likely that the values of -9.0 to -9.5 bars obtained in these experiments more closely approximate the field situation.

Photosynthesis and transpiration responded similarly to decreasing ψ_c, although net photosynthesis was affected to a greater extent at any particular value of ψ_c in both plants. Both net photosynthesis and transpiration were decreased slight by ψ_c values near -8 bars, but did not exhibit large decreases until values of -11 to -12 bars were reached. Sequential short term responses of leaf elongation, net photosynthesis, and transpiration have not been measured previously although Boyer (1970a) related photosynthesis and leaf elongation to the ψ_c of corn in a water stress study lasting several days and found a similar pattern to that illustrated in Figure 36.

Calculation of the diffusion resistances to CO_2 transfer showed that the decrease in net photosynthesis was due to increases in both the mesophyll (r_m) and stomatal resistances (r_s) (Figure 37). The increases in both r_s and r_m followed the same pattern and appeared to begin at approximately the same degree of stress. The mesophyll resistance increased a little more than the stomatal resistance with increasing stress, but the ratio of the resistances remained approximately the same. The increases in r_m, which indicate a degree of nonstomatal control over net photosynthesis during water stress may result from physical, photochemical, biochemical, or metabolic factors affecting the rate of net photosynthesis. These can not be specifically identified because r_m was calculated as a residual term. A number of workers have recently reported similar increases in r_m under water stress conditions (Slatyer, 1973; Hansen, 1971; Redshaw and Meidner, 1972). Redshaw and Meidner (1972) concluded that the increases in r_m of water stressed tobacco plants were probably due to an increase in the rate of CO_2 evolution or an increase in the chemical resistance to CO_2 fixation. An increase in the respiration rate that increased the compensation point above zero, would have produced an artificial increase in r_m in this experiment as the assumption $[CO_2]_{chl}=0$ would no longer be correct. However, Wesselius and Brouwer (1972) reported the respiration rate of water

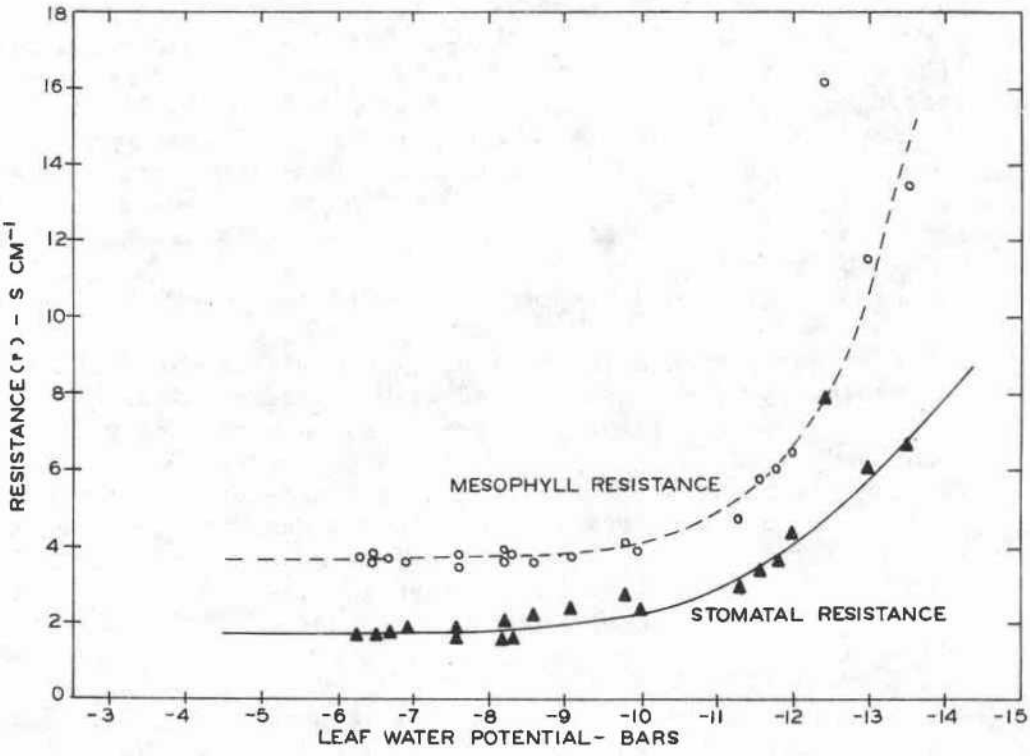

Figure 37. The stomatal and mesophyll resistances to carbon dioxide transfer of the 5th leaf of a 7 leaf corn plant, as a function of the water potential of that leaf.

stressed corn to increase by less than 2 percent, and, therefore, it is unlikely that increased respiration rate was the cause of the increase in r_m in this experiment. Boyer (1971) and Wesselius and Brouwer (1972) demonstrated nonstomatal influences on photosynthesis, in water stressed sunflower and corn plants by using elevated CO_2 concentrations. Boyer and Bowen (1970) illustrated that the reduction of photosynthesis in sunflower leaves was paralleled by the loss of Hill reaction activity in vitro.

In summary it would appear that the nonstomatal factors influencing photosynthesis could be physical constrictions impeding the transfer of CO_2 to the fixation sites, a loss of photochemical activity, or biochemical inhibition of carboxylation reactions. All these mechanisms have been proposed by Neales and Incoll (1968) as possible consequences of photosynthate accumulations in the photosynthetic source leaf. Therefore the possible mechanisms of nonstomatal control of photosynthesis are at least consistent with the source-sink hypothesis under consideration. Although photosynthate levels were not measured in this experiment, the different sensitivity of leaf elongation and photosynthesis to water stress (Figures 35 and 36) would make the accumulation of photosynthate likely at moderate water stresses (-8 to -11 bars). However, this experiment did not establish a cause and effect relationship.

The parallel responses of net photosynthesis and transpiration to increasing water stress, coupled with an increase in r_m, recorded in this study, are worthy of further comment because they illustrate, aptly, a point made by Hsiao (1973) in a recent review of water stress effects on growth. Although much of the evidence in favor of a dominant stomatal control of photosynthesis during water stress is based on studies showing a close parallel between photosynthesis and transpiration responses to water stress (Brix, 1972; Barrs, 1968; Boyer, 1970b; Hansen, 1971), this does not rule out the possibility of nonstomatal involvement particularly if the stomata are regulated by CO_2 concentration inside the leaf.

Finally the rapid physiological responses of the young corn plants to water stress illustrated in this experiment may be indicative of plant response in the field to the diurnal cycle of water stress. The sensitivity of leaf elongation to high light intensity, soil temperature, and ψ_c reported is in good agreement with earlier observations by Loomis (1934) that leaf elongation is reduced, frequently, by adverse environmental conditions in the field, and often may be restricted to dark periods. Grobbelaar (1963) in a study of the responses of young corn plants to root temperature found that leaf area, rather than net dry matter production per unit weight (photosynthesis) was the main determinant of differences in relative growth rate. Leaf enlargement may be a very important factor limiting production in similar situations.

EFFECT OF REDUCED LEAF ELONGATION ON PHOTOSYNTHESIS

Introduction

Results of the experiments discussed above suggested that a moderate water stress (-9 to -12 bars) may cause an accumulation of photosynthate in the sink leaf and ultimately in the source leaf by decreasing the size of the growth sink within the rapidly expanding young leaf. It was proposed that this carbohydrate accumulation in the source leaf could be one of the nonstomatal factors causing the photosynthetic rate to decrease during mild water stress. Several other workers also have proposed that decreased leaf elongation (Wardlaw, 1969; Boyer, 1970a) or decreased translocation of photosynthate (Zolkevick, Drusakova, and Lizandr, 1958; Hartt, 1963) could lead to accumulation of photosynthate in the source leaf thus regulating the photosynthetic rate. However none of these workers have directly measured photosynthesis in relation to photosynthate accumulation in the whole plant situation. It was pointed out above that the direct association of photosynthate accumulation with reductions in rate of photosynthesis is of prime importance in establishing the validity of the source-sink hypothesis where applied to plant reactions to water stress.

Experiments were designed seeking to establish a relationship between sink size, photosynthate accumulation, and photosynthetic rate by manipulating the rate of leaf elongation with the aid of changes in soil or apical meristem temperature. It was reasoned that if photosynthate accumulates in the plant in response to a decrease in the size of the growth sink, then the pattern of photosynthate accumulation in plants stressed by lowering the soil temperature should be different from that of plants stressed by lowering the temperature of the apical meristem. It was shown that lowering the soil temperature adversely affected the rate of elongation of the 7th leaf, by decreasing the temperature of the apical meristem, as well as by decreasing the plant water potential. This decrease in ψ_c also would reduce the rate of cell enlargement of the 6th leaf, which is importing little photosynthate (Hofstra and Nelson, 1969) but is still expanding. Therefore if the growth sink in this leaf is reduced, photosynthate produced in this leaf may accumulate. Consequently lowering the soil temperature may result in the accumulation of photosynthate in the source leaf 5, the independent leaf 6, and the sink leaf 7.

In contrast, inhibiting leaf elongation by lowering the temperature of the apical meristem may result in the accumulation of photosynthate only in the source leaf 5 and the sink leaf 7. Photosynthate may not accumulate in the independent leaf 6 because this leaf is growing predominately by cell expansion using its own photosynthate (Sharman, 1942) and the low temperature of the meristem should not affect its growth.

Methods and Materials

Corn plants in the 7 leaf stage were placed in the temperature controlled root chamber of the carbon assimilation system in an identical manner to that described above. An initial nonstress measurement of leaf elongation, net photosynthesis, and ψ_c were taken at a soil temperature of 27.5 C. The soil temperature was then rapidly lowered to 15 C and net photosynthesis, leaf elongation, and ψ_c were monitored for 6 hours at this soil temperature. At the end of the 6 hour period samples were taken from leaves 5, 6, and 7 and placed in a freezer at -15 C to be analyzed for soluble carbohydrate content. The entire leaf and sheath portions of leaves 6 and 7 were sampled, whereas only the leaf chamber portion of leaf 5 was sampled. Control plants for carbohydrate analysis were grown at a soil temperature of 27.5 C for the same duration and under identical light intensities (381 w m^{-2}). Each experiment was replicated three times.

Apical meristem temperature was lowered by passing 6 C water through the lucite meristem collars described above. The experimental procedure was the same as described for the soil temperature experiment with the exception that control plants without meristem collars were run concurrently in this experiment.

Soluble carbohydrates were extracted with 80 percent ethanol and measured by the anthrone method. As the dry weight of the sampled leaves could not be determined, the dry weight of the 80 percent-ethanol-insoluble residue was determined. Soluble carbohydrate content then was reported as a percentage of the 80 percent-ethanol-insoluble residue.

Results and Discussion

Lowering the soil temperature to 15 C for 6 hours caused ψ_c to decrease rapidly to values between -8.5 and -9.5 bars. There was a tendency for ψ_c to continue to decrease slightly during the 6 hour stress period but these decreases never exceeded 1.0 bar and ψ_c did not fall below -10 bars in any treatment. The small decrease in the leaf elongation between 80 and 360 minutes (Figure 38), is probably a result of these small decreases in ψ_c. The net photosynthetic rate was more than 80 percent of the initial nonstress rate, when ψ_c was greater than -10 bars (Figure 34). Therefore it is unlikely that the 47 percent reduction in the rate of net photosynthesis after 360 minutes at a soil temperature of 15 C was due to a decrease in ψ_c *per se* (Figure 38).

The soluble carbohydrate levels of leaves 5, 6 and 7 were increased significantly by the 6 hour stress period at a soil temperature of 15 C (Table 26). Although the carbohydrate increases in leaves 6 and 7 were 1 1/2 to 2 times that in leaf 5, this may not be significant because leaf 5 was more mature and only the blade portion within the leaf chamber

was analyzed. These increases in soluble carbohydrates indicate that the 80 to 90 percent reduction in leaf elongation (leaf 7) caused by the soil temperature stress, effectively reduced the size of the leaf growth photosynthate sinks. Lowering ψ_c caused photosynthate accumulations of approximately the same magnitude in the sink leaf 7 and the independent leaf 6. This was predicted because of the general effect of decreased ψ_c on cell enlargement (Boyer, 1968; Green, 1968).

Table 26. Effect of lowering the soil temperature from 27.5 C to 15 C for 6 hours on the rates of leaf elongation (leaf 7), net photosynthesis (leaf 5), and the soluble carbohydrate content of leaves 5, 6, and 7.

Parameter	Stress	Control	Significance	Difference
Soluble carbohydrates (% Res. wt.)			$LSD_{0.05}$	% of Control
Leaf 5	37.6	29.5	3.2	127.4
Leaf 6	43.3	29.4	7.2	147.3
Leaf 7	71.3	49.2	11.4	144.9
Photosynthesis ($mg\ CO_2 dm^{-2} hr^{-1}$)	14.1	26.4	6.6	53.4
Leaf elongation ($\mu m\ min^{-1}$)	7.5	56.2	8.7	13.3

The decrease in the size of the photosynthate sink in leaf 7, and possibly other photosynthate sinks in the plant as well caused the soluble carbohydrate level of the source leaf 5 to increase by 27 percent. This increase was accompanied by a 47 percent decrease of the net photosynthetic rate of this leaf. The pattern of decrease in the photosynthetic rate was almost linear from 97 percent to 53 percent of the initial rate. In contrast, leaf elongation decreased rapidly to 25 percent of its prestress rate and declined very slowly for the remainder of the stress period (Figure 39). If photosynthesis is regarded as a measure of source activity and leaf elongation as a measure of sink size, it follows that the pattern illustrated in Figure 39 corroborates the present concept of source-sink regulation (Neales and Incoll, 1968). Namely, that a large decrease in sink size is followed by a gradual decline in source activity as photosynthate accumulates, first at the sink and then at the source.

When leaf elongation was decreased by lowering the temperature of the apical meristem region to 6 C the ψ_c remained relatively constant and did not fall below -7 bars throughout the experiments. The pattern of reaction of photosynthesis and leaf elongation to this treatment was similar to that produced by lowering the soil temperature (Figure 39). However there were some important differences.

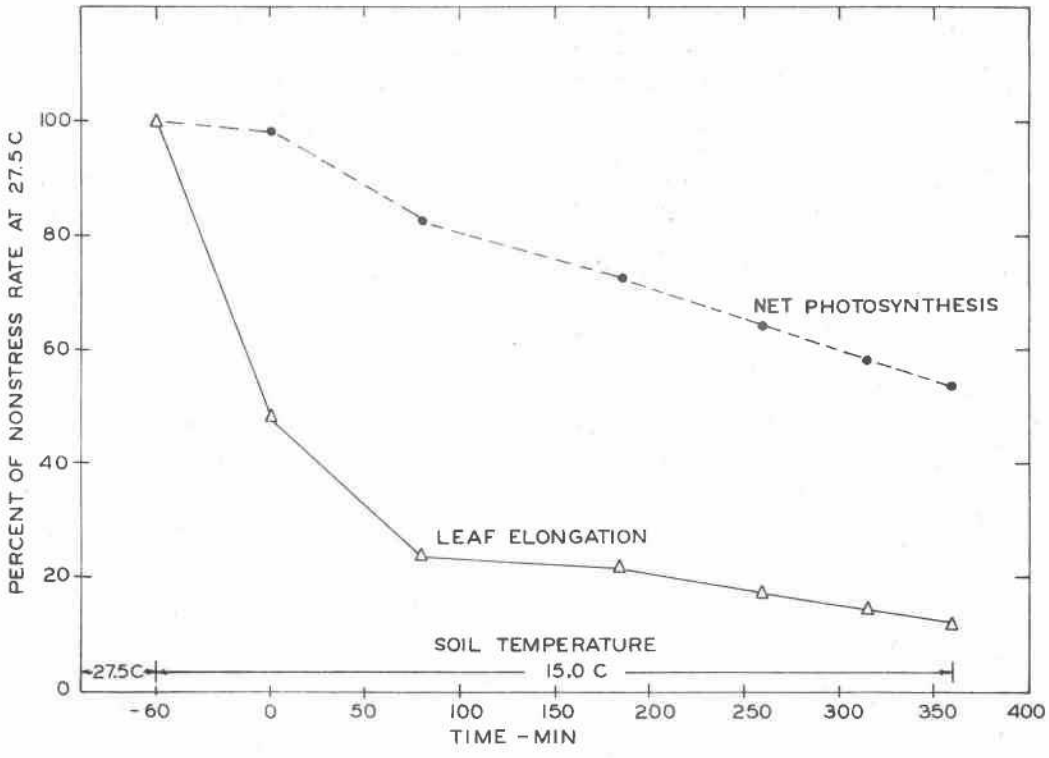

Figure 38. Effect of lowering the soil temperature from 27.5 C to 15 C on the rates of leaf elongation (leaf 7) and net photosynthesis (leaf 5) of a 7 leaf corn plant.

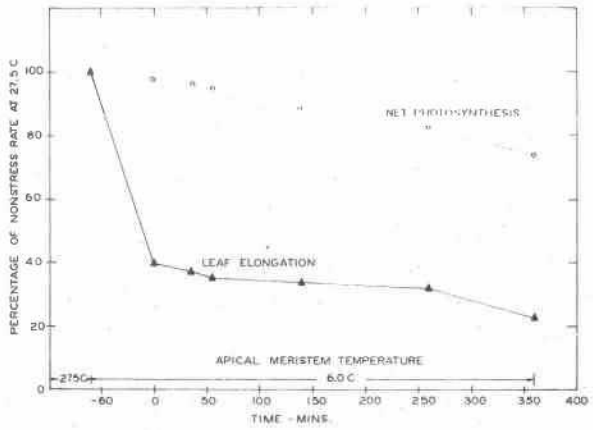

Figure 39. Effect of lowering the shoot apical meristem temperature from 27.5 to 6.0 C on the rates of leaf elongation (leaf 7) and net photosynthesis (leaf 5) of a 7 leaf corn plant.

The reduction in net photosynthetic rate of 24 percent caused by the decrease in the size of the photosynthetic sink was approximately one-half that caused by lowering the soil temperature to 15 C (Table 27). There are two possible explanations for this result. Firstly, the reduction in the rate of leaf elongation was smaller than that produced by lowering the soil temperature. Secondly, as predicted in the introduction, the meristem collar produced a more specific metabolic effect than the general water stress produced by the soil temperature treatment. This more specific effect would affect fewer photosynthate sinks within the plant. Although Hofstra and Nelson (1969) found leaf 7 to be the major photosynthate sink for leaf 5, the sum of all other sinks in the plant accounted for more of the photosynthate produced in leaf 5 than did leaf 7. The lack of a significant increase in the soluble carbohydrate level in leaf 6 is further evidence to support this point (Table 27).

Table 27. Effect of lowering the shoot apical meristem temperature from 27.5 C to 6 C for 6 hours on the rates of leaf elongation (leaf 7), net photosynthesis (leaf 5), and the soluble carbohydrate content of leaves 5, 6, and 7.

Parameter	Stress	Control	Significance	Difference
Soluble carbohydrates (% Res. wt.)			$LSD_{0.05}$	% of Control
Leaf 5	38.2	31.1	4.2	122.8
Leaf 6	30.2	31.4	n.s.	96.5
Leaf 7	73.6	52.7	7.1	139.7
Photosynthesis ($mg\ CO_2 dm^{-2} hr^{-1}$)	19.2	25.2	1.1	76.2
Leaf elongation ($\mu m\ min^{-1}$)	10.3	48.3	8.5	21.3

The significant increase in the soluble carbohydrate levels of leaves 5 and 7, but not leaf 6, when leaf elongation is decreased by lowering the temperature of the apical meristem, is consistent with the hypothesis put forward in the introduction of this chapter. Therefore, the photosynthate accumulations measured in this experiment are a result of a decrease in the size of the photosynthate sinks. More specifically, the large reductions in the rate of leaf elongation that occur under mild water stress conditions can lead to photosynthate accumulations in the source leaf and a subsequent reduction in photosynthetic rate. This indirect effect of water stress on net photosynthesis had not been previously demonstrated.

BIBLIOGRAPHY

Acevedo, E., T. C. Hsiao, and D. W. Henderson. 1971. Immediate and subsequent growth responses of maize leaves to changes in water status. Plant Physiol. 48:631-636.

Balls, W. L. 1908. The cotton plant in Egypt. MacMillan, London.

Bange, G. G. L. 1953. On the quantitative explanation of stomatal transpiration. Acta Bot. Neerl. 2:255-297.

Barlow, E. W. R. and L. Boersma. 1972. Growth response of corn to changes in root temperature and soil water suction measured with an LVDT. Crop Sci. 12:251-252.

Barrs, H. D. 1968. Effect of cyclic variations in gas exchange under constant environmental conditions on the ratio of transpiration to net photosynthesis. Physiol. Plant. 21:918-929.

Beauchamp, E. G. and J. K. Torrance. 1969. Temperature gradients within young maize plant stalks as influenced by aerial and root zone temperature. Plant and Soil 30:241-251.

Bierhuizen, J. F. and R. O. Slatyer. 1964. An apparatus for the continuous and simultaneous measurement of photosynthesis and transpiration under controlled environmental conditions. CSIRO Div. Land Res. Tech. Paper 24.

Boussingault, J. B. 1868. Agronomic, chimie agricole et physiologie 2nd Ed. Mallet Bachelier, Paris. (quoted by Neales and Incoll, 1968).

Boyer, J. S. 1968. Relationship of water potential to growth of leaves. Plant Physiol. 43:1056-1062.

Boyer, J. S. 1970a. Leaf enlargement and metabolic rates in corn, soybean, and sunflower at various leaf water potentials. Plant Physiol. 46:233-235.

Boyer, J. S. 1970b. Differing sensitivity of photosynthesis to leaf water potentials in corn and soybean. Plant Physiol. 46:236-239.

Boyer, J. S. 1971. Nonstomatal inhibition of photosynthesis in sunflower at low leaf water potentials and high light intensities. Plant Physiol. 48:532-536.

Boyer, J. S. and B. L. Bowen. 1970. Inhibition of oxygen evolution in chloroplasts isolated from leaves with low water potentials. Plant Physiol. 45:612-615.

Brix. H. 1962. The effect of water stress on the rates of photosynthesis and respiration in tomato plants and loblolly pine seedlings. Physiol. Plant. 15:10-20.

Brouwer, R. 1964. Response of bean plants to root temperature. I. Root temperature and growth in the vegetative phase. Jaarb. I.B.S. 11-22. Wageningen, The Netherlands.

Burt, R. L. 1966. Some affects of temperature on carbohydrate utilization and plant growth. Aust. J. Biol. Sci. 19:711-714.

Campbell, G. S. and M. D. Campbell. 1974. Evaluation of a thermocouple hygrometer for measuring leaf water potential *in situ*. Agron. J. (in press).

Carbon, B. A. 1973. Diurnal water stress in plants grown on a coarse soil. Aust. J. Soil Res. 11:33-42.

Chao, M. D. and W. E. Loomis. 1948. Temperature coefficients of cell enlargement. Bot. Gaz. 109:225-231.

Coombs, J., C. W. Baldry, and C. Bucke. 1973. The C-4 pathway in *Pennisetum purpureum*. I. The Allosteric Nature of PEP Carboxylase. Planta 110:95-107.

Forrester, M. L., G. Krotkov, and C. D. Nelson. 1966. Effect of oxygen on photosynthesis, photorespiration, and respiration in detached leaves. II. Corn and other monocotyledons. Plant Physiol. 41:428-431.

Fuller, E. N., P. D. Schettler, and J. C. Giddings. 1966. A new method for prediction of binary gas phase diffusion coefficients. Ind. Eng. Chem. 58:18-27.

Gaastra, P. 1959. Photosynthesis of crop plants as influenced by light, carbon dioxide, temperature, and stomatal diffusion resistance. Meded. Landbouwhogeschool, Wageningen, The Netherlands. 59:1-68.

Green, P. B. 1968. Growth physics in *Nitella*: A method for continuous *in vivo* analysis of extensibility based on a micromanometer technique for turgor pressure. Plant Physiol. 43:1169-1184.

Grobbelaar, W. P. 1963. Responses of young maize plants to root temperatures. Meded. Landbouwhogeschool, Wageningen, The Netherlands. 63(5):1-71.

Hansen, G. K. 1971. Photosynthesis, transpiration, and diffusion resistance in relation to water potential in leaves during water stress. Acta. Agr. Scand. 21:163-171.

Hartt, C. E. 1963. Translocation as a factor in photosynthesis. Naturwissenschaften 21:666-667.

Hesketh, J. 1967. Enhancement of photosynthetic CO_2 assimilation in the absence of oxygen as dependent upon species and temperature. Planta. 76:371-374.

Hofstra, G. and C. D. Nelson, 1969. The translocation of photosynthetically assimilated ^{14}C in corn. Can. J. Bot. 47:1435-1442.

Hope, A. B. and P. A. Aschberger. 1970. Effects of temperature on membrane permeability to ions. Aust. J. Biol. Sci. 23:1047-1060.

Hsiao, T. C. 1970. Rapid changes in levels of polyribosomes in Zea mays in response to water stress. Plant Physiol. 46:281-285.

Hsiao, T. C. 1973. Plant responses to water stress. Ann. Rev. Plant Physiol. 24:519-570.

Hsiao, T. C., E. Acevedo, and D. W. Henderson. 1970. Maize leaf elongation: continuous measurements and close dependence on plant water status. Science 168:590-591.

Humphries, E. C. 1963. Dependence of net assimilation rate on root growth of isolated leaves. Ann. Bot. 27:175-183.

Iljin, W. S. 1957. Drought resistance in plants and physiological processes. Ann. Rev. Plant Physiol. 8: 257-274.

Janac, J., J. Catsky, and P. G. Jarvis. 1971. Infra-red gas analysers and other physical analysers. p. 111-193. In: Z. Sestak, J. Catsky and P. G. Jarvis (ed.). Plant Photosynthetic Production. Manual of Methods. Dr. W. Junk. The Hague, The Netherlands.

Jarman, G. D., E. W. R. Barlow, and L. Boersma. 1974. An application of long-arc xenon lighting for plant growth experiments. Crop Sci. (in press).

Jarvis, P. G. 1971. The estimation of resistances to carbon dioxide transfer. p. 566-622. In: Z. Sestak, J. Catsky and P. G. Jarvis (ed.). Plant Photosynthetic Production. Manual of Methods. Dr. W. Junk. The Hague, The Netherlands.

Kemp, A., G. S. P. Groot and H. J. Reitsma. 1969. Oxidative phosphorylation as a function of temperature. Biochim. Biophys. Acta 180:28-34.

King, R. W., I. F. Wardlaw, and L. T. Evans. 1967. Effect of assimilate utilization on photosynthetic rate in wheat. Planta 77:261-276.

Kleinendorst, A. and R. Brouwer. 1970. The effect of temperature of root medium and of the growing point of the shoot on growth, water content and sugar content of maize leaves. Neth. J. Agr. Sci. 18:140-148.

Kramer, D. 1969. Plant and soil water relationships. A modern synthesis. McGraw-Hill, New York.

Kriedemann, P. E. and R. E. Smart. 1971. Effects of irradiance, temperature and leaf water potential on photosynthesis of vine leaves. Photosynthetica 5:6-15.

Kuiper, P. J. C. 1964. Water uptake of higher plants as affected by root temperature. Meded. Landbouwhogeschool, Wageningen, The Netherlands. 64:1-11.

Kuiper, P. J. C. 1972. Water transport across membranes. Ann. Rev. Plant Physiol. 23:157-172.

Loomis, W. E. 1934. Daily growth of maize. Am. J. Bot. 21:1-6.

Lyons, J, M. and J. K. Raison. 1970. Oxidative activity of mitochondria isolated from plant tissues sensitive and resistant to chilling injury. Plant Physiol. 45:386-389.

Meidner, H. 1962. The minimum intercellular space CO_2 concentration of maize leaves and its influence on stomatal movements. J. Exp. Bot. 13:284-293.

Meyer, R. F. and J. S. Boyer. 1972. Sensitivity of cell division and cell elongation to low water potentials in soybean hypocotyls. Planta 108:77-87.

Moss, D. N. 1971. Carbon dioxide compensation in plants with C_4 characteristics. In: M. D. Hatch, C. B. Osmond, and R. O. Slatyer (ed.). Photosynthesis and photorespiration. Wiley-Interscience, New York.

Neales, T. F. and L. D. Incoll. 1968. The control of leaf photosynthesis rate by the level of assimilate concentration in the leaf: a review of the hypotesis. Bot. Rev. 34:107-124.

Neumann, H. H. and G. W. Thurtell. 1972. A peltier cooled thermocouple dewpoint hygrometer for in situ measurement of water potentials. In: R. H. Brown and B. P. VanHavenen (eds.). Pyshcrometry in water relations research. Utah Agr. Exp. St. Logan.

Nir, I. and A. Poljakoff-Mayber. 1967. Effect of water stress on the photochemical activity of chloroplasts. Nature 213:418-419.

Preiss, J. and K. Kosuge. 1970. Regulation of enzyme activity in photosynthetic systems. Ann. Rev. Plant Physiol. 21:433-466.

Redshaw, A. M. and H. Meidner. 1972. Effects of water stress on the resistance to uptake of carbon dioxide in tobacco. J. Exp. Bot. 23:229-240.

Sachs, R. M. 1965. Stem elongation. Ann. Rev. Plant Physiol. 16:73-96.

Santarius, K. A. 1967. Das verhalten von Hill-reaktion und photophosphorylierung und ATP-synthese intakter Blattzellen in abhangigkeit vom Wassergehalt. Planta 73:228-242.

Sharman, B. C. 1942. Developmental anatomy of the shoot of Zea mays L. Ann. Bot. 6:245-285.

Slavik, B. 1965. The influence of decreasing hydration level on photosynthetic rate in the thalli of the hepatic Conacephallum concum. In: B. Slavik (ed.). Water stress in plants. Dr. W. Junk, The Hague, The Netherlands.

Slatyer, R. O. 1969. Physiological significance of internal water relations to crop yield. In: J. D. Eastin, F. A. Haskins, C. Y. Sullivan, and C. H. M. VanBavel (ed.). Physiological aspects of crop yield. American Society of Agronomy, Madison, Wisconsin.

Slatyer, R. O. 1973. Effects of short periods of water stress on leaf photosynthesis. In: R. O. Slatyer (ed.). Plant response to climatic factors. UNESCO. Paris.

Slatyer, R. O. and J. F. Bierhuizen. 1964. A differential psychrometer for continuous measurement of transpiration. Plant Physiol. 39:1051-1056.

Sweet, G. B. and P. F. Wareing. 1966. Role of plant growth in regulating photosynthesis. Nature 210:77-79.

Thrower, S. L. 1965. Translocation of labelled assimilates in soybean. IV. Some effects of low temperatures on translocation. Aust. J. Biol. Sci. 18:449-461.

Troughton, J. H. 1969. Plant water status and carbon dioxide exchange of cotton leaves. Aust. J. Biol. Sci. 22:289-302.

Turner, N. C. and J. E. Begg. 1973. Stomatal behavior and water stress on maize, sorghum and tobacco under field conditions. Plant Physiol. 51:31-36.

Wardlaw, I. F. 1969. The effect of water stress on translocation in relation to photosynthesis and growth. II. Effect during leaf development in Lolium temulentum. L. Aust. J. Biol. Sci. 22:1-16.

Watts, W. R. 1972a. Leaf extension in Zea mays L. I. Leaf extension and water potential in relation to root zone and air temperature. J. Exp. Bot. 23:704-712.

Watts, W. R. 1972b. Leaf extension in Zea mays L. II. Leaf extension in response to independent variation of the temperature of the apical meristem, of the air around the leaves, and of the root zone. J. Exp. Bot. 23:713-721.

Weatherley, P. E. and B. T. Watson. 1969. Some low temperature effects on sieve tube translocation in Salix viminalis. Ann. Bot. 33:843-853.

Wesselius, J. C. and R. Brouwer. 1972. Influence of water stress on photosynthesis, respiration and leaf growth of Zea maize L. Meded. Landbouwhogeschool, Wageningen, The Netherlands. 72(33):1-15.

Whiteman, P. C. and P. C. Koller. 1968. Estimation of mesophyll resistance to diffusion of carbon dioxide and water vapor. p. 415-419. In; F. E. Eckart (ed.). Functioning of Terrestrial Ecosystems at the Primary Production Level. UNESCO. Paris.

Zolkevick, V. N., L. D. Drusakova, and A. A. Lizandr. 1958. Translocation of assimilates and respiration of conductive tissue in relation to soil moisture. Fiziol. Rast. 5:337-344.

APPENDIX I

Outline of the Theory and Methodology Involved in the Computation of the Diffusive Resistances to Carbon Dioxide Flow During Photosynthesis

The ease with which CO_2 moves into a leaf in the process of photosynthesis and the ease with which water vapor moves out of the leaf in the process of transpiration, exerts a large influence on the rates of these processes. The resistances encountered by CO_2 molecules moving into the leaf to the fixation sites in the chloroplasts, may be used to quantitatively describe the physiological responses that may limit the rate of photosynthesis. The resistances encountered by water vapor molecules may be used in a similar manner. Along each diffusion pathway there are several discrete segments which may be identified by position or transfer mechanism. As several of these pathway segments are common to both CO_2 and water vapor, the simultaneous measurement of photosynthesis and transpiration enables all resistances to be either measured or calculated.

The diffusion resistances encountered by water vapor leaving the leaf are r_s the stomatal resistance and r_a the boundary layer resistance. CO_2 entering the leaf follows the same pathway and therefore encounters the same boundary layer and stomatal resistances. However, as CO_2 must also diffuse from the substomatal cavity to the carbon fixation sites in the mesophyll or bundle sheath cells, a further CO_2 resistance, the mesophyll resistance (r_m) is defined (Gaastra, 1959). As these resistances are in series the total resistance is equal to the sum of the individual resistances (Bange, 1953). Neglecting the negligible CO_2 and water vapor transfer through the cuticle (Jarvis, 1971) the total resistances to CO_2 and water vapor transfer may be written

$$\Sigma r_{H_2O} = r_a + r_s \qquad \text{A-1}$$

and

$$\Sigma r_{CO_2} = r_a + r_s + r_m \, . \qquad \text{A-2}$$

The resistances are quantified in the following manner. The transfer of CO_2 into and water vapor out of the leaf occurs by molecular diffusion, therefore by Fick's first law, the net flux of mass per unit area and time q_v, anywhere within the pathway is proportional to the gradient of partial pressure, or at atmospheric pressure, the gradient of concentration dc/dz so that,

$$q_v = -D_v \frac{dc}{dz} \, , \qquad \text{A-3}$$

where D_v is the effective molecular diffusivity of water vapor or CO_2 in air (after Jarvis, 1971). The diffusion resistance r_v is then defined by

$$r_v = \int_{z_1}^{z_2} \frac{dz}{D_v} \quad [s\ m^{-1}] \ , \qquad \text{A-4}$$

and hence

$$q_v = \frac{c_1 - c_2}{r_v} \quad [Kg\ m^{-2} s^{-1}] \ , \qquad \text{A-5}$$

and

$$r_v = \frac{c_1 - c_2}{q_v} \quad [s\ m^{-1}] \ . \qquad \text{A-6}$$

Based on equations A-6 and A-1 the total resistance to water vapor transfer can be obtained as,

$$\Sigma r_{H_2O} = r_a + r_s = \frac{[H_2O]_c - [H_2O]_a}{E} \quad [s\ m^{-1}] \ , \qquad \text{A-7}$$

where E is the transpiration rate $[Kg\ m^{-2} s^{-1}]$, $[H_2O]_a$ and $[H_2O]_c$ are the water vapor concentration $[Kg\ m^{-3}]$ in the air and interior of the leaf respectively. The stomatal resistance (r_s) can be obtained by first estimating the boundary layer resistance (r_a).

$$r_s = \Sigma r_{H_2O} - r_a \ . \qquad \text{A-8}$$

The boundary layer resistance r_a can be measured by determining the rate of water loss from blotting paper leaf models with similar geometry to the leaf. The total resistance to CO_2 transfer is obtained from the equation

$$\Sigma r_{CO_2} = r_a + r_s + r_{me} = \frac{[CO_2]_a - [CO_2]_{chl}}{P_N} \ [s\ m^{-1}] \ , \qquad \text{A-9}$$

where P_N is the net photosynthetic rate $[Kg\ m^{-2} s^{-1}]$, $[CO_2]_a$ and $[CO_2]_{chl}$ are the CO_2 concentrations in the air and at the chloroplast fixation sites respectively, As r_a and r_s have already been

calculated from the transpiration rate, the mesophyll resistance (r_m) can be calculated from the equation

$$r_m = \Sigma r_{CO_2} - (r_s + r_a)\left(\frac{D_{H_2O}}{D_{CO_2}}\right) \qquad \text{A-10}$$

where the correction term (D_{H_2O}/D_{CO_2}) is necessary to account for the difference in effective molecular diffusivities of CO_2 and water vapor.

Although the mesophyll resistance was defined as a diffusion resistance, its estimation as a residual resistance by the above method means that it contains all that is not accounted for by the stomatal and boundary layer resistances and therefore includes photochemical and biochemical processes unrelated to the transfer of CO_2 through the cell. In this study the use of mesophyll resistance as a residual term was practically expedient, because the study aimed to differentiate between stomatal and nonstomatal influences reducing the photosynthetic rate during plant water stress.

APPENDIX II

Calculation of Transpiration Rates From Differential Psychrometer Readings

Data From Chart Recorder

ΔT_1: the temperature difference between reference and sample wet bulbs was 101 μV

ΔT_2: the temperature difference between reference wet bulb and water bath B_2 (27.5 C) was -240 μV

thermocouple calibration was 41 μV per degree C.

Therefore,

$$\Delta T_1 = 2.46 \text{ C}$$

and

$$\Delta T_2 = -5.85 \text{ C} .$$

As reference temperature was 27.5,

T_r, temperature of reference wet bulb is 21.65 C (27.50-5.85)

T_s, temperature of sample wet bulb is 24.11 C ($T_r + \Delta T_1$) .

From Equation 26,

$$\Delta e = e_s - e_r = A(t_{ws}-t_{wr}) + (e_{ws}-e_{wr}) ,$$

where ($t_{ws} - t_{wr}$) is ΔT_1 and e_{ws} and e_{wr} are the saturated vapor pressures at T_s and T_r respectively. A, the psychrometric constant, is 0.667 mb vapor pressure per degree C, so that

$$\Delta e = (0.667 \times 2.46) + (30.011 - 25.871) ,$$

$$\Delta e = 5.78 \text{ mb}$$

The saturated vapor pressure (e_s) at 27.5 C is 36.71 mb and the density of water vapor (ρ) in saturated air at 27.5 C is 26.46 mg L^{-1}.

From Equation 27,

$$c = \rho\left(\frac{\Delta e}{e_s}\right) ,$$

$$c = 26.46 \text{ x } (5.78/36.71) ,$$

$$c = 4.17 \text{ mg } L^{-1} .$$

If the leaf area in the chamber is 40 cm^2 and the flow rate through the chamber is 3.63 L min^{-1}, the transpiration rate E is,

$$E = 4.17 \text{ x } (3.63/40) ,$$

$$E = 0.378 \text{ mg } cm^{-2} min^{-1} ,$$

$$E = 2.271 \text{ g } dm^{-2} hr^{-1} .$$

Calculation of CO_2 Transfer Resistances From Photosynthesis, Transpiration, and Leaf Temperature Data

$P_n = 30.9$ mg CO_2 $dm^{-2} hr^{-1} = 0.086$ µg CO_2 $cm^{-2} s^{-1}$

$E = 2.407$ g H_2O $dm^{-2} hr^{-1} = 6.686$ µg H_2O $cm^{-2} s^{-1}$

$T_c = 30.00$ C

T_a = temperature of air entering the chamber = 27.50 C

T_r = temperature of reference wet bulb = 21.65 C

$r_a = 0.96$ s cm^{-1}

$[CO_2]_a = 345$ vpm $= 0.610$ µg cm^{-2}

$[CO_2]_{chl} = 0$ vpm

The saturated vapor pressure at 21.65 C is 25.87 mb and the density of water vapor in saturated air at 27.5 C is 26.46 µg cm^{-3}.

The water vapor concentration of the air entering the leaf chamber is

$$[H_2O]_a = 26.46\ (25.87/36.71)$$

$$= 18.65\ \mu g\ cm^{-3}\ .$$

The water vapor concentration inside the leaf is the water vapor density of saturated air at 30.00 C, which is 30.34 $\mu g\ cm^{-3}$

$$[H_2O]_c = 30.34\ \mu g\ cm^{-3}\ .$$

Substituting in Equation 30

$$\Sigma r_{H_2O} = \frac{[H_2O]_c - [H_2O]_a}{E}\ ,$$

$$= \frac{30.34 - 18.65}{6.686}\ s\ cm^{-1}\ ,$$

$$= 1.75\ s\ cm^{-1}\ .$$

The total resistance to CO_2 transfer is calculated from Equation 31,

$$\Sigma r_{CO_2} = \frac{[CO_2]_a - [CO_2]_{chl}}{P_n}\ ,$$

$$= 0.610/0.86\ s\ cm^{-1}\ ,$$

$$= 7.09\ s\ cm^{-1}\ .$$

As D_{H_2O}/D_{CO_2} is 1.60 and r_a is 0.96 s cm^{-1} the stomatal resistance to CO_2 transfer is,

$$r_s = \Sigma r_{H_2O}\left(\frac{D_{H_2O}}{D_{CO_2}}\right) - r_a\ ,$$

$$= (1.75 \times 1.60) - 0.96\ ,$$

$$= 1.84\ s\ cm^{-1}\ .$$

The mesophyll resistance to CO_2 transfer is

$$r_m = \Sigma r_{CO_2} - (r_a + r_s)\ ,$$

$$= 7.09 - 2.8\ ,$$

$$= 4.29\ s\ cm^{-1}\ .$$

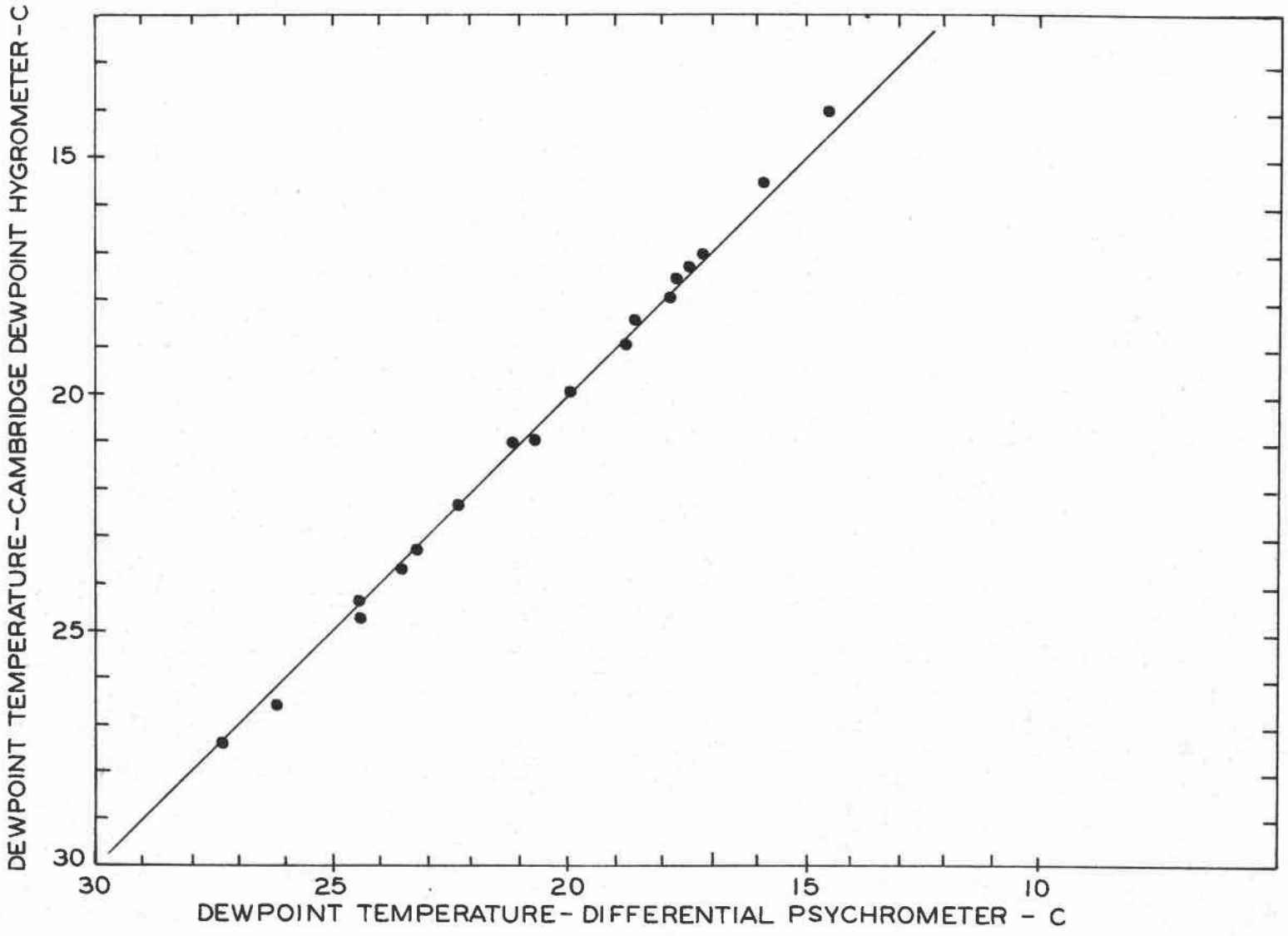
DEWPOINT TEMPERATURE-CAMBRIDGE DEWPOINT HYGROMETER-C
15
20
25
30
30
25
20
15
10
DEWPOINT TEMPERATURE- DIFFERENTIAL PSYCHROMETER - C